Numerical and Experimental Studies of Droplet Combustion
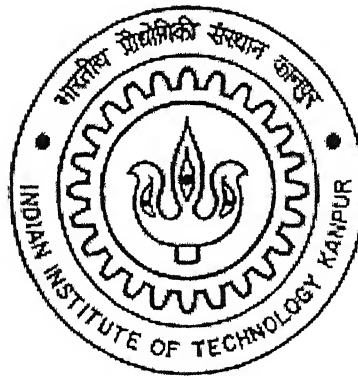
A Thesis Submitted

In Partial Fulfillments of the Requirements
for the Degree of

Master of Technology

by

Amit Majee

to the

Department of Aerospace Engineering
Indian Institute of Technology Kanpur, India
July, 2005

Certificate

It is certify that the work contained in the thesis titled, **"Numerical and Experimental Studies of Droplet Combustion"** by **Amit Majee,** has been carried out under my supervision and that this work has not been submitted elsewhere for the award of a degree.
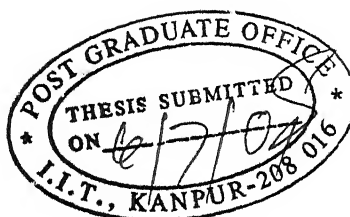
July, 2005

(Dr. D. P. Mishra)

Assistant Professor,

Department of Aerospace Engineering,

Indian Institute of Technology, Kanpur.

DEDICATED TO MY UNCLE

SRI UDDHAB KUMAR MAJEE

AND

OTHER RELATIVES

Acknowledgement

This is a great opportunity for me to express my sincere gratitude towards my thesis supervisor Dr. D. P. Mishra for his inspiration and valuable guidance during the period of this work. His constant concern and personal guidance has led the present investigation to a fulfill completion.

During the course of my research work, I got an opportunity to interact with Prof. Keshav Kant of Mechanical Engineering Department and Dr. Abhijit Kushari for which I grateful to their help.

I must acknowledge heartily the spontaneous assistance and cooperation extended by Ashok Singh, Ajay Naik and Manoj Naik of Combustion Lab, Department of Aerospace Engineering. I am grateful for the help and cooperation of my friends Sudhir, Kiran and Ugandhar for completing this thesis successfully and I will be remembering their plangent company throughout my life .

For my experimental works I am thankful to Mr. Arun Kumar Mishra and other staffs of Aerospace Engineering Workshop. Beside this the services rendered by the staffs of central Workshop are acknowledged heartily.

I am also very much thankful to my hostel mates Sunny Bhai (Md. Rabius Sunny), Kumareshda (Kumaresh Bagchi), Sanjoyda (Sanjoy Saha), Kanchanda (Kanchan Dutta) and Rabi (Rabi Sankar Ghosh Bag) for their affectionate support.

Finally I am eternally indebted to my family for the sacrifice they have made for me and for the utmost patience with which they have borne. Thanking them is just the beginning.

July, 2005

(Amit Majee)

ABSTRACT

The understanding of liquid fuel droplet combustion is very important for designing and developing low emission and energy efficient combustion systems. The present thesis is devoted to investigate the combustion aspects of a single isolated droplet numerically and experimentally. Droplet combustion experiments for both single and multi component fuels at normal pressure and temperature are performed under normal gravity condition. The d^2 law diameter regression rate behavior is observed for both single and multicomponent fuel. The burning rate constant for multicomponent fuel droplet combustion lies between that for its individual constituents. The droplet combustion is modeled by solving one dimensional, unsteady governing equations numerically. In this CFD code, variable properties, gray gas model for radiation heat transfer are included. The effects of ambient oxygen level on droplet combustion are very important to study as it varies in the course of combustion. Burning rate constant as well as the flame diameter increases with the increase in ambient oxygen level. The flame temperature is increased leading to gasification of fuel droplet. The inclusion of gray gas model for radiation heat transfer improves the prediction of droplet burning rate and flame temperature. It was found out that radiation heat transfer (heat loss at low ambient temperature and heat gain at high ambient temperature) for bigger size droplet is more predominant compared to smaller droplet. As a result opposite influence of the initial droplet diameter on the droplet combustion can be observed between the higher and lower temperature. The burning rate constant with increase in initial droplet diameters is increased and decreased at high and low ambient temperature respectively. In the third phase, the multicomponent fuel droplet combustion is investigated by using distillation curve model. The transient analysis of the surface properties with different fuel composition has also been carried out extensively in the study. The data presented in the present study matches well with the available previous study. It was found out that multicomponent fuel droplet combustion has three dominant periods, 2 d^2 law periods separated by transition period with a gradual change.

Contents

LIST OF FIGURES

LIST OF TABLES

NOMENCLATURE

English Symbols:

a	Thermal diffusivity (m^2/s)
a_0	Thermal diffusivity at standard ambient conditions (m^2/s)
a,b,c,d	Elements in Tri-diagonal Matrix
A	Pre-exponential factor
B	Spanding's transfer number
C_p	Constant pressure specific heat $(Jule/\,kmol\text{-}K)$
C_{M_i}	Concentration of chemical species i.
D_i	Diffusion coefficients of species $i\,(m^2/s)$
Dn	Damköhler number
E_a	Activation Energy
$\Delta h_{f,i}^0$	Enthalpy of formation for i^{th} species
k	proportionality constant
K_b	Burning rate
$Le_{i,0}$	Reference Lewis Number of ith species
L_i	Latent heat of vaporization of the ith species
m,n	Exponent
M	Molecular weight
p	Pressure in Pascal
P	Pressure in bar
q_R	Radiation term
R_0	Initial droplet radius
R_u	Universal gas constant
St	Non dimensional term
t	Time
t_b	Burning time
t_1	Preheated time
T	Temperature
v_g	Gas phase radial velocity
x	Non dimensional liquid phase radius
X	Mole fraction

Y Mass fraction

Greek Symbols:

α	Absorptivity
$\alpha, \beta, \gamma, \varphi$	Some temporary terms used for calculation
η	Non dimensional gas phase radius
ρ	Density
ε	Fractional mass gasification rate
$\dot{\omega}_{g,i}$	Species generation for i^{th} species in gas phase
Θ	Non dimensional term
λ	Thermal conductivity
$\nu_i^{'}$	stoichiometric coefficient of the ith reactant
$\nu_i^{''}$	stoichiometric coefficient of the ith product

Subscripts:

0	At the standard or starting conditins
d	Droplet
f	Fuel
g	For gas phase
i	For i^{th} species
j	Time step
l	Liquid phase

Superscripts:

*	Non dimensional terms

Chapter 1

INTRODUCTION

1.1. Background

The first step in human civilization is the invention of fire. The further mastery over combustion and its applications played most vital role to drive the human civilizations. Industrial era was started with the invention of steam engine by James Watt. This was the first step to convert the heat of combustion to the mechanical power. Even today 90% of the energy used by the human being is being obtained by burning of fuels such as, coal, petroleum oils, biomass, etc. The phenomenon of combustion finds applications in several modern systems such as internal combustion engine used in most of the automobiles, gas turbine engines in aircraft and power plant, boiler used for power generation and lots of other applications.

However, the over exploitation of combustion process to meet the energy demands of modern man has created unmitigated problems of emissions which is a threat to very existence of life on the earth. The air pollutants such as carbon monoxide, NO_X, SO_X, unburnt hydrocarbons, etc. are generated due to incomplete combustion of fuel. Combustion process also produces large amount of smoke, ash, odors, noxious and benign gases. These gases have damage the environment around to a large extent for which there is a global concern to reduce the emission from the combustion systems. Beside this there is scarcity of fossil fuel across the globe. Hence, it is important to utilize the available fossil fuel and enhance the efficiency of the combustion systems. For which, there is an urgent need to understand the processes involved in the combustion and develop energy efficient and low emission combustion systems.

Generally the liquid fuel is used in most of the combustion devices due to easy storage and high energy density. However, it can not be burnt itself efficiently like any other gaseous fuel. In order to increase the burning rate the contact area between the liquid surface and the ambient oxygen has to be increased, which can be possible by disintegrating the liquid fuel into smaller droplets. Disintegrating a bigger droplet into n numbers of smaller droplet total surface area can be increased by n times. Hence the fuel can be burnt n^2 time faster than the previous case. For example, burning time can be enhanced by 10^6 times to disintegrate a 3 mm

diameter bigger droplet into 10^3 numbers of 300 μm diameter droplets. In any liquid fuel combustion system, fuel is atomized into spray containing large numbers of droplets with different diameters. But the understanding of spray combustion is impeded by the complex processes involved in it. However the whole spray consisting of a wide range of droplet diameters can be well represented by a single droplet diameter generally in terms of Sutter Mean Diameter (SMD). The SMD of a spray is used as an important parameter during the design of a combustor. Hence the study of the droplet combustion is very important to understand the physical mechanism during its combustion process.

1.2. Droplet Combustion
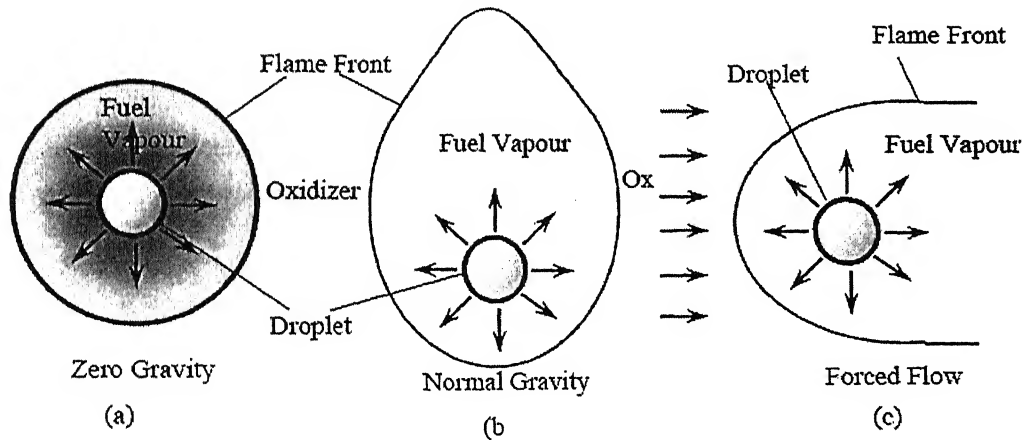
Fig. 1.1: Liquid fuel droplet combustion in (a) Micro gravity (b) Normal gravity (c) Forced convection conditions [47]

The processes involved in the combustion of a single droplet under three different conditions such as (a) Microgravity, (b) Normal Gravity and (c) Forced Flow are described in Fig. 1.1. During droplet combustion, liquid fuel vaporizes and mixes with the air due to mass diffusion. As the temperature outside the droplet is higher than the self ignition temperature of the fuel, combustion takes place. Heat and products are generated, which are transferred due to heat and mass diffusion respectively. When the droplet is burnt under **normal gravity** condition, the high temperature product gas moves upward due to buoyancy force and natural convection heat transfer takes place, as shown in Fig. 1.1(b). The burning rate is

enhanced considerably due to convection heat transfer. However under **zero** or **micro gravity** conditions the flame surface becomes almost spherosymmetric as shown in Fig. 1.1(a). For this case the ratio of the flame radius to the droplet radius is defined as **flame stand-off ratio**. When the flow takes place over the droplet surface as shown in Fig. 1.1(c), the flame is aligned along the free stream velocity.

Classical Theory on Droplet Combustion:

For simplicity, droplet burning is considered as follows in the classical theory of droplet combustion;

(1) Spherical symmetry; (2) No spray effect; (3) Combustion rate controlled by mass transfer to the flame due to diffusion; (4) Constant pressure process; (5) Thin flame approximation; (6) Constant gas phase properties; (7) Quasi steady process assumption; (8) Constant and uniform droplet temperature; (9) Neglecting Soret, Dufour and radiation effect, (10) unity Lewis number, (11) No radiation heat loss.

By using this approximation the instantaneous droplet diameter can be represented by the initial droplet diameter and the burning time as follows;

$$d^2 = d_0^2 - K_b t \qquad (2.1)$$

where, d and d_0 are the instantaneous droplet diameter at time t and initial droplet diameter. K_b is the burning constant (also known as **effective burning rate** in literature) which can be expressed as

$$K_b = \frac{\partial r_d^2}{\partial t} = \frac{8\rho_g a_s}{\rho_l} \ln(1 + B) \qquad (2.2)$$

where, ρ_g and ρ_l -are the gas and liquid phase density. a_g is the gas phase thermal diffusivity at the surface and B is the Spalding transfer number. And the total burning time can be represented as $t_b = \dfrac{d_0^2}{K_b}$.

1.3. Motivation for the Present Work

In any combustion device, the performance and size of combustor are strongly dependent on the total allowable time provided to burn the droplet. If the droplet does not get the required time to burn, unburnt hydrocarbons are exhausted out to the atmosphere. As a result the efficiency of the combustion systems is reduced drastically while releasing large amount of pollutants to the atmosphere. Most of the time, the liquid fuel droplet are burnt under high pressure and temperature. Beside this the concentration of oxygen level in the combustor may get changed with time, which affects its burning efficiency. Hence it is very important to study the effects of temperature, effects of oxygen concentration on the droplet burning, which is not being addressed adequately in the literature.

Most of the practical liquid fossil fuel generally consists of several blends of hydrocarbons with different physical and chemical properties. However, the literature review reveals that the understanding of the multicomponent fuel droplet combustion is at infancy stage. Hence, in this thesis an attempt is made to study the multicomponent fuel droplet combustion by using both experimental and numerical tools.

1.4. Objective

The main objectives of the current work are the followings.

i)   Design and develop an experimental setup to investigate the single isolated droplet combustion under normal gravity.

ii)   To study the single and multi component fuel droplet combustion under normal atmospheric pressure.

iii)   To develop unsteady, 1-D, variable properties, single step chemistry, numerical model for droplet combustion under microgravity for single and multi component fuel droplet combustion.

iv)   To study the transient variation of droplet diameter square, flame structure, surface parameters such as surface temperature gasification rate, etc.

v)   Effect of ambient oxygen concentration on the single component fuel droplet combustion.

vi)   Study the effects of radiation heat transfer on the droplet combustion.

vii)   Study the inverse influences of the initial diameter in high and low ambient

temperature.

viii) Study of multicomponent fuel droplet combustion. Changing in surface parameters during multicomponent fuel droplet combustion.

1.5. Organization of the Thesis

The background, motivation and objective of this research are contained in the present chapter. Previous research on the field of droplet combustion is discussed in brief in chapter 2. The major previous experimental and numerical works are reviewed critically in this chapter reporting the anomalies present in the literature. Based on the literature survey the objectives of the present thesis are set out. The experimental setup and the results of the present work are discussed in chapter 3. In chapter 4, the mathematical model for this analysis is elaborated, which is followed by the numerical results and discussion in chapter 5. Results and discussions are presented in two sections Section 5.1 containing the simulation results for single component fuel droplet combustion followed by the results for the multicomponent fuel droplet combustion in Section 5.2. The effects of initial oxygen concentrations, effects of radiations are discussed extensively for single component fuel droplet combustion. However, the effects of compositions on the transient variation of different burning parameters are being discussed for multicomponent fuel droplet combustion. The last chapter (Chapter 6) contains the conclusion and the recommendations for the further studies.

1.6. Summary

In the present chapter a brief insight into the basics of the droplet combustion is presented. It is quite clear from the study that droplet combustion is very important to study. The processes involved during the combustion of single isolated droplet under three different conditions such as, normal gravity, micro-gravity and forced flow conditions are being discussed briefly. The classical theory of droplet combustion is enumerated briefly highlighting the universality of d^2 law. The motivation of the present work is described mentioning the current issues to be addressed in this thesis. The objectives of the present thesis are enumerated adequately.

Chapter 2
LITERATURE REVIEW

2.1. Classical Theories on Liquid Fuel Droplet Combustion

First successful and remarkable investigations of droplet combustion were carried out theoretically by G A E Godsave [18] and D B Spalding [68] independently in 1953. Godsave [18] presented two distinct models such as (i) Low Temperature Evaporation and (ii) High Temperature Evaporation and Combustion. He found out that Low Temperature Evaporation is more likely to occur when the temperature difference between the droplet and the ambient is less. On the other hand, the High Temperature Evaporation and Combustion can occur when the difference in temperature between the droplet and surround atmosphere is considerable. He concluded that the volatility of the fuel, expressed in terms of vapor pressure, does not have a predominant effect on the burning rate. However the instantaneous mass rate of burning is proportional to its diameter.

Spalding [68] was first to introduce a non-dimensional transfer number, B in his quasi steady state model that controls the mass burning rate. Subsequently this was leveled as *Spalding's transfer number*. The mass transfer from liquid fuel droplet surface depends only on *Spalding's transfer no, B*. In this model, the rate controlling phenomenons were found to be dependent on the physical properties, heat and mass transfer. However the chemical kinetics associated with combustion does not play any critical role.

2.2. Experimental Studies

Experimental studies on droplet combustion was pioneered by Kumagai, S., and Isoda, H. [28] in 1955. Subsequently they investigated the combustion of a single isolated droplet in microgravity successfully in 1957 [30]. In that experiment they studied the effects of gravity on the droplet combustion in terms of flame structure and the droplet burning rate.

In 1971, Kumagai, Sakai and Okajima [31] performed the first unsupported droplet combustion experiments using a 0.8 s drop tower. In these experiment, the burning rate of n-heptane was reported to be nearly constant, 0.78 mm^2/s. Considerable numbers of experiments supported their findings (Yang and Avedisian

[80]; Hara and Kumagai [20]). Hence the burning rate constant for an isolated n-heptane droplet was remained as a fundamental parameter for more than two decades. Later on, advanced theories supported by experimental data revealed the earlier conclusion not to be right.

2.3. Parametric Studies of Droplet Combustion

The droplet combustion at high pressure was modeled by Rosner [60], Chervinsky [7]. They found out that burning rate is proportional to $p^{1/3}$. Faeth et al. [13] also conducted supercritical combustion studies up to pressure of 100 atm., under micro-gravity conditions. Their experimental results supported the previous modeling results. Later on the transient variation of droplet combustion by varying operating parameters for a wide range were investigated extensively by several research groups such as, Hubbard et al. [24], Law [36], Law and Sirignano [37], Saitoh and Nagano [61]. Among all the results of Hubbard et al. [24] are very closer to the existing experimental data. Prakash and Sirignano [57], [58] modeled the internal circulation in the droplet due to shear generated at its surface depicting the liquid and air interaction.

Egawa et al. [12] examined the pressure effects on combustion of fuel droplet under zero gravity. They concluded that the evaporation constant increases with increase in pressure and its effects on the evaporation constant are very small. Flame stand-off ratio decreases with pressure and its variation cannot be explained by the classical quasi-steady theory. Subsequently Sato et al. [64] carried out experiments on the effects of natural convection on high pressure droplet combustion. They studied the burning of n-octane fuel droplet under both normal and microgravity conditions. They concluded that the burning rate increases in the sub-critical zone and decreased in the super-critical zone in both micro and normal gravity condition with the increase in pressure and attains a maximum value at the critical pressure. The burning rate increases with the natural convection and its effects are relatively pronounced at high ambient pressure.

The effect of acoustical excitation on the droplet evaporation and combustion was studied experimentally by Saito et al. [63] in 1995. They concluded that the acoustical excitation promotes the mixing between the fuel vapor and the surrounding gases leading to augmentation in heat and mass transfer during the

combustion process. As a result the burning rate was enhanced. Ghenai et al. [15] extended it further and concluded that burning rate increases more that 20% when the droplet is situated at the pressure node (velocity anti-node) of the acoustic wave. In contrast no such effects were observed at velocity node (pressure anti-node).

2.4. Effects of Radiation on Droplet Burning

Radiations heat losses from the flame surface are two types: luminous radiation and non-luminous radiation. Non-luminous radiations are mainly associated with the combustion gases, such as CO_2 and H_2O. In contrast, oxygen and nitrogen are considered as transparent to the thermal radiations. Carbon particles or soot are responsible for the luminous radiation (Tien and Lee [70]).

The classical quasi-steady theory does not take account of the radiation effects on the droplet combustion. However, the effect of radiation was analyzed by Godsave [18] by considering the heat directly transferred from hot flame zone to the cold droplet surface. The reflection and radiative losses from the droplet was not considered in this model. Total heat gain due to radiation at droplet was approximated as, $q_R = A\alpha_d\alpha_f\sigma_E T_f^4$; where, A is the drop surface area, α_d is the absorptivity of drop surface, α_f is the absorptivity of flame front and σ_E is the Stefan-Boltzman's constant. In this analysis, the flame temperature, mean droplet surface were assumed to be 2000 K, 323 K. Beside this they also approximated the flame surface and drop surface absorptivity to be 0.03 and 0.05 respectively during the burning of 1.42 mm diameter benzene droplet. In his study it was concluded that 20% of heat is transferred at droplet surface due to radiation and absorbed radiation is proportional to the diameter of the droplet. It was suggested that the radiation effect can be neglected for smaller droplets.

In another study, Beer and Howarth [5] concluded that any small gas volume in any thermodynamic system must be in a thermodynamic equilibrium. The product species such as H_2O and CO_2 are the considered to be the major contributors for radiative heat transfer. According to the study of Abdel-Khalik et al. [1], 40% of total heat is transferred due to radiation. Out of which 30% is contributed by the soot radiation, while 70% is due to gas phase radiation. In their study H_2O and CO_2 were considered as only the participating gases.

Currently, two types of radiation models such as Gray gas and Non-gray gas

model are being used in the literatures. In Gray gas model the radiation properties are assumed to be remained constant with the wavelengths. However, the variations of radiation properties with the wave-lengths are considered in non-gray gas narrow and wide band models. In the weighted sum gray gas model, the gas is represented by a number of gray gases with different absorption coefficients.

In most of the studies such as, Saitoh et al. [62], Marchese and Dryer [43], Marchese et al. [44], Kumar et al. [33], Kazakov et al. [27], gray gas modeling originally pioneered by Viskanta and Merriam [75] had been used. Saitoh et al. [62] used a constant Planck mean absorption coefficient equal to 0.35 m^{-1}. While Marchese and Dryer [43], Marchese et al. [44], Kazakov et al. [27], Kumar et al. [33] had employed the variable Planck mean absorption coefficients, which was evaluated locally based on the partial pressure weighted sum of mean absorption coefficient for each participating gas at the local grid temperature.

In 1992 a comprehensive mathematical model incorporating multi-component molecular diffusion, complex chemistry, and heterogeneous process to investigate a variety of chemically reacting flow problem was introduced by Cho et al. [10]. This model emphasized the elementary chemical and physical process rather than complex flow geometry. They concluded that extinction of smaller droplets is caused by purely finite-kinetics, while extinction of larger droplets is caused by excessive radiative heat loss which eventually limited the kinetics.

Effects of non-luminous thermal radiation in micro-gravity droplet combustion were examined by Marchese and Dryer [43]. They numerically simulated the transient combustion of methanol-water mixture droplets. Their results also indicate that the effect of radiative heat loss cannot be neglected for larger initial droplet diameters.

Transient combustion of spherical single and multicomponent n-Alkane droplets with non-luminous gas phase radiative heat transfer with complex chemical kinetics was numerically simulated by Marchese et al. [44]. By including radiation in this model, a significant decrease in maximum flame temperature was observed. The normalized flame position decreases as a consequence of radiative losses. With increase in initial diameter, their model predicts lower burning rate and eventually leading to radiative extinction.

Baek et al [4] investigated the influence of non-gray radiation on the droplet combustion using weighted sum of gray gas model assuming CO_2 and H_2O to be

the major contributors. By using a constant Planck mean absorption coefficient of $2.0 \, m^{-1}$ they found out a good agreement between the results of gray-gas model and non gray gas model.

To investigate the effect of initial droplet diameter on combustion at different ambient temperature, Xu et al. [79] performed their experimental analysis of a single isolated n-heptane droplet at 298 K, 633 K and 1093 K. Their result predicted the inverse influences of initial droplet diameter in cold and hot ambiences. The burning rate respectively decrease and increase with the increase in droplet diameter for former and later case. The differences between the radiation heat gain by the droplet and heat loss to the ambience was suggested to be responsible for this. Subsequently this phenomenon at room temperature was reported in the numerical and experimental analysis of Kazakov et al. [27].

2.5. Droplets Interaction

In actual combustion systems, droplet never burns in an isolated manner without any interaction among the adjacent droplets. Under this situation, the droplet-droplet (and flame-flame) interaction will affect the flame shape, flame dynamics, burning rates and extinction behaviors. Early investigations using linear arrays of droplets were performed by Miyasaka and Law [48], Xiong et al. [78]. Their results indicated that the average burning rate for the droplet arrays is lower than that of an isolated droplet. This phenomenon is attributed to oxygen starvation. Further studies indicated that burning rate increases with the decrease in separation parameter, which is defined by l/d_0, where l is the distance between two droplet centre and d_0 is the initial droplet diameter. Recently, the study performed by Mikami et al. [46] concluded that for both micro gravity and normal gravity, there are reductions in the burning time (increase in burning rate) as the separation parameter; l/d_0 is decreased from infinity (corresponding to isolated droplet combustion). For normal gravity results, as the separation distance is reduced, oxygen transport to the flame is enhanced due to natural convection around each droplet. However additional reduction in separation distance is resulted in oxygen starvation, which increases the burning time (decrease in burning rate) drastically. In the case of microgravity, the radiation heat gain at the droplet surface initially increases when l/d_0 is decreased from infinity resulting in the decrease in burning

time. Further decrease in l/d_0 creates the oxygen starvation effect and burning time increase dramatically. Explanation of such behavior of droplet burning rate for micro-gravity was provided by Okai et al. [51] in the experimental result of droplet near wall.

2.6. Multicomponent Fuel Droplet Combustion

Most of the fuels used in practical combustors are multi-component in nature. The processes involved in the burning of multicomponent fuel droplet are much more complex than single component fuel combustion which is mainly due to liquid phase mass transfer. The phase change characteristics of a multicomponent fuel depend on the extent of miscibility among its constituents. Several models for the multi-component fuel droplet combustion are being put forwarded by researchers. Distillation curve model, diffusion limit model and shell model are some of the important models for liquid phase mass transfer during multicomponent fuel droplet combustion. In diffusion limit model, liquid phase transport is considered to be due to the mass diffusion. It is generally assumed that there is no any internal circulation present inside the liquid phase. In contrast, liquid phase transport is considered to occur due to internal circulation in distillation curve model resulting in uniform distribution of fuel constituents inside the droplet. Hence, the species concentrations are assumed not to be varied spatially. The rapid mixing or distillation curve model of multi-component droplet burning was initially investigated by Faeth [14], and Law [36]. In 1976 Law [36] introduced the shell model assuming that single-component fuel vaporizes in each shell. By further simplifications he obtained the results which were closely approximated to the bulk vaporization behavior as described in the distillation curve model.

Law and Law [40] developed a model for asymptotic analysis on diffusion limited quasi-steady regime assuming the extremely slow rate of liquid phase mass diffusion. No changes in the temperature and mass fraction profile on the liquid phase were considered in their study. Their results predicted that the fraction of mass flux leaving the droplet surface for any species was equal to the initial liquid mass fraction of that species and d^2 law prevails during the burning of multicomponent fuel droplet combustion. Experimental results obtained for alchohal-alkane binary droplet combustion by them confirm the d^2 law behavior.

Results presented for 50% Undecane and 50% Octanol mixture is shown in Fig.2.1.
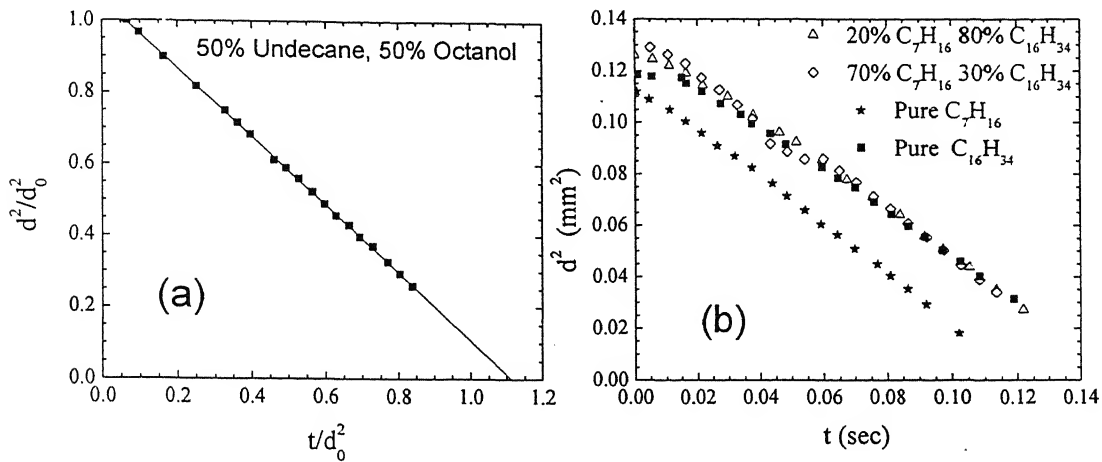
Fig. 2.1: Experimental results for **(a)** the existence of d^2 for multicomponent fuel droplet combustion by Law and Law [40], **(b)** temporal variation of the droplet diameter square with time for heptane/hexadecane droplet by Wang et al. [76].

Combustion and Micro-explosion studies on a freely falling multicomponent fuel droplets carried out by Wang et al. [76]. The combustion characteristics of isolated, low Reynolds number, multicomponent droplets falling in a hot, oxidizing gas flow were studied. Three staged combustion behavior were reported and the mass diffusion were reported as dominant liquid phase transport mechanism. It was concluded that, during multicomponent fuel droplet combustion there exists an initial period when the volatile components in the surface layer gets vaporized droplet temperature remain relatively cold. Followed by a transition period when droplet surface temperature increases rapidly. In this period the burning rate is extremely low, the size shrinks and the temperature diminishes. Finally a quasi-steady period sustains during which the droplet interior concentration distribution remains almost constant and the surface region is more concentrated with the less volatile component. The results of the heptane/hexadecane droplet combustion presented in their study are shown in Fig. 2.1 (b). The results for the micro-explosion of a multicomponent fuel droplet consisting 60% propanol, 30% hexadecane, and 10% surfactant during the transitional droplet heating period is shown in Fig. 2.2 (b). It may happen during burning of droplet when less volatile constituents are at outside and the more volatile constituents are at the center shells. Thus the more volatile components superheat and try to come outside fast due to extra pressure generated during superheat. This may start homogeneous nucleation,

whose extremely fast gasification rate may lead to sufficient pressure build up and thus the droplet may eventually fragment.
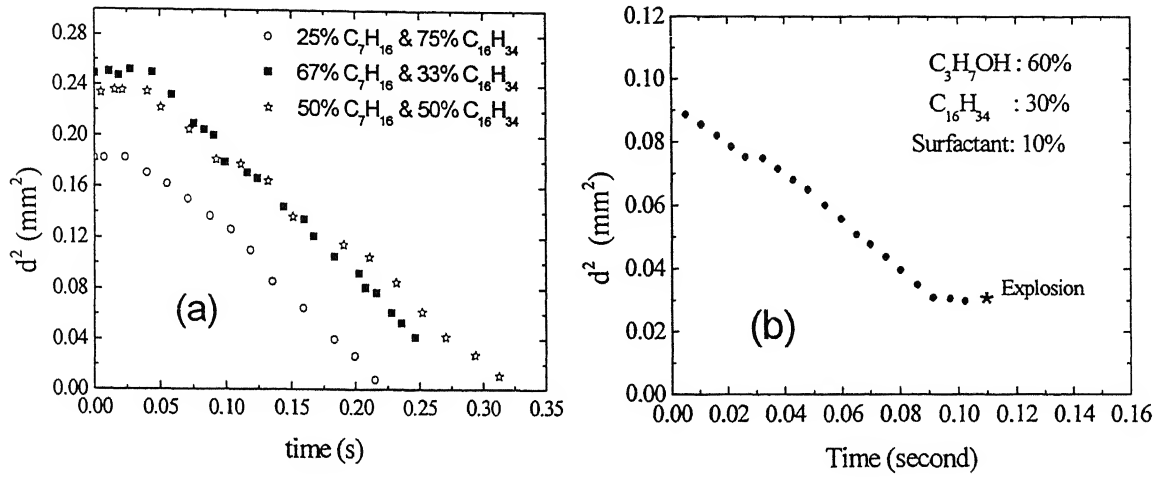
Fig. 2.2: Experimental measurement of the square of droplet diameter vs. time for **(a)** hexadecane/heptane droplet burning in 1 atm. air (Yang and Avedisian, [80]); **(b)** A droplet consisting of 60% propanol, 30% hexadecane, and 10% surfactant (C.H. Wang, X.Q. Liu and C.K.Law, [76]).

Tong and Sirignano [71] modeled the multicomponent transient droplet vaporization with internal circulation. The liquid phase internal circulation, transient droplet heating and species diffusion were taken care in their model.

In the study of the major controlling parameters in the gasification behavior of multicomponent droplets Makino and Law [41] in 1988 concluded that the liquid phase Lewis number is not the appropriate parameter to indicate the influence of liquid phase diffusional resistance on the droplet gasification behavior. However, it was found out that Peclet number, which is defined as the ratio of a reference surface regression rate to the liquid phase mass diffusivity, have a crucial role in controlling the gasification from the liquid fuel surface.

The experiment of unsupported hexane and hexadecane mixture under micro gravity was performed by Yang and Avedisian [80] using 1.2 s drop tower. Their results are plotted in Fig. 2.2 (a). Their data concluded that the evaluation of droplet diameter was similar to that of the classical d^2 law for a single droplet. In order to investigate the d^2 law behavior of multicomponent fuel droplet conclusion, Law and Law [40] concluded the similar nature of d^2 law.

To resolve the above anomalies between the results, predicting the nature of the burning history (d^2 law) for multicomponent fuel droplet, Shaw [66] extended this study of Law and Law [40]. His study on the multicomponent fuel droplet concluded that the droplet species profile change is slow relative to the change of droplet size. Hence, d^2 law surface regression closely followed. The mass flux fraction of a given species of the droplet surface is approximately equal to the volume averaged mass fraction of that species within the droplet. The ratio of the liquid phase species diffusion coefficient can be treated as a small parameter in contrast to the burning rate constant.

The evolution of liquid-phase mass fraction and temperature profiles during combustion of fuel droplets composed of binary miscible mixtures of low volatility and high volatility constituents was studied by Shaw and Williams [67]. They assumed the small initial mass fractions of low volatility material or slow introduction of low volatility material into the liquid phase by absorption from the gas phase. The gas phase was considered to remain quasi-steady and the liquid temperatures were considered to be spatially uniform. Their result shows that at the droplet surface a boundary layer was developed in which the mass fraction of the low volatility components were increases with time. Both the d^2 law and non-d^2 law behaviors of the droplet surface regression were discussed. Their study concluded that for small initial values of the initial impurity mass fraction, the surface regression approximately follows the d^2 law nature until the mass fraction of the impurity reaches near unity. Meanwhile, for sufficiently large values of the initial impurity, their numerical results demonstrated appreciable departures from the d^2 law behavior.

A fully transient numerical study for multicomponent liquid fuel droplet was carried out by Mawid and Agarwal [45]. This numerical result demonstrate that due to the process of fuel vapor accumulation within the inner region to the flame and to the high liquid-phase mass diffusional resistance, a situation is reached where the concentration of fuel vapor in the inner zone of the flame or in the immediate vicinity of the droplet surface exceeds that at the droplet surface for certain values of the liquid phase Lewis number. This result gives negative vaporization rate and no indication of flame extinction. Typical variation of d^2 with time for 50-50 heptane-decane mixture as reported by them is shown in fig. 2.3 (a).
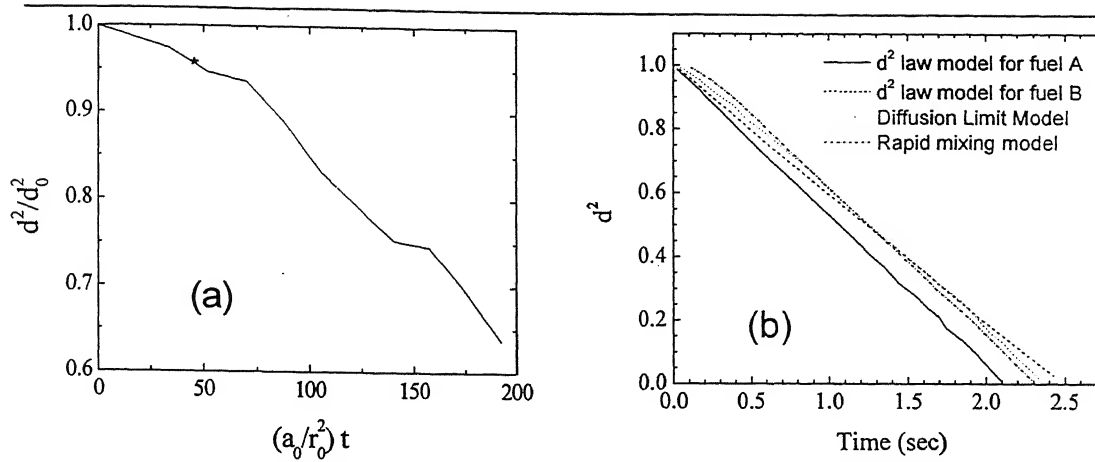
Fig. 2.3: **(a)** Temporal variation of the droplet radius squared for the base case. The asterisk indicates the time when suppression of vaporization occurs (Mawid and Aggarwal [45]). **(b)** Predicted square of the droplet diameter vs. time for d^2 law, distillation curve and diffusion limited model (Glassman [17]).

The results predicted by Glassman [17] are shown in Fig. 2.3 (b). The heat up period predicted by the rapid mixing model is longer since more heat is required to raise the temperature of the entire droplet (relative to the diffusion limit model).To study the effect of water concentration on flame luminosity and sooting tendency and disruptive burning, Jackson and Avedisian, [25] performed the experimental study of combustion of unsupported n-heptane droplets emulsified with water in microgravity. They concluded that the sooting is minimized for emulsions relative to pure heptane. A period was reported near the end of burning during which the droplet diameter is nearly constant, followed by disruptive burning events.

Mandal [42] studied the combustion behavior of single isolated multi component fuel droplet using finite element method. He used adaptive grid generation method and variable gas and liquid phase properties. A highly efficient semi-analytical model was also developed. Both the models exhibit three dominant period of droplet burning, two d^2-law periods separated by a transition period which exhibits a gradual change. In both the models, it was considered that the liquid phase mass transport occur only due to diffusion process and internal circulation, which is more likely to be occurred in the actual situation, was not considered..

Very recently in 2003, droplet evaporation study by using distillation curve model for kerosene fuel at normal and elevated pressure was performed by Burger et al. [6]. Their results were in good agreement to the diffusion limit model at different pressure.

2.6.1. Comparison of Results Available in Literature

In the earlier section the investigations on the multicomponent fuel droplet combustion available in the open literature were discussed extensively. This works can be categorized broadly into two groups such as (i) the experimental and numerical studies presented by Law and Law [40], Yang and Avedisian [80], and Shaw [66], those predicts the classical d^2 law and (ii) Wang et al. [76], Mawid and Aggarwal [45], those have reported the staged behavior of d^2 law. On the critical examination of the experimental data available in the literature, it was found out that there is large discrepancies exist in the data by various researchers even for the almost same composition of fuels. The variation of droplet diameter square with time reported by Wang et al. [76] and Yang and Avedisian [80] for heptane hexadecane mixture are compiled and plotted in Fig. 2.4 (a). It can be observed that the results presented by Wang et al. [76] exhibited non d^2 law behavior. In contrast the results of Yang & Avedisian [80] departed from the data of Wang et al. [76] and while retaining the classical d^2 law behavior.
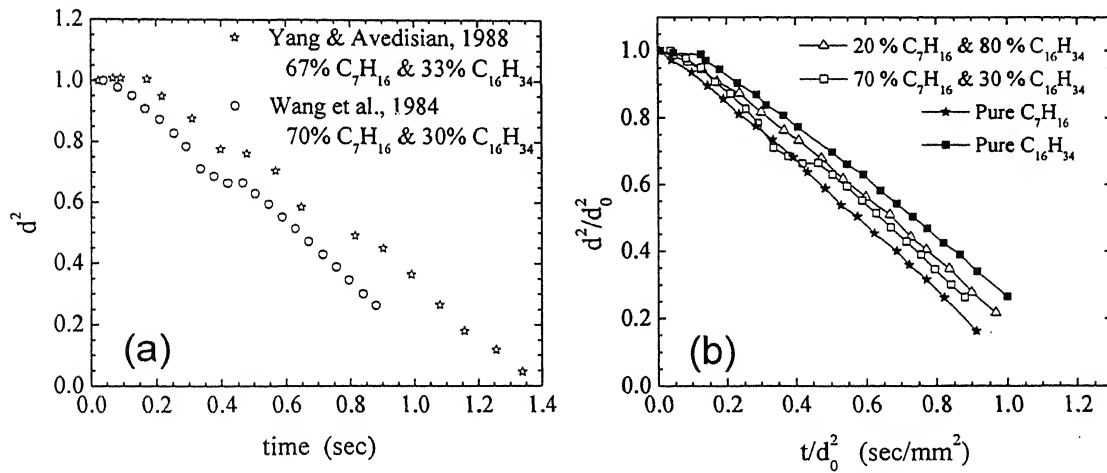
Fig. 2.4: Comparison of results: **(a)** The results predicted by Yang & Avedisian [80] and Wang et al. [76] for burning of heptane-hexadecane fuel mixture. **(b)** Results presented by Wang et al. [76].

It can be noted that Wang et al. [76] claimed the experimental data to follow staged d^2 law behavior. However it is conjectured that this changed in slope of diameter square with time may be due to experimental error. In order to asses their results critically all the data are compiled and presented in the standard normalized form (d^2/d_0^2 vs. t/d_0^2) in Fig. 2.4 (b). It can be observed that their data for

multicomponent fuel droplet combustion for two different compositions exhibit both the classical d^2 law and non d^2 law behavior. The diameter square change with time for multicomponent fuel droplet with composition of 20 % heptane and 80 % hexadecane follows the classical d^2 law. In contrast multicomponent fuel droplet with composition of 70 % heptane and 30 % hexadecane departs slightly from the classical d^2 law. However the results presented by Yang & Avedisian [80] for almost same composition of fuels depict d^2 law behavior.

2.7. Conclusions

The most important step in the study of droplet combustion was the development of the classical quasi-steady theory. Initial droplet combustion research efforts were directed towards ascertaining the validity of the classical quasi-steady theory. Though the d^2 law predicted by the classical theory can corroborate to the experimental data, but the flame stand off distance predicted by the classical quasi-steady theory departs substantially from that of the experimental data. The addition of radiation heat transfer effects in the theoretical model predicts the flame stand off ratio reasonably. Although several radiation heat transfer models have been developed the droplet burning rate, but several discrepancies exists in the literatures which needs to be addressed. Recently the experimental data reported by Xu et al. [79] revealed an interesting feature of opposite influence of the initial diameter to the burning rate constant particularly at high temperature. And this behavior of droplet burning has not been investigated numerically to best of our knowledge. Beside this, the effect of ambient oxygen concentration on the single component fuel droplet combustion has not been addressed adequately, which will be investigated in detail in the present thesis.

Several numerical and experimental studies on the multicomponent fuel droplet combustion have been reviewed in the present chapter. It was found out that three major models such as distillation curve model, diffusion limit model and shell model for liquid phase mass transport have been put forwarded by the researchers. It seems that the results of distillation curve model in comparison to the other model are closer to the experimental data. Hence, there is a need to develop a better model for multicomponent fuel droplet combustion. The surface parameters during multicomponent fuel droplet combustion are very important to study.

Chapter 3

EXPERIMENTAL STUDIES

3.1. Introduction

In order to study the droplet combustion, an experimental setup has been deigned and developed from the scratch in the lab. It can withstand maximum pressure of 5 MPa. The design calculation was done with the help of ASME Boiler and Pressure Vessel Design Code [3]. In this case the factor of safety of 3 is employed. Stainless steel is chosen as material for combustion chamber. The detailed description of the experimental setup and the experimental results are discussed below.

3.2. Experimental Setup:
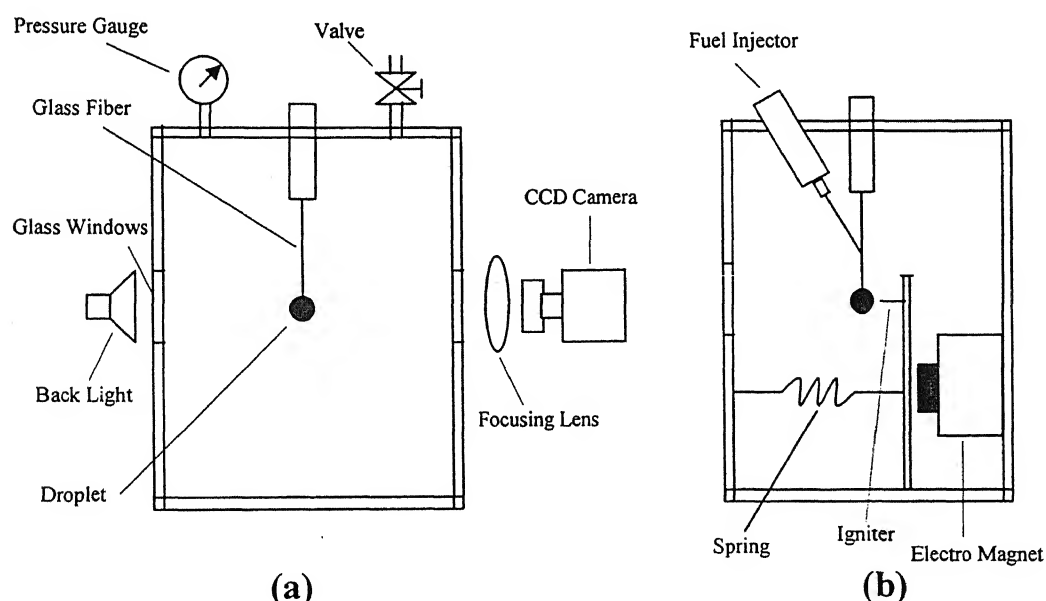
Fig. 3.1: Schematic of the experimental setup (a) Front view (b) Side view.

Two orthogonal views (Front and Side view) of experimental setup used for the present study are shown schematically in Fig. 3.1. The stainless steel box of dimension, 160 mm×160 mm×180 mm is used as a combustion chamber. All the walls of the combustion chamber are welded except the top wall, which is fixed by nut and bolt. The three side walls of the combustion chamber are equipped with circular glass windows in such a way that the droplet remains along the optical axis

of these windows during experimentation. A glass fiber of diameter 0.16 mm is used to suspend the droplet. This fiber is attached to the top wall with a specially designed holder. In order to hold a droplet at the tip of the glass fiber a bid of 0.2 mm diameter is used for the present experiments. Care is taken during the combustion process such that the droplet remains at the center of the chamber. Fuel droplet is generated by using a specially designed fuel delivery system, which consists of a hypodermic tube and piston cylinder assembly. Resistance type igniter is designed and developed in the lab for igniting the droplet. The igniter is retracted just after the ignition by an electro magnet. The igniter and the electro magnet is control through an electrically control timer circuit and a relay as shown in Fig. 3.2. A 12 V DC power supply is used both for the igniter and electro magnet. The droplet diameter change during the burning is visualized by using shadowgraph. A backlight is used behind the droplet. The flame shape and the droplet diameter change during the combustion are recorded through a microscopic lens of 100 mm focal length and a 24 frame per second Hi 8 CCD camera. The droplet burning is recorded as a movie and extracted to the frames using a computer. There it can be analyzed frame by frame using image processing technique. The time between consecutive frames is constant, which 1/fps. The diameter of the droplet is calculated with respect to the support fiber.
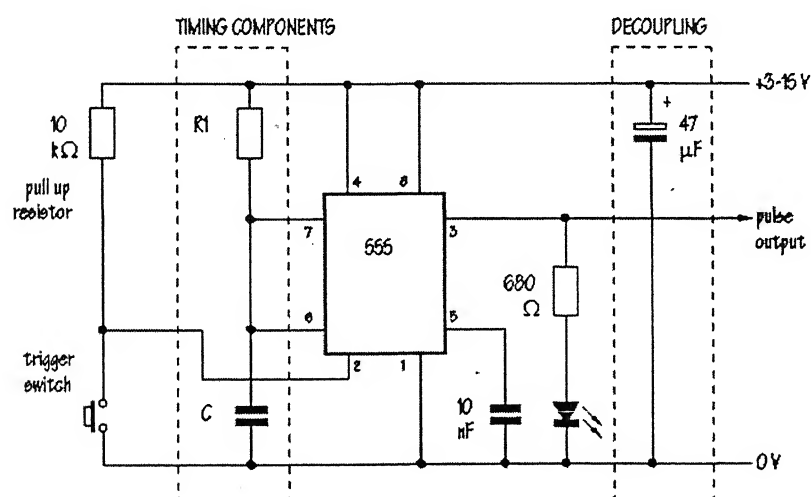
Fig. 3.2: Timer circuit

3.3. Experimental Procedures:

The experimental procedures are discussed in this section:

i)   The fuel is injected to the droplet holder for making a droplet at the tip of the droplet holder.

ii)   The shadowgraph system is made operational for the experiments.

iii)   The CCD video camera is focused on the droplet by using the microscopic lens.

iv)   The recording of the droplet photograph is initiated.

v)   The ignition system is switched on by triggering the ignition circuit.

vi)   The burning history of the fuel droplet is recorded till its end in video format.

vii)   The frames are extracted from the video images by using image processing software.

viii) These photographs of flame and droplet surfaces are modified to the gray scale images of 256 steps (0-255) in brightness.

ix)   The flame and droplet boundaries are obtained by examining the contrast level of the pixels by using edge detection technique.

x)   The droplet diameter and the flame boundaries are analyzed.

xi)   As at the starting of the combustion there is the igniter, the droplet burning is being affected due to this. Hence the initial images have been removed and not considered in the diameter regression and flame analysis.

3.4. Results and Discussions :

The photograph of flame and the droplet during the combustion of n-heptane with initial diameter of 0.82 mm and n-Decane with initial diameter of 1.0 mm are shown in Fig. 3.3 and 3.4 respectively. It can be noted that the experiments is conducted under normal gravity conditions. Hence, the hot combustion products are moved in upward direction due to natural convection resulting in an oval flame shape as shown below. The upper part of the flame for both the case of n-Heptane and n-Decane burning is very luminous as compared to the lower part. The yellow color of the flame can be due to the presence of soot particles. Below this zone there is a small zone of reddish color which may arises due to radiation from CO_2 and

water vapor. The lower most portion of the flame is observed to be blue due to complete combustion in the presence of sufficient oxygen level. As a result the maximum temperature is likely to occur in this zone.
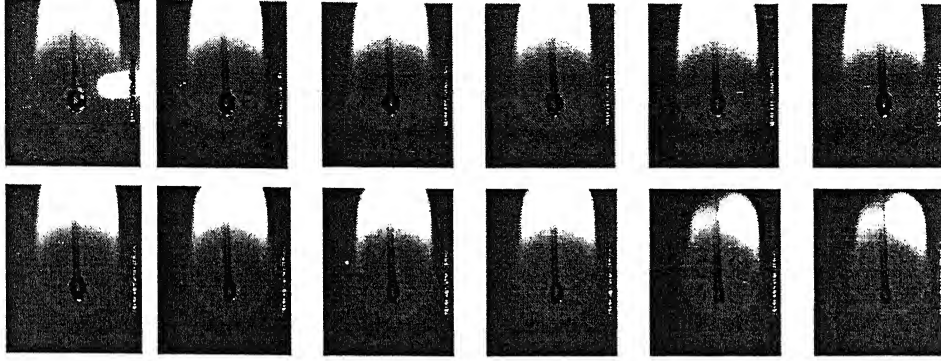
Fig. 3.3: Burning history of n-Heptane droplet of diameter 0.82 mm
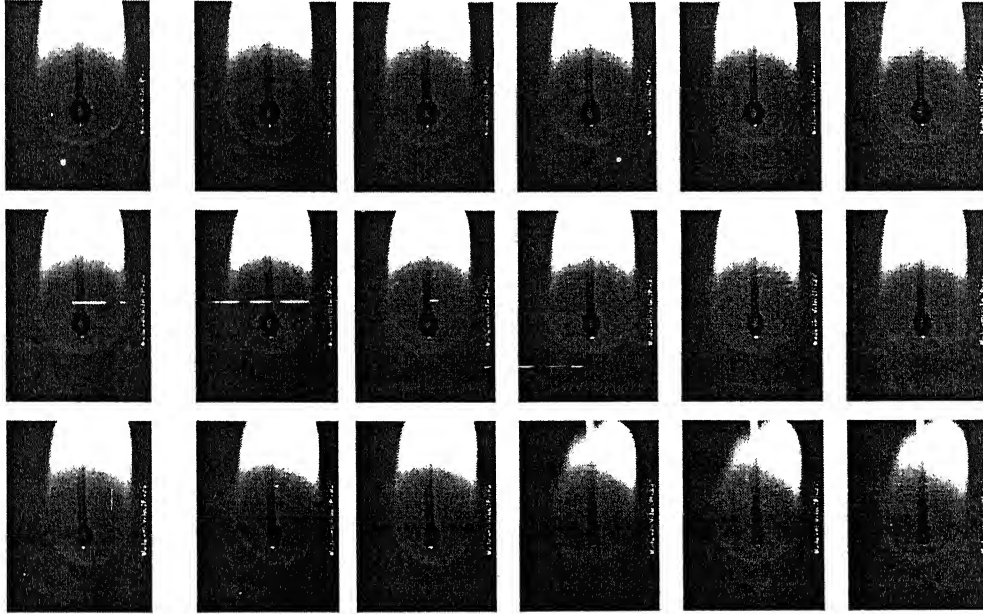
Fig. 3.4: Burning history of n-Decane droplet of diameter 1.0 mm

Due to buoyancy and the surface tension of the fuel and the support fiber, the droplet is not spherical. It is like as shown in Fig.3.5. The droplet diameter is approximated by equivalent volume diameter of the droplet as stated by Kumagai and et al. [31]. If the major axis diameter is a and the minor axis is b, then the equivalent diameter is $d = \sqrt[3]{ab^2}$. The schematic representation of the flame envelop during droplet burning is shown in Fig. 3.5. The bottom edge of the flame envelop from the center of the droplet along its radius is represented by h_1 as shown in Fig.

3.5. Since the droplet flame envelop is non spherical in geometry due to the natural convection, another dimension needs to be defined for characterization of the flame shape (Kumagai et al. [31]). For the present case the side edge of the flame envelop from the droplet center along the radius is represented by h_2 as shown in Fig. 3.5. Digitally captured photographs of flame and droplet surfaces were modified to the gray scale images of 256 steps (0-255) in brightness. The flame and droplet boundaries are obtained by examining the contrast level of the pixels by using edge detection technique.
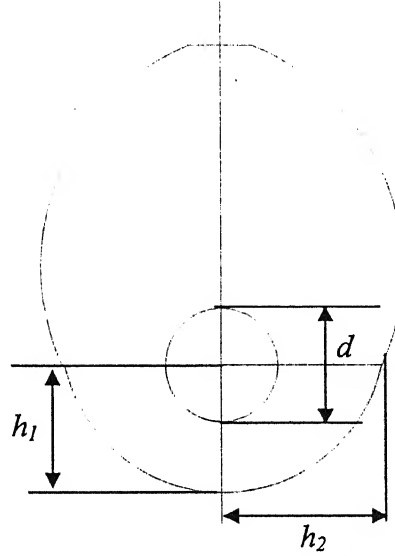
Fig. 3.5: Schematic presentation of droplet burning.

As per classical theory of droplet combustion the droplet diameter square difference, $\left(d_0^2 - d^2\right)$ is proportional to burning time. The normalized diameter square, d^2/d_0^2 is plotted against the normalized time, t/d_0^2 in Fig. 3.6 for n-Heptane droplet burning of initial droplet diameter 0.82 mm. It can be observed from the Fig. 3.6 that droplet diameter decreases with time as per the d^2 law of Classical theory. The slop of the curve d^2/d_0^2 vs. t/d_0^2 known as the burning rate constant, K_b, become almost constant in this case which is equal to 1.12 with the experimental error is within 4 %. However, the value of K_b obtained from the experimental data of Kumagai & Isoda [29] for n-Heptane droplet burning of diameter 1.3 mm at normal gravity is approximately equal to 1.04. This small difference may be due to use of different initial droplet diameter. For bigger size droplet the radiation loss becomes more predominant and is resulted in decrease in the burning rate constant.
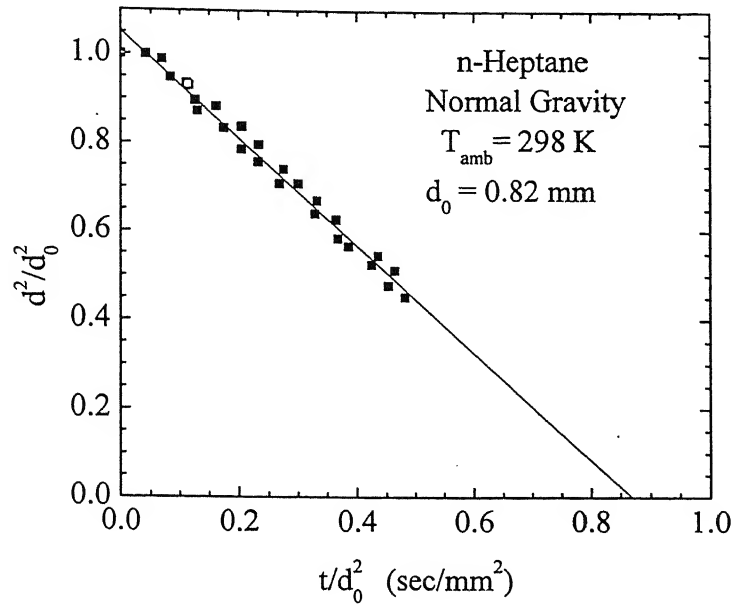
Fig. 3.6: Variation of normalized droplet diameter square with normalized time for burning of n-heptane fuel droplet of diameter 0.82 mm.
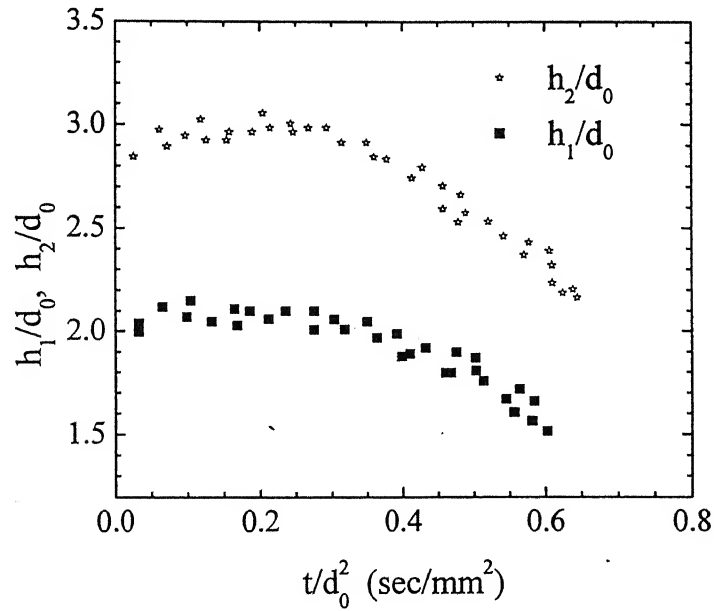
Fig. 3.7: Variation of normalized flame boundaries with normalized time for burning of n-heptane fuel droplet of diameter 0.82 mm.

The flame boundaries, h_1/d_0, h_2/d_0, obtained from digitally captured as described in previous section are also plotted in Fig.3.7. It can be observed that the flame boundary initially increases with time and subsequently decreases with the

droplet diameter. This may be due to fact that fuel gets vaporized in the beginning with the initial ignition energy. Subsequently it diffuses outwardly and comes in contact with the ambient oxygen at stoichiometric ratio leading to the formation of the flame surface at a shorter distance from the surface. As the burning of the droplet continues further, flame surface moves outwardly in search of requisite oxygen for complete burning. The flame boundaries continue to move outwardly till a threshold flame radius beyond which sufficient oxygen is available for complete combustion. After this the flame radius starts decreasing with the reduction in droplet diameter.
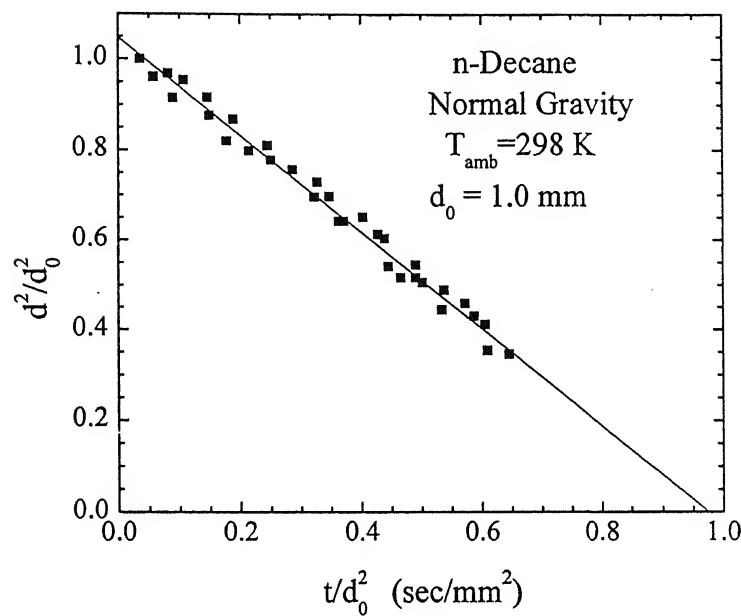
Fig. 3.8: Variation of normalized droplet diameter square with normalized time for burning of n-decane fuel droplet of diameter 1.0 mm.

Normalized droplet diameter square and the flame boundaries are plotted in Fig. 3.8 and 3.9 respectively for combustion of n-Decane fuel droplet of initial diameter 1.0 mm. The experimental uncertainty lies within 5 % in this case. The burning time for n-Decane fuel droplet is found to be more as compared to n-Heptane fuel droplet. This difference in burning time may be attributed to the lower volatility of n-Decane. Interestingly the flame of heptane fuel droplet is established at a smaller distance from the droplet surface as compared to that of the decane. This phenomenon can also be explained in terms of the gasification rate. As it is already known the gasification rate is higher in case of heptane fuel due to its low

boiling point temperature. The more amount of fuel vapor is likely to be released from the droplet surface which spreads for longer distance to get consumed by the oxygen. Hence, the flame surface for n-Heptane is located at a larger distance from its center as compared to the n-Decane.
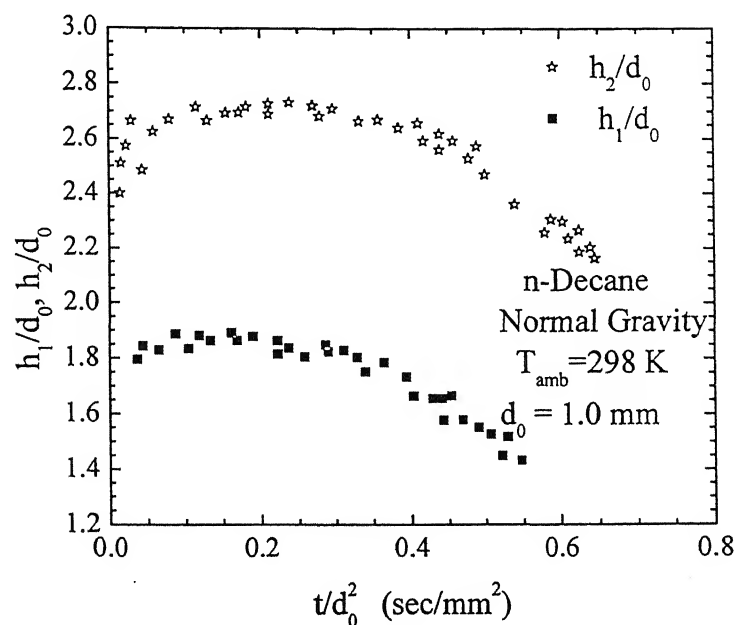
Fig. 3.9: Variation of normalized flame boundaries with normalized time for burning of n-decane fuel droplet of diameter 1.0 mm.
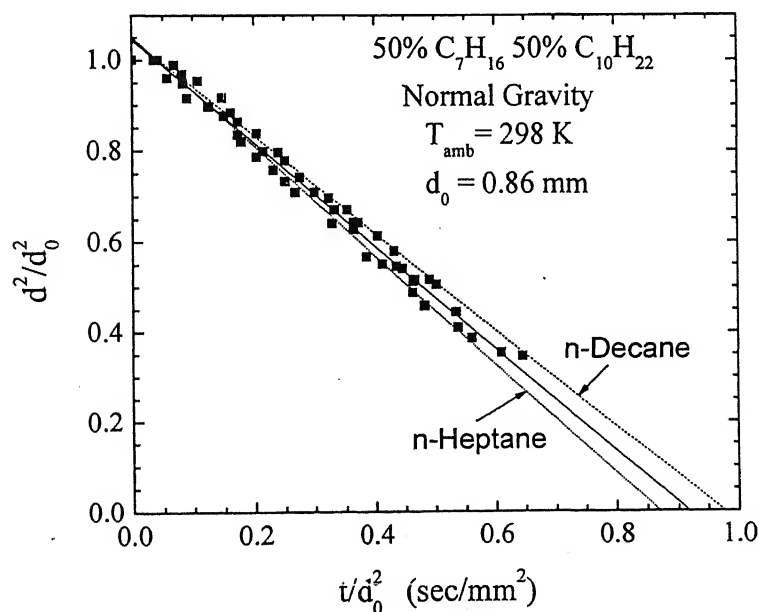
Fig. 3.10: Variation of normalized droplet diameter square with normalized time for burning of 50 % 50% n-heptane n-decane mixture droplet of diameter 0.86 mm.
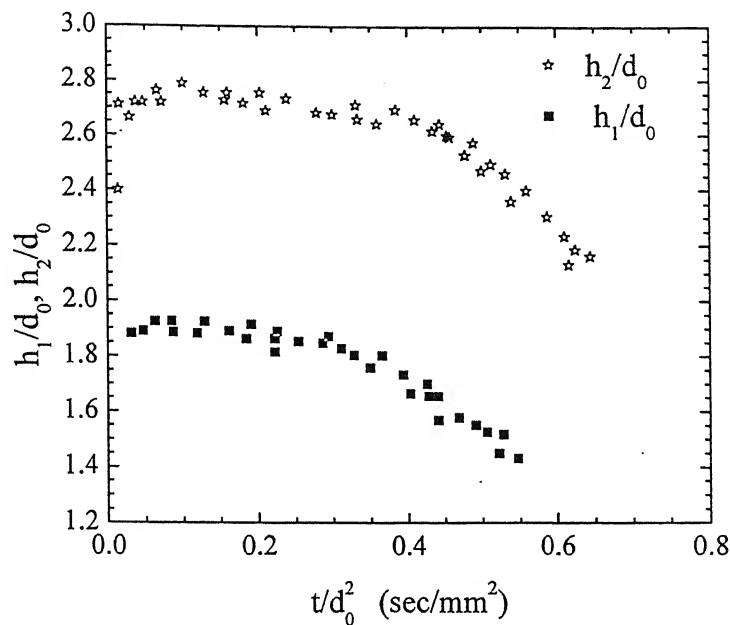
Fig. 3.11: Variation normalized flame boundaries with normalized time for burning of 50 % 50% n-heptane n-decane mixture droplet of diameter 0.86 mm.

An attempt is taken to study the multicomponent fuel droplet combustion. A fuel mixture of 50% n-Heptane and 50% n-Decane is taken. The normalized droplet diameter square and the flame boundaries for combustion of 50 % -50 % n-heptane and n-Decane mixture droplet of diameter 0.86 mm are respectively plotted in Fig. 3.10-11. The results found out here qualitatively similar to the results of Wang et al. [76]. The stepped d^2 law found out in the case of 70% heptane and 30% hexadecane may be due to some numerical error. The d^2-law behavior of burning is observed here. The burning rate constant is found to be almost equal to 1.1 with the experimental error is within 5%. This is in between the burning rate constant for single n-Heptane and n-Decane burning. The droplet boundaries are also in between the droplet boundaries found out for these two single pure fuel burnings.

3.5. Conclusions

The experimental studies on single and multicomponent fuel droplet combustion are carried out under normal gravity conditions at normal pressure and temperature. The droplet diameter regression for both single component and multicomponent fuel burning follow the d^2 law behavior. Flame boundaries are first increase and subsequently decreases with time. The slope of the d^2 law curve known as burning rate constant, K_b, are almost constant for droplet burning. For n-Heptane and n-Decane droplet burning under normal gravity the burning rate constant are found to be 1.12 and 1.03. In the case of multicomponent fuel, composed with 50% heptane and 50% decane, droplet combustion the burning rate constant lies in between the burning rate constants of the two fuel droplet combustion.

Chapter 4

MATHEMETICAL MODELING

4.1. Problem Definition

In the present chapter, the mathematical modeling of droplet combustion is described. The schematic of the model for single isolated fuel droplet is shown in Fig. 4.1. In this case, droplet is burning in a hot, stagnant ambience with the assumption of spherical symmetry, which is possible only when there is no buoyancy force due to gravity. Here the burning is considered to be initiated by creating a spherically symmetric high temperature zone around the droplet. Due to high temperature around the droplet, the vaporization is started from the surface of droplet. Subsequently fuel vapor gets transported by diffusion process and comes in contact with the ambient oxygen. Since the gas phase is at high temperature, exothermic reactions take place where the fuel vapor and oxidizer meets at their stoichiometric ratio. And this zone is defined as flame, which is located at *flame stand off distance* (r_f) from the droplet surface as shown in Fig. 4.1. Both the heat and the products from this flame zone are transferred to the either sides due to heat and mass transfer. The heat transferred from the flame surface causes the droplet to vaporize further. For modeling of the droplet combustion one dimension, unsteady governing equations such as mass, momentum, energy and species equations are considered with the following assumptions.
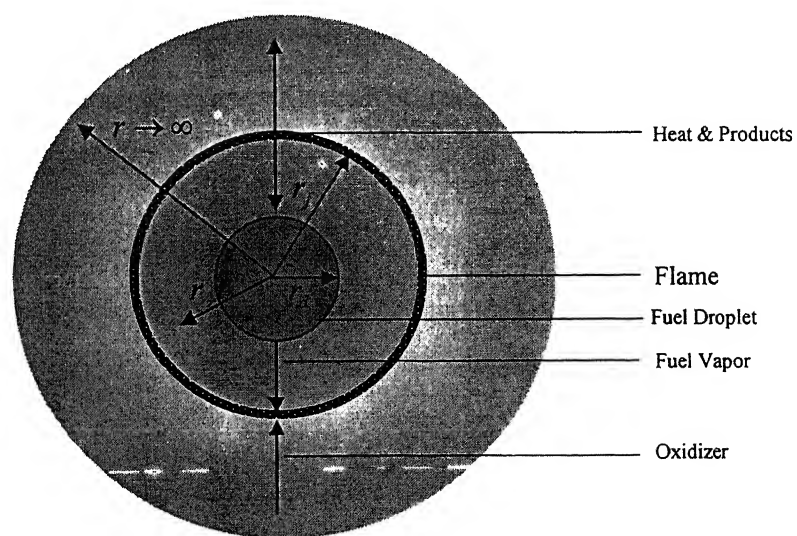
Fig. 4.1: Schematic of a single isolated liquid droplet burning in an infinite oxidizing medium.

Assumptions

i) The droplet is stationary in the quiescent atmosphere.

ii) The droplet combustion process is considered to be spherically symmetric during whole burning period. This assumption is more appropriate only when burning takes place under micro-gravity conditions.

iii) One dimensional unsteady inviscid flow.

iv) The pressure is assumed to be constant, so that the momentum equations need not to be solved.

v) Dufour-Soret effects and viscous effects are considered to be negligible.

vi) The combustion is modeled using single step *Arrhenius* second order reaction for simplicity.

vii) Soot radiation is neglected.

In the present model variable thermodynamic and transport properties are employed to achieve the realistic prediction. A simple gray gas radiation model is considered for gas phase radiation.

4.2. Liquid Phase Conservation Equations

4.2.1. Energy Equation

The droplet is heated only by the heat supplied from the flame surface. As the interior temperature of the liquid droplet is low, the radiation from the liquid phase can be neglected. Liquid phase velocity v_r is also very low as compared to the gas phase velocity. Hence it can be neglected. Considering above points the energy equation for the liquid phase becomes

$$\frac{\partial T_l}{\partial t} = \frac{1}{r^2 \rho_l C_{P,l}} \frac{\partial}{\partial r}\left(\lambda_l r^2 \frac{\partial T_l}{\partial r} \right) \tag{4.1}$$

Where, ρ_l, λ_l, $C_{P,l}$ are liquid phase density, heat conductivity and specific heat respectively. T_l is the liquid phase temperature.

4.2.2. Liquid Phase Species Equation

For single component fuel droplet combustion gas phase solubility is negligible at low pressure. Hence, there is no need to solve species equation for the liquid phase. However, the species equations are to be solved for multicomponent fuel droplet combustion. Several models are reported in literature for multicomponent fuel droplet combustion. In Diffusion Limit model, the liquid phase mass transfer is occurring only due to the molecular diffusion. The governing equation for this model is as follows;

$$\rho_l \frac{\partial Y_{l,i}}{\partial t} = \frac{1}{r^2} \frac{\partial}{\partial r} \left(r^2 \rho_l D_{l,i} \frac{\partial Y_{l,i}}{\partial r} \right)$$ (4.2)

where, $Y_{l,i}$ is the mass fraction of ith species in liquid phase. $D_{l,i}$ is the liquid phase mass diffusivity of ith species in liquid mixture.

During the combustion of multicomponent fuel droplet, the high volatile fuel as compared to the other constituent fuels vaporizes at a faster rate from the outer shell of the droplet. As a result the scarcity of high volatile substance is likely to be occurred at the outer shell. This high volatile fuel vapor can not be transported from the inner shell only due to diffusion process. Hence, only the low volatile fuel is likely to be present in the outer shell. In contrast both the high and low volatile fuels are present in the inner shell. Then there is a chance that high volatile component fuel gets superheated due to transfer of heat into the core region of the droplet. As a result high pressure can be generated in the core region due to vaporization at high pressure, leading to formation of internal circulation inside the droplet. This internal fuel circulation can create uniformly distributed species concentration over the spatial domain of the liquid droplet. This kind of model is known as Distillation Curve Model, which is described as follows;

$$\left(\frac{4}{3} \pi r_d^3 \rho_{l,i} Y_{l,i} \right)_{j+1} = \left(\frac{4}{3} \pi r_d^3 \rho_{l,i} Y_{l,i} \right)_j - \left(4\pi r_d^2 \dot{r}_d \Delta t \rho_{l,i} \varepsilon_i \right)_j$$ (4.3)

here, r_d is the droplet radius. ε_i is the fractional mass gasification rate for species i, which is defined as,

$$\varepsilon_i = \left(\frac{\dot{Y}_{l,i}}{\sum_i \dot{Y}_{l,i}} \right)_{r = r_d}$$ (4.4)

The first term in the Eqn. 4.3 denotes the total mass of the fuel at $(j+1)^{th}$ time step, which is equal to the remaining mass of the fuel at the jth time step after vaporization of the fuel from its surface.

4.3. Gas Phase Conservation Equations

4.3.1. Mass Conservation

The mass conservation equation for gas phase is given below;

$$\frac{\partial \rho_g}{\partial t} + \frac{1}{r^2}\frac{\partial}{\partial r}(\rho_g r^2 v_g) = 0 \tag{4.5}$$

where, ρ_g is the gas phase density, v_g is the gas phase radial velocity.

3.3.2. Species Conservation Equation

The gas phase species equation is,

$$\rho\left(\frac{\partial Y_{g,i}}{\partial t} + v_g\frac{\partial Y_{g,i}}{\partial r}\right) = \frac{1}{r^2}\frac{\partial}{\partial r}\left(r^2 \rho_g D_{g,i}\frac{\partial Y_{g,i}}{\partial r}\right) + \dot{\omega}_{g,i} \tag{4.6}$$

here, $Y_{g,i}$ is the ith species in the gas phase. $\dot{\omega}_{g,i}$ is the generation of ith species due to reaction. $D_{g,i}$ is the gas phase diffusional coefficient of species i.

4.3.3. Energy Conservation Equation

Considering heat generation due to exothermic reaction, heat conduction, radial convection and gas phase radiation of heat, the energy conservation equation for gas phase becomes;

$$\rho_g C_{P,g}\left(\frac{\partial T_g}{\partial t} + v_g\frac{\partial T_g}{\partial r}\right) = \frac{1}{r^2}\frac{\partial}{\partial r}\left(\lambda_g r^2\frac{\partial T_g}{\partial r}\right) - \sum_{i=1}^{N}\dot{\omega}_{g,i}\,\Delta h^0_{f,i} - \nabla\cdot q_R \tag{4.7}$$

Here, $C_{P,g}$, λ_g are the specific heat and heat conductivity of the gas phase mixture. $\Delta h^0_{f,i}$, $\nabla\cdot q_R$ are the enthalpy of formation for i^{th} species and radiation term respectively.

$$\nabla\cdot q_R = \frac{1}{r^2}\frac{\partial}{\partial r}(r^2 q_R) \tag{4.8}$$

4.3.4. Equation of State

Considering ideal gas, the pressure, temperature, density and mass fraction can be related using the equation of state as given below;

$$p = \rho R_u T \sum_{i=1}^{N} \frac{Y_i}{M_i}$$

$$\rho = \frac{p}{R_u T \sum_{i=1}^{N} \frac{Y_i}{M_i}} \tag{4.9}$$

4.4. Reaction Modeling

During the actual combustion process, several intermediate species are participated in the large number of chemical reactions. Some reaction occurs at very first rate, some very slowly. The generalized chemical reaction of arbitrary complexity can be represented by the following stoichiometric equation given below;

$$\sum_{i=1}^{N} v_i' M_i = \sum_{i=1}^{N} v_i'' M_i \tag{4.10}$$

where, v_i' is the stoichiometric coefficient of the ith reactant, v_i'' is the stoichiometric coefficient of the ith product, M is the molecular weight of all chemical species, and N is the total number of components involved. Then the reaction rate, RR can be expressed as

$$RR = k \prod_{i=1}^{N} (C_{M_i})^{v_i'} \tag{4.11}$$

where, k is the proportionality constant called the *specific reaction rate constant*. For a given chemical reaction, k is independent of the concentrations, C_{M_i} and depends only on the temperature. The value of k can be determined using *Arrhenius Law*, which is expressed as;

$$k = A \exp\left(-\frac{E_a}{R_u T}\right) \tag{4.12}$$

Here, A is pre-exponential factor representing the collision frequency and E_a is the activation energy.

$$\dot{\omega} = k(Y_{f_1})^m (Y_{O_2})^n \tag{4.13}$$

In the study of single component fuel droplet combustion, a single step global chemistry model for n-Heptane-air is considered as follows;

$$C_7H_{16} + 11O_2 = 7CO_2 + 8H_2O \qquad (4.14)$$
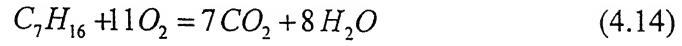
However, for multicomponent fuel droplet combustion, two single step kinetics of n-Heptane and n-Decane are used as given below.

$$C_7H_{16} + 11O_2 = 7CO_2 + 8H_2O$$
$$C_{10}H_{22} + 15.5O_2 = 10CO_2 + 11H_2O \qquad (4.15)$$
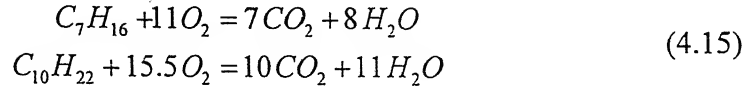
For finding out the reaction rates of the above reactions, the values of A, δ, E_a, m and n are taken from Turns [73].

4.5. Initial Conditions

The selections of proper initial conditions are of paramount importance in making the numerical process stable. High gradients in the temperature and species profile may lead to numerical instability. Hence, suitable initial temperature, oxygen and fuel species profiles are chosen (Saitoh and Nagano [61]). Initial profiles with the transformed coordinate system are shown in Fig. 4.2 and 4.3. Far away from the droplet (at infinity), standard ambient conditions, with standard air composition, has been used. At ambient $T_0 = 298.15$ K with ambient mass fraction values of O_2, CO_2, H_2O taken as 0.232, 0.00045 and 0.0188 respectively.

At time, $t = 0$:

$$T_{g,0} = fn(r), \quad T_{l,0} = fn(r), \quad Y_{g,f} = fn(r), \quad Y_{g,O_2} = fn(r)$$

$$Y_{g,CO_2} = 0.00045, \quad Y_{g,H_2O} = 0.0188, \quad Y_{l,f} = Y_{l,f,0} \qquad (4.16)$$

4.6. Boundary Conditions

4.6.1. At Droplet Center ($r=0$)

Due to symmetry at the droplet centre, the temperature and species concentration gradients are zero. Hence, the boundary conditions can be written as

$$\frac{\partial Y_{l,j}}{\partial r} = 0$$
$$\frac{\partial T}{\partial r} = 0 \qquad (4.17)$$

4.6.2. At Droplet Surface ($r=r_d$)

Mass Balance: At the droplet surface the liquid fuel gets vaporized into gas satisfying the mass conservation as stated below;

$$\rho_g v_g = -\rho_l v_l = -\rho_l \frac{\partial r_d}{\partial t} \tag{4.18}$$

Species Balance: In both of the phases, species are transported due to both convection and diffusion. Therefore, species flux is governed by;

$$\rho_g D_{g,i} \left. \frac{\partial Y_{g,i}}{\partial r} \right|_{r=r_d} = \rho_g v_g Y_{g,i,r=r_d} \qquad i = O_2, CO_2, H_2O \tag{4.19}$$

$$-\rho_g D_{g,f} \left. \frac{\partial Y_{g,f}}{\partial r} \right|_{r=r_d} = \rho_g v_g (\varepsilon_f - Y_{g,f,r=r_d}) \quad f = f_1, f_2 \tag{4.20}$$

$$-\rho_l D_{l,f} \left. \frac{\partial Y_{l,f}}{\partial r} \right|_{r=r_d} = \rho_l v_l (\varepsilon_f - Y_{l,f,r=r_d}) \quad f = f_1, f_2 \tag{4.21}$$

Energy Balance: At droplet surface certain amount of heat from the gas phase is transported to the liquid droplet. The heat balance equation at the liquid-gas phase interface can be written as,

$$\lambda_g \frac{\partial T_g}{\partial r} = \lambda_l \frac{\partial T_l}{\partial r} - \rho_l \frac{\partial r_d}{\partial t} \sum_{i=1}^{N} \varepsilon_i L_i + q_R \tag{4.22}$$

The first term is pertaining to heat transfer due gas phase conduction; second term represents heat absorption by the liquid due to heat conduction. While the third term represents the latent heat of vaporization. The forth term is associated with the radiation.

Phase Equilibrium at Liquid Vapor Interface: The phase equilibrium at the liquid vapor interface of the droplet surface is governed by the Clausius Clapeyron's equation and the Roult's Law as stated below [54];

$$X_{i,d}(T_d) = \frac{1}{P} \exp \left\{ \frac{L_i M_i}{R_u} \left(\frac{1}{T_{b,i}} - \frac{1}{T_S} \right) \right\} \tag{4.23}$$

Here, T_S is the surface temperature, $T_{b,i}$ is the boiling point temperature evaluated at the normal atmospheric pressure, P is the prevailing system pressure in bar and M_i and L_i are the molecular weight and latent heat of vaporization

respectively for the ith species, and R_u is the universal gas constant. It can be noted that the above expression for phase equilibrium at liquid vapor interface is only valid for ideal gas case. Hence, it cannot be used for combustion process at high pressure.

4.6.3. At Infinity ($r=\infty$)

At the ambient, the temperature or species profiles are not affected by the droplet burning. Hence at the ambient, the temperature and species profile remain constant throughout the burning process, which is expressed as;

$$
\begin{aligned}
T &= T_\infty \\
Y_{g,f} &= 0 \\
Y_{g,i} &= Y_{i,\infty}
\end{aligned}
\tag{4.24}
$$

4.7. Non-dimensionalization and Co-ordinate Transformation

4.7.1. Non-dimensionalization

The droplet surface regresses with the burning of fuel droplet, which creates additional complexities in the modeling. In order to overcome this complexities co-ordinate trans-formation is required. The governing equations are non-dimensionalized by using the following non-dimensional terms;

$$
r^* = \frac{r}{R_0}, \qquad r_d^* = \frac{r_d}{R_0}, \qquad t^* = \frac{a_0 t}{R_0^2}, \qquad (T_l^*, T_g^*) = \left(\frac{C_{P,0}\alpha_f}{\Delta h_{C0}}\right)(T_l, T_g),
$$

$$
v^* = \frac{R_0 v}{a_0}, \qquad \Theta = \frac{E}{R_u}\frac{C_{P,0}\alpha_f}{\Delta h_{C,0}}, \qquad q_R^* = \frac{R_0 q_R}{a_0 \rho_l \sum_{i=1}^{N} \varepsilon_i L_i}, \qquad Y_i^* = \alpha_i Y_i \tag{4.25}
$$

where, the co-efficient, α_i is known as absorptivity and can be defined as follows:

$$
\alpha_i = -\frac{M}{(v_i^{''} - v_i^{'})M_i} \quad \text{and} \quad M = \sum_{i=1}^{N} v_i^{'} M_i = \sum_{i=1}^{N} v_i^{''} M_i \tag{4.26}
$$

All thermo-physical properties are non-dimensionalized by their reference value taken at the ambient condition. The non-dimensionalized expressions are;

$$a^* = \frac{a}{a_0}, \qquad D_i^* = \frac{D_i}{D_{i,0}}, \qquad \rho^* = \frac{\rho}{\rho_0}, \qquad C_P^* = \frac{C_P}{C_{P,0}}, \qquad \lambda^* = \frac{\lambda}{\lambda_0} \qquad (4.27)$$

The a_0 and $D_{i,0}$ are further non-dimensionalized with the Lewis No. of the species i, $Le_{i,0}$

$$Le_{i,0} = \frac{a_0}{D_{i,0}} \qquad (4.28)$$

The asterisk (*) mark indicates the non-dimensional quantities.

4.7.2. Co-ordinate Transformation

In order to overcome the problem of moving boundary at the droplet surface it is convenient to transform the moving boundary to a fixed boundary. In liquid phase the gradients do not vary much over the spatial domain, however, for gas phase the gradients are found to be quite high between the droplet surface and the flame. Hence, to compute efficiently, very fine grids are to be provided within this zone. On the other hand the gradients of dependent variables are found to be low between the flame and the ambient. Hence, course grid should be used to save computational time. To overcome these difficulties the co-ordinate transformations are adopted from the work of Saitoh and Nagano [61].

For liquid phase the following transformation is employed;

$$x = \frac{r}{r_d} = \frac{r^*}{r_d^*} \qquad (4.29)$$

Note that, the above transformation converts the liquid region to a fixed domain from $x = 0$ (at the droplet centre) to $x = 1$ (at the droplet surface).

For the gas phase, the following transformation is used.

$$\eta = \ln\left(\frac{r}{r_d}\right) = \ln\left(\frac{r^*}{r_d^*}\right) \qquad (4.30)$$

This transformation converts the gas phase to a fixed domain. At the droplet surface, $\eta = 0$ and $\eta = 5$ is considered at far distance ($r \rightarrow \infty$) from the center of the droplet. With this transformation the grid become finer between droplet surface and the flame and coarser beyond the flame region.

4.7.3. Transformed and Non-dimensionalized Governing Equations

i) *Non dimensional energy equation in liquid phase:*

The energy conservation equation (Eq. 4.1) is transformed to

$$\frac{\partial T_l^*}{\partial t^*} = \frac{a_l^*}{r_d^{*2}} \frac{\partial^2 T_l^*}{\partial x^2} + \left(\frac{2a_l^*}{x r_d^{*2}} + \frac{1}{\rho_l^* C_{P,l}^* r_d^{*2}} \frac{\partial \lambda_l^*}{\partial x} \right) \frac{\partial T_l^*}{\partial x} \qquad (4.31)$$

ii) *Non dimensional species equation in liquid phase:*

The diffusion limited species conservation equation (Eq. 4.2) is transformed to

$$\frac{\partial Y_{l,i}^*}{\partial t^*} = \frac{D_{l,i}^*}{Le_{i,0} r_d^{*2}} \frac{\partial^2 Y_{l,i}^*}{\partial x^2} + \left(\frac{2 D_{l,i}^*}{x r_d^{*2}} + \frac{1}{r_d^{*2}} \frac{\partial D_{l,i}^*}{\partial x} \right) \frac{\partial Y_{l,i}^*}{\partial x} \qquad (4.32)$$

The equation of species profiles for distillation curve (Eq. 4.3) model becomes

$$\left(\frac{4}{3} \pi \left(r_d^* \right)^3 \rho_{l,i}^* Y_{l,i}^* \right)_{j+1} = \left(\frac{4}{3} \pi \left(r_d^* \right)^3 \rho_{l,i}^* Y_{l,i}^* \right)_j - \left(4\pi \alpha_i \left(r_d^* \right)^2 \dot{r}_d^* \Delta t^* \rho_{l,i}^* \varepsilon_i \right)_j \qquad (4.33)$$

iii) *Non dimensional Gas phase mass conservation equation:*

The mass conservation equation (Eq. 4.5) becomes,

$$\frac{\partial \rho_g^*}{\partial t^*} - \left(\frac{\dot{r}_d^*}{r_d^*} \right) \frac{\partial \rho_g^*}{\partial \eta} + \frac{1}{r^{*3}} \frac{\partial (r^{*2} \rho_g^* v_g^*)}{\partial \eta} = 0 \qquad (4.34)$$

iv) *Non dimensional gas phase species conservation equation:*

The species conservation equation (Eq. 4.6) can be derived as

$$\frac{\partial Y_{g,i}^*}{\partial t^*} = \frac{D_{g,i}^*}{Le_{i,0} r^{*2}} \frac{\partial^2 Y_{g,i}^*}{\partial \eta^2} + \left(\frac{2 D_{g,i}^*}{Le_{i,0} r^{*2}} - \frac{v_g^*}{r^*} + \frac{1}{Le_{i,0} r^{*2} \rho_{g,i}^*} \frac{\partial \left(\rho_{g,i}^* D_{g,i}^* \right)}{\partial \eta} \right)$$

$$\frac{\partial Y_{g,i}^*}{\partial \eta} - Dn \left(\rho_g^* \right)^{m+n-1} \left(Y_f^* \right)^m \left(Y_{O_2}^* \right)^n \exp \left(-\frac{\Theta}{T_g^*} \right) \qquad (4.35)$$

v) *Non dimensional gas phase energy conservation equation:*

The transformed non dimensional energy conservation equation (Eq. 4.7) is

$$\frac{\partial T_g^*}{\partial t^*} = \frac{a_g^*}{r^{*2}} \frac{\partial^2 T_g^*}{\partial \eta^2} + \left(\frac{2a_g^*}{r^{*2}} - \frac{v_g^*}{r^*} + \frac{1}{r^{*2} \rho_g^* C_{P,g}^*} \frac{\partial \left(\lambda_g^* \right)}{\partial \eta} \right) \frac{\partial T_g^*}{\partial \eta}$$

$$- \frac{1}{r^{*3} \rho_g^* C_{P,g}^*} \frac{\partial}{\partial \eta} (r^{*-2} q_R) + \frac{Dn}{C_{P,g}^*} \left(\rho_g^* \right)^{m+n-1} \left(Y_f^* \right)^m \left(Y_{O_2}^* \right)^n \exp\left(-\frac{\Theta}{T_g^*} \right) \tag{4.36}$$

where, the *Damköhler number*, Dn, is defined by,

$$Dn = \frac{\lambda_g (\rho_0)^{m+n-1} M R_0^2}{\left(\alpha_f M_f \right)^m \left(\alpha_{O_2} M_{O_2} \right)^n} \tag{4.37}$$

4.7.4. Transformed and Non-dimensionalized Initial Conditions

For liquid phase at $t^* = 0$,

$$T_l^* = T_l^*(x), \qquad Y_{l,f}^* = Y_{l,f,0}^* \qquad \text{for } 0 \le x \le 1 \tag{4.38}$$

For gas phase at $t^* = 0$,

$$T_g^* = T_g^*(\eta), \qquad Y_{g,f}^* = Y_{g,f}^*(\eta), \qquad Y_{g,O_2}^* = Y_{g,O_2}^*(\eta) \qquad \text{for } 0 \le \eta < \infty \tag{4.39}$$

Initial temperature, fuel and oxygen species are chosen as shown in Fig.4.2-3 with the transformed coordinate system grids.
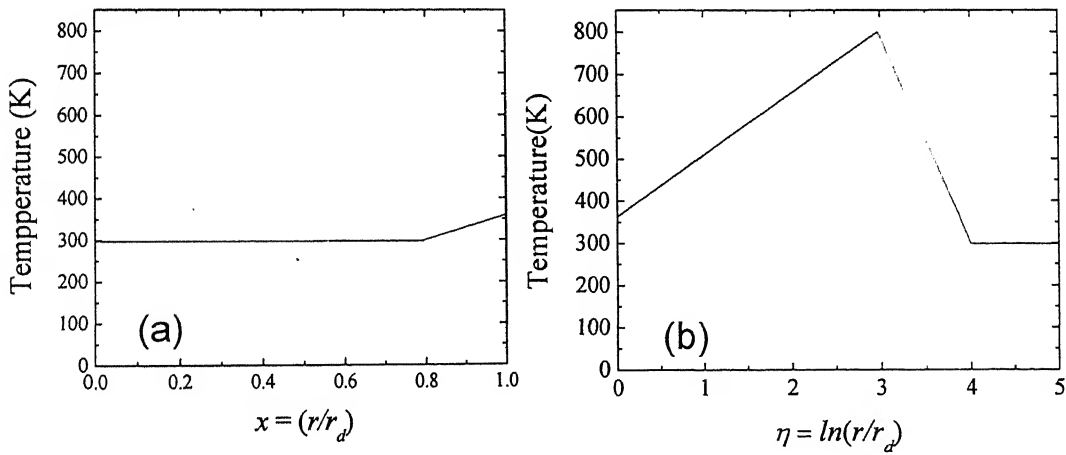
Fig.4.2: Initial Temperature Profile for **(a)** Liquid Phase and **(b)** Gas Phase.
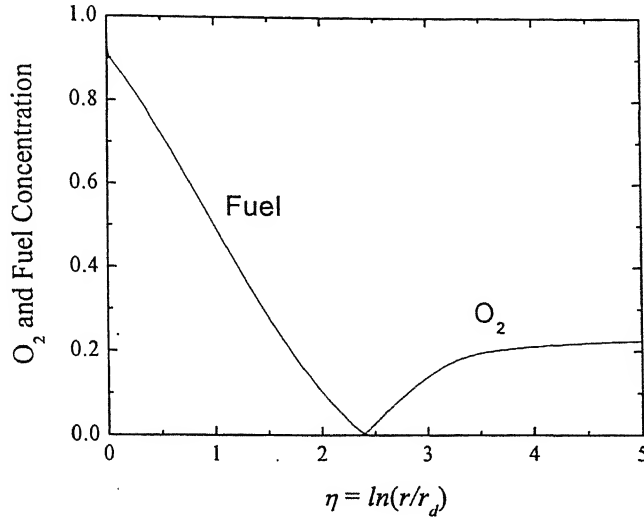
Fig.4.3: Initial Oxygen and Fuel Concentration Profiles.

4.7.5. Transformed and Non-dimensionalized Boundary Conditions

(i)   At droplet center, $x = 0$, the equation 4.17 becomes,

$$\frac{\partial Y_{l,i}^*}{\partial x} = 0$$

$$\frac{\partial T_l^*}{\partial x} = 0 \qquad\qquad (4.40)$$

(ii)   At droplet Surface, $x = 1$, mass conservation equation (Eq. 4.18) is converted to

$$\rho_g^* \mathrm{v}_g^* = -\rho_l^* \mathrm{v}_l^* = -\rho_l^* \frac{\partial r_d^*}{\partial t^*} \qquad\qquad (4.41)$$

(iii) At droplet surface species conservation equations (Eqs. 4.19-21) can be transformed to;

$$\left.\frac{\partial Y_{g,i}^*}{\partial x}\right|_{x=1} = \frac{Le_{i,0}\, r_d^*}{D_{g,i}^*} \mathrm{v}_g^* Y_{g,i,r=r_d}^* \qquad i = O_2, CO_2, H_2O \quad (4.42)$$

$$-\left.\frac{\partial Y_{g,f}^*}{\partial x}\right|_{x=1} = \frac{Le_{f,0}\, r_d^*}{D_{g,i}^*} \mathrm{v}_g^* \left(\varepsilon_f \alpha_f - Y_{g,f,r=r_d}^*\right) \quad f = f_1, f_2 \qquad (4.43)$$

$$-\left.\frac{\partial Y_{l,f}^*}{\partial x}\right|_{x=1} = \frac{Le_{f,0}\, r_d^*}{D_{l,i}^*} \mathrm{v}_l^* \left(\varepsilon_f \alpha_f - Y_{l,f,r=r_d}^*\right) \quad f = f_1, f_2 \qquad (4.44)$$

(iv)   Energy balance equation at the droplet surface (Eq. 4.22) becomes

$$\frac{\partial r_d^*}{\partial t^*} = \frac{St}{r^*}\left(\lambda_l^* \frac{\partial T_l^*}{\partial x} - \lambda_g^* \frac{\partial T_g^*}{\partial \eta} \right) + q_R^* \qquad (4.45)$$

where, St is a non-dimensional number defined as:

$$St = \frac{\rho_0 \, \Delta h_{CO}}{\alpha_f \rho_l \sum\limits_{i=1}^{N} \varepsilon_i L_i} \qquad (4.46)$$

4.8.   Numerical Technique (Discretization)

One dimensional, unsteady, equations for mass, species and energy equations for both liquid and gas phases governing the combustion processes of a single droplet fuel are solved numerically as described below. The Cranck-Nicolson finite difference scheme (Anderson, [2]) is employed for the discretization of governing equations. The unsteady term can be discretized as follows;

$$\frac{\partial T}{\partial t} = \frac{T_i^{n+1} - T_i^n}{\Delta t} \qquad (4.47)$$

The second derivative terms are discretized by using central time step, central spacing (CTCS) as described below;

$$\frac{\partial^2 T}{\partial \eta^2} = \frac{1}{2}\left[\left(\frac{T_{i-1} - 2T_i + T_{i+1}}{(\Delta \eta)^2} \right)^{n+1} + \left(\frac{T_{i-1} - 2T_i + T_{i+1}}{(\Delta \eta)^2} \right)^n \right] \qquad (4.48)$$

Diffusion terms are also expressed by using central time step, central spacing. The discretized diffusion terms is shown below;

$$\frac{\partial T}{\partial \eta} = \frac{1}{2}\left[\left(\frac{T_{i+1} - T_{i-1}}{2\Delta \eta} \right)^{n+1} + \left(\frac{T_{i+1} - T_{i-1}}{2\Delta \eta} \right)^n \right] \qquad (4.49)$$

The terms, $\dfrac{\partial \lambda}{\partial \eta}$, $\dfrac{\partial D}{\partial \eta}$ are discretized by using backward time spacing, for the previous time steps, as;

$$\frac{\partial \lambda}{\partial \eta} = \left(\frac{\lambda_{i+1} - \lambda_{i-1}}{2\Delta \eta} \right)^n \qquad (4.50)$$

For discretizing of the species equation at the droplet boundary, the following discretizations are employed.

$$\frac{\partial Y}{\partial \eta}\bigg|_{\eta = 0} = \frac{1}{2}\left[\left(\frac{Y_2 - Y_1}{\Delta \eta}\right)^{n+1} + \left(\frac{Y_2 - Y_1}{\Delta \eta}\right)^{n}\right] \tag{4.51}$$

For solving the mass conservation equation for the gas phase the interior grid points are discretized by higher order central spacing and the points adjacent to boundary are discretized using second order central spacing technique.

$$\frac{\partial \rho}{\partial \eta} = \frac{-3\rho_i + 4\rho_{i+1} - \rho_{i+2}}{2\Delta \eta} \qquad for \quad i = 2$$

$$\frac{\partial \rho}{\partial \eta} = \frac{-\rho_{i+2} + 8\rho_{i+1} - 8\rho_{i-1} + \rho_{i-2}}{12\Delta \eta} \qquad for \quad i = 3\ to\ m-2 \tag{4.52}$$

$$\frac{\partial \rho}{\partial \eta} = \frac{3\rho_i - 4\rho_{i+1} + \rho_{i-2}}{2\Delta \eta} \qquad for \quad i = m-1$$

The non dimensional energy conservation equation for gas phase is discretized using Crank-Nicolson finite difference scheme as given below.

$$\frac{T_i^{n+1} - T_i^n}{\Delta t^*} = \frac{\alpha}{2}\left[\left(\frac{T_{i-1} - 2T_i + T_{i+1}}{(\Delta \eta)^2}\right)^{n+1} + \left(\frac{T_{i-1} - 2T_i + T_{i+1}}{(\Delta \eta)^2}\right)^{n}\right]$$
$$+ \frac{\beta}{2}\left[\left(\frac{T_{i+1} - T_{i-1}}{2\Delta \eta}\right)^{n+1} + \left(\frac{T_{i+1} - T_{i-1}}{2\Delta \eta}\right)^{n}\right] - \gamma + \varphi \qquad for\ i = 2\ to\ m\text{-}1 \tag{4.53}$$

In the above equation T_g^* is replaced by T for convenience. The terms α, β, γ and φ are defined as follows;

$$\alpha = \frac{a_g^*}{r^{*2}} \tag{4.54}$$

$$\beta = \left(\frac{2a_g^*}{r^{*2}} - \frac{v_g^*}{r^*} + \frac{1}{r^{*2}\rho_g^* C_{P,g}^*}\frac{\left(\lambda_g^*\right)_{i+1}^n - \left(\lambda_g^*\right)_{i-1}^n}{2\Delta \eta}\right) \tag{4.55}$$

$$\gamma = \frac{1}{r^{*3}\rho_g^* C_{P,g}^*}\frac{\partial}{\partial \eta}(r^{*-2} q_R) \tag{4.56}$$

$$\varphi = \frac{Dn}{C_{P,g}^*}\left(\rho_g^*\right)^{m+n-1}\left(Y_f^*\right)^m\left(Y_{O_2}^*\right)^n \exp\left(-\frac{\Theta}{T_g^*}\right) \tag{4.57}$$

Equation 4.53 becomes

$$\left(1+\frac{\alpha\,\Delta t^*}{\Delta\eta^2}\right)T_i^{n+1}+\left(-\frac{\alpha\,\Delta t^*}{2\Delta\eta^2}-\frac{\beta}{4\Delta\eta}\right)T_{i+1}^{n+1}+\left(-\frac{\alpha\,\Delta t^*}{2\Delta\eta^2}+\frac{\beta}{4\Delta\eta}\right)T_{i-1}^{n+1}=$$

$$\left(1-\frac{\alpha\,\Delta t^*}{\Delta\eta^2}\right)T_i^{n}+\left(\frac{\alpha\,\Delta t^*}{2\Delta\eta^2}+\frac{\beta}{4\Delta\eta}\right)T_{i+1}^{n}+\left(\frac{\alpha\,\Delta t^*}{2\Delta\eta^2}-\frac{\beta}{4\Delta\eta}\right)T_{i-1}^{n}-\gamma\,\Delta t^*+\varphi\,\Delta t^* \quad (4.58)$$

In these way, this equation can be represented as a tri diagonal matrix form as shown below.

$$\begin{bmatrix} a_1 & b_1 & & & & \\ c_2 & a_2 & b_2 & & & \\ & \ddots & \ddots & \ddots & & \\ & & c_{m-1} & a_{m-1} & b_{m-1} \\ & & & c_m & a_m \end{bmatrix}\begin{bmatrix} T_1^{n+1} \\ T_2^{n+1} \\ \vdots \\ T_{m-1}^{n+1} \\ T_m^{n+1} \end{bmatrix}=\begin{bmatrix} d_1 \\ d_2 \\ \vdots \\ d_{m-1} \\ d_m \end{bmatrix} \quad (4.59)$$

For $i=2$ to $m-1$

$$a_i=\left(1+\frac{\alpha\,\Delta t^*}{\Delta\eta^2}\right),\ b_i=\left(-\frac{\alpha\,\Delta t^*}{2\Delta\eta^2}-\frac{\beta}{4\Delta\eta}\right),\ c_i=\left(-\frac{\alpha\,\Delta t^*}{2\Delta\eta^2}+\frac{\beta}{4\Delta\eta}\right)\ \text{and}$$

$$d_i=\left(1-\frac{\alpha\,\Delta t^*}{\Delta\eta^2}\right)T_i^{n}+\left(\frac{\alpha\,\Delta t^*}{2\Delta\eta^2}+\frac{\beta}{4\Delta\eta}\right)T_{i+1}^{n}+\left(\frac{\alpha\,\Delta t^*}{2\Delta\eta^2}-\frac{\beta}{4\Delta\eta}\right)T_{i-1}^{n}-\gamma\,\Delta t^*+\varphi\,\Delta t^* \quad (4.60)$$

The values of a_1, b_1, a_m, c_m can be obtained from the boundary conditions. This matrix is solved very efficiently by using *Thoma's Algorithm*. Similarly the other governing equations for species and energy, (Eqs. 4.31, 4.32, 4.35) with appropriate boundary conditions are resulted in tri-diagonal matrices and are solved by using the same algorithm. The solution procedure for the present model is described in details in section 4.11.

4.9. Radiation Heat Transfer Modeling

For gas radiation, the gray gas model has been used. In this model, carbon dioxide and water vapor are assumed to be the major contributors for the radiative heat transfer. The Planck mean absorption coefficient $k_{P,g}$ is evaluated locally from mass- fraction weighted summation of each participating species as follows:

$$k_{P,g}=P\left(X_{CO_2}k_{CO_2}+X_{H_2O}k_{H_2O}\right) \quad (4.61)$$

Here, X_{CO_2} and X_{H_2O} are the mole fractions of CO₂ and H₂O, respectively. P is the atmospheric pressure in bar. The Planck mean absorption coefficient for CO₂ and H₂O are represented by k_{CO_2} and k_{H_2O} respectively. These are determined by the curve-fitted data taken from RADCAL program 1993[19].

The radiation term involved in the energy equation has been calculated by using radiative transfer equation with the assumption of isotropic scattering, given by Viskanta and Merriam [75] for a concentric sphere. The same modeling has also been used by Saitoh et al., [62], Marchese et al. [43] and Kumar et al., [32], [33].

$$\nabla \cdot q_R = \frac{1}{r^2} \frac{\partial}{\partial r} \left(r^2 q_R \right)$$
$$= 4 \, k_{P,g} \sigma_E T_g^4 - k_{P,g} \, G(\tau) \tag{4.62}$$

where, q_R is radiation flux, σ_E is the Stephan-Boltzman constant, G is the radiation absorption by the gas shell. The first term is associated with radiation emission and the second term corresponds to the absorption; however, the scattering term gets canceled out.

The radiation absorption can be expressed as,

$$G(\tau) = \frac{2\sigma_E}{\tau} \left[T_d^4 \, g_1(\tau) + T_\infty^4 \, g_2(\tau) + \int_{\tau_1}^{\tau_2} K(\tau,\xi) T_g^4 \, d\xi \right] \tag{4.63}$$

Here, $g_1(\tau)$ is associated with the radiation absorption by any shell from the droplet surface. The term, $g_2(\tau)$ corresponds to the absorption of radiation heat from the ambience. The Kernel term, $K(\tau,\xi)$ represents the radiation absorption between the shells. τ is the optical path length defined as:

$$\tau = \int_0^r k_{P,g} d\xi \tag{4.64}$$

τ_1 and τ_2 are the optical path length at the drop surface and infinity respectively. The functions $g_1(\tau)$ and $g_2(\tau)$ are defined as:

$$g_1(\tau) = \tau_1 \, E_2(\tau - \tau_1) - E_3(\tau - \tau_1) + E_3(\tau^*) \tag{4.65}$$

$$g_2(\tau) = \tau_2 \, E_2(\tau_2 - \tau) - E_3(\tau_2 - \tau) - \tau_2^* \, E_2(\tau_2^* + \tau^*) - E_3(\tau_2^* + \tau^*) \tag{4.66}$$

Here τ^* and τ_2^* are as follows:

$$\tau^* = \sqrt{(\tau^2 - \tau_1^2)}, \quad \tau_2^* = \sqrt{(\tau_2^2 - \tau_1^2)} \tag{4.67}$$

Kernel $K(\tau, \xi)$ is represented by:

$$K(\tau, \xi) = E_1\left(|\tau - \xi|\right) - E_1\left(|\tau^* - \xi^*|\right) \times \xi^* \tag{4.68}$$

where, $\xi^* = \sqrt{\left(\xi^2 - \tau_1^2\right)}$ and the exponential integral function, $E_n(\tau)$ is defined as;

$$E_n(\tau) = \int_0^\infty \zeta^{-n} \exp(-\tau \zeta) d\zeta \tag{4.69}$$

The radiation properties have been calculated with high accuracy in this way. The close form solutions [85] for Exponential Integral Functions are used.

4.10. Thermodynamic, Transport and Radiation Properties

The gas phase and liquid phase transport, thermal and radiation properties are discussed in details in Appendix A. The gas mixture consists of fuel vapor, O_2, CO_2, H_2O and N_2. The transport properties of the liquid and gas phase have been estimated from the kinetic theory of gases and liquids as discussed in Reid et al. [59] and Hirschfelder et al. [22]. These estimated are compared with the experimental data (Vargaftik, [74] and Toulokian, [72]). The species transport and thermal data are taken mostly from Sandia Database.

4.11. Solution Procedure

The flow chart of the solution is shown in Fig.4.4. For the present study a computer code has been developed by using C with this algorithm.

(1) At $t^* = 0$, suitable initial temperature and species profiles are chosen.

(2) The vaporization rate data for initial conditions is estimated from the classical theory of droplet vaporization and combustion.

(3) Calculation of variable gas and liquid phases' properties with temperature.

(4) Temperature of a single component fuel droplet at its surface can be calculated by using the liquid vapour phase equilibrium equations (Clausius-Clapeyron's equation and Roult's Law). In the case of Multi-component fuel

droplet surface temperature can be calculated by mass fraction weighted summation.

(5)   To find out the axi-symmetric velocity, v_g, mass conservation equation has to be solved.

(6)   Determination of the Radiation heat transfer and irradiance.

(7)   Solution of Gas phase energy conservation equation to find out the temperature profile.

(8)   Then species equation (fuel, O_2, CO_2, H_2O) has to be calculated respectively to find out the species profiles. The species profile of N_2 is determined from species balance.

(9)   Calculation of the energy equation for the liquid phase to find out the temperature inside the droplet.

(10)   For multi-component fuel droplet combustion the species equation in the liquid phase are solved. For distillation curve (rapid mixing) model uniform species concentration are considered inside the droplet and for the diffusion limit model diffusion limited governing equation for the liquid phase species equation have to be solved.

(11)   Determination of the regression rate $\left(\dfrac{\partial r_d^*}{\partial t}\right)$ at surface of the fuel droplet using the energy conservation equation.

(12)   Check convergence criterion. If $\dfrac{\left|\left(\dfrac{\partial r_d^*}{\partial t}\right)_{new} - \left(\dfrac{\partial r_d^*}{\partial t}\right)_{old}\right|}{\left(\dfrac{\partial r_d^*}{\partial t}\right)_{old}} \leq 10^{-4}$, then go to the next step, else, do the same process 3-11.

(13)   Droplet radius for the next time step has to be calculated, $r_{j+1} = r_j + \left(\dfrac{\partial r}{\partial t}\right)\Delta t$.

(14)   Check the stopping criterion.

(15)   Proceed to the next time step.

All the computations are carried out in the present thesis using Linux based Pentium IV (3.4 GHz) IBM PC. The time required for a typical case in this machine is around 1 CPU hours.

$t = 0$

Selection of Suitable Initial Profile

Approximation of Vaporization Rate from Classical Theory

Calculation of Variable Liquid and Gas Phase Properties with Temperature

Determination of Droplet Surface from Liquid-Vapor Phase Equilibrium

Calculation of Gas Phase Velocity: Using Continuity Equation

Determination of Radiation Heat Transfer and Irradiance

Calculation of Gas Phase Temperature Distribution: Using Energy Equation

Estimation of Gas Phase Species Mass Fraction: Using Species Equation

Determination of Temperature Distribution inside the Droplet: Using Liquid Phase Energy Equation

Solution of Liquid Phase Species Mass Fraction: Using Species Equation for Liquid Phase

Determination of Regression Rate from the Energy Balance at Droplet Surface

NO

Check Convergence Criterion

YES

Calculation of Droplet Radius for the Next Time Step

NO $t = t + \Delta t$

Check Stopping Criterion

YES

STOP

Fig. 4.4: Flow Chart of the Solution Procedure

4.12. Selection of Grid Sizes, Time Step and Domain Boundary

Ideally, the outermost boundary lies at infinity. However for numerical simulation, outer boundary is generally taken at considerable distance from the droplet centre. In the present numerical model the outermost boundary is taken at approximately 150 times away from the droplet radius ($\eta = 5.0$). In order to choose the appropriate semi-infinite domain for computation, the effect of outer boundary distances on the results of regression rate are investigated by varying the value of $\eta = 4$, 5, 6, for an n-heptane droplet at normal ambient temperature and pressure. The results of d^2-law for these cases are plotted in Fig. 4.5. It can be observed that all three curves are pretty closer to each other. The errors are within 0.01% as compared to the total burning time. Hence, the outer boundary distance, η of 5 is chosen for all the computations reported in this thesis.
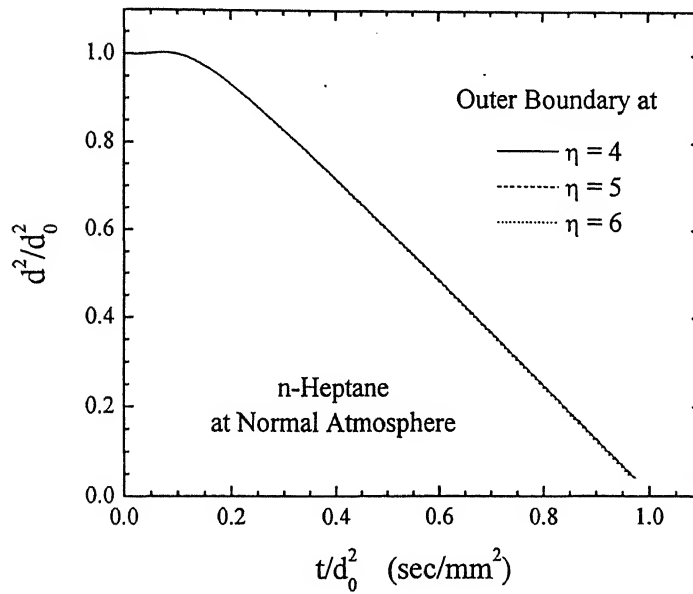
Fig. 4.5: The results of d^2 law for n-Heptane burning in normal atmosphere by varying the boundary distance, $\eta = 4, 5, 6$ ($\Delta t^* = 5 \times 10^{-4}$ and $\Delta \eta = 0.02$).

A uniform non dimensional time step (Δt^*) of 5×10-4 has been used. To check the accuracy of time step chosen the following test has been performed. In Figure 4.6(a), the d^2 with time for n-Heptane burning in normal atmosphere is plotted with, Δt^*, of 2×10^{-4}, 5×10^{-4} and 1×10^{-3} with $\Delta \eta = 0.02$ and at ambient η is considered equal to 5.0. From this figure, it has been fond that $\Delta t^* = 5 \times 10^{-4}$ is

the optimum grid size, as there are negligible differences in the result for $\Delta t^* = 5 \times 10^{-4}$ and $\Delta t^* = 2 \times 10^{-4}$ (0.2% of error as compared to the total burning time). Hence, $\Delta t^* = 5 \times 10^{-4}$ is taken for the entire calculation.
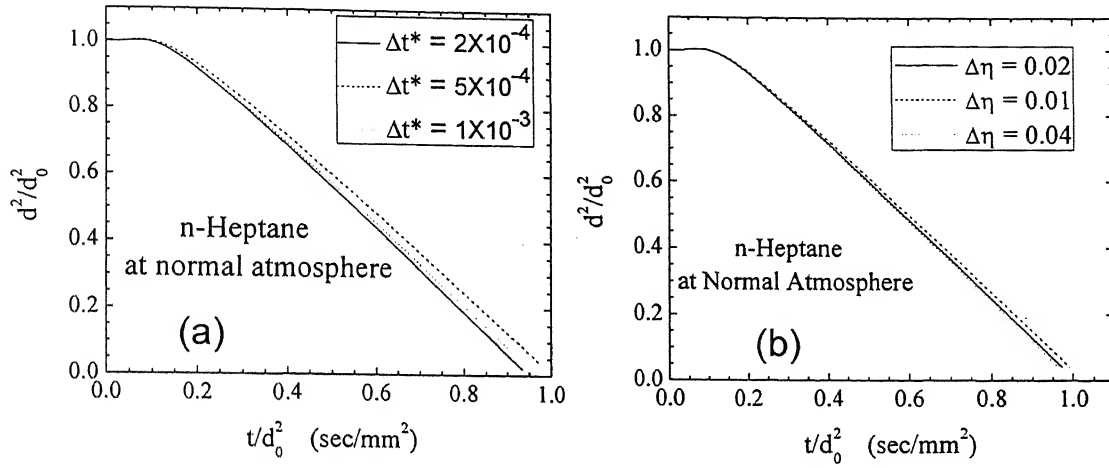
Fig. 4.6: The results of d^2 law for n-Heptane burning in normal atmosphere with (a) Different Δt^* of 2×10^{-4}, 5×10^{-4} and 1×10^{-3} ($\Delta \eta = 0.02$, at ambient η is considered equal to 5.0) and (b) different $\Delta \eta$ of 0.01, 0.02 and 0.04 ($\Delta t^* = 5 \times 10^{-4}$, at ambient η is considered equal to 5.0).

The logarithmic grid is used $\Delta \eta = 0.02$. In order to select optimum grid size grid sensitivity test has performed. The results of the variation of burning history with the different grid size taken are plotted in Fig. 4.6 (b). It is depicted from the figure that, burning time does not depend much on the grid chosen. For $\Delta \eta = 0.02$ and 0.04 the relative in within 0.1 %. Hence to save the computational times the value of $\Delta \eta$ is chosen 0.02 for entire calculations in the thesis.

Chapter 5

RESULTS AND DISCUSSION

In this chapter, the results achieved from the numerical studies of single component and multicomponent fuel droplet combustion are discussed. The results are compared with the present experimental data and others data available in the literature. First section (Sec. 5.1) contains the studies of single component fuel droplet combustion followed by multicomponent fuel droplet combustion in the next section (Sec. 5.2).

5.1. Single Component Fuel Droplet Combustion

This section is mainly devoted to the numerical studies of single component fuel droplet combustion. In the first phase, the numerical experiments are carried out without including the radiation effects. A single n-Heptane fuel droplet of initial diameter of 1 mm is being investigated. The results of this study is presented in subsequent subsection in terms of droplet burning history, flame structure, flame stand-off ratio and flame location and gas and liquid phase temperature distribution. The numerical data such as droplet burning history and the flame location are compared with the present experimental data and other experimental data available in the literature. In the next subsection the effects of radiation heat transfer are being discussed extensively. The effects of initial droplet diameter on the burning rate at different ambient temperature are investigated and compared with the existing experimental data. Subsequently the results of droplet burning at different ambient oxygen level are presented.

5.1.1. Transient Variation of Burning Parameters without Radiation

Droplet Burning History

The normalized droplet diameter square, d^2/d_0^2 and the burning rate constant, K_b are plotted with normalized time, t/d_0^2 in Fig. 5.1(a) and 5.1(b) respectively. The variation of droplet diameter square with time is compared with the numerical data presented by Saito & Nagano [61] and the experimental data by Okajima and Kumagai [52]. It can be observed from the Fig. 5.1(a) that, the present numerical prediction burning rate is higher than the experimentally observed burning rate by

Okajima and Kumagai [52]. In contrast, the numerical results of burning rate considering constant property and without radiation predicted by Saito and Nagano [61] matches well with the experimental data of Okajima and Kumagai [52]. In the present experimental study under normal gravity the burning rate is observed to be higher than the microgravity experimental data. However, the present numerical study without radiation heat transfer is closer to the present experimental data.

It can be noted that, radiation heat loss is not considered in the present model. Hence, burning rate must be greater than the experimental results, as experimental data can not be free from radiation heat loss. In contrast the numerical results presented by Saito and Nagano [61] predict well the burning rate experimental data of Okajima and Kumagai [52]. This is contrary to the expectation. This matching of numerical prediction with the experimental data is considered to matter of mere coincidence. However, the present model using variable properties are supposed to be superior as compared to the numerical modeling with constant properties of Saito and Nagano [61].

In the present experiments under normal gravity, natural convection is occurred due to which turbulence is likely to be generated in the gas phase. Hence, gas phase heat and mass transfer are increased to a larger extent resulting in increase in droplet burning rate. The increase in burning rate under normal gravity condition is mainly contributed by the natural convection rather than the radiative heat loss.
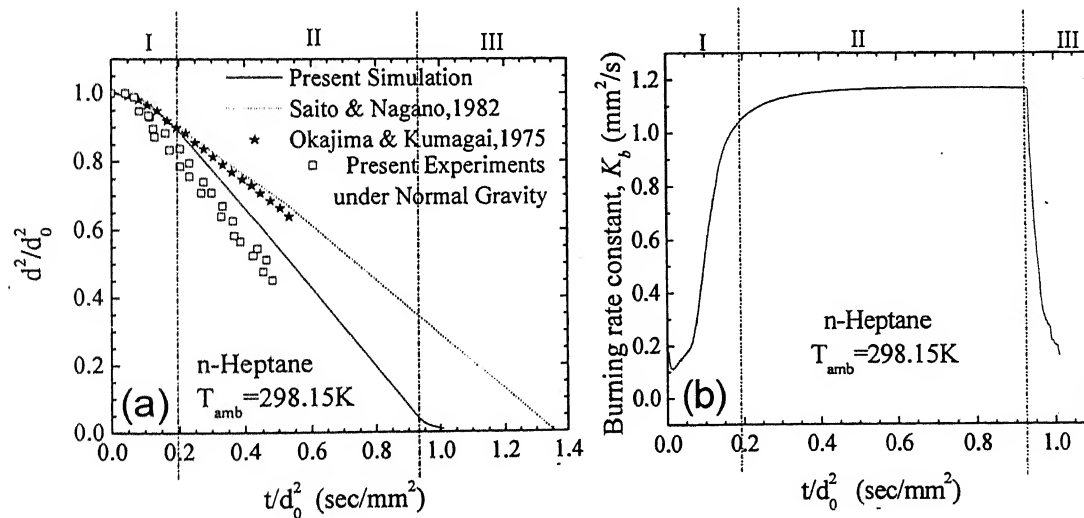
Fig. 5.1: Variation of the (a) Droplet diameter square and (b) Burning rate constant, K_b with time.

The transient variations of droplet center temperature, droplet surface temperature and flame temperature are plotted in Fig. 5.2. It can be noted that the numerical calculation of droplet combustion are initiated with some initial temperature and species profile.
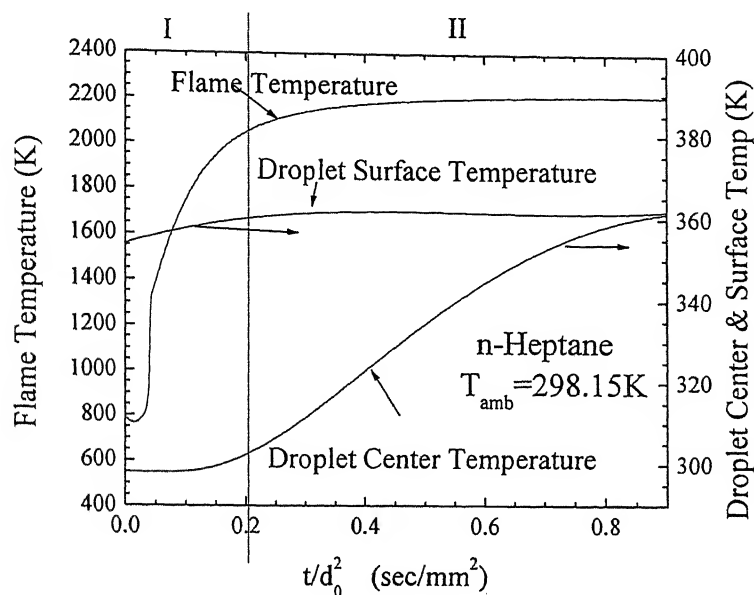
Fig. 5.2: Variation of droplet surface temperature, droplet center temperature and flame temperature with time.

Fig. 5.2 indicates that the temperature profiles change its slope indicating the effect of initial transients. The heat generated through the combustion is used to build up the temperature in the gas phase. However in this period the flame temperature as well as the droplet surface temperature are increased to a certain value and become almost stable. During this period the burning rate constant, K_b, is increased at a faster rate and attains a maximum value as can be seen in Fig. 5.1(b). This period is defined as initial preheated period. In the numerical study this initial preheat period is a depended on the initial temperature and species profiles. After initial transient period, the droplet burning rate, K_b remains almost constant. After this, the gas phase temperature increases marginally to its asymptotic value as can be seen in Fig. 5.2. During this period the heat generated due to reaction is almost balanced by the heat transferred to the ambient and liquid phase. As a result the burning rate constant, K_b, remains almost constant. The droplet surface temperature as shown in Fig. 5.2 becomes almost constant during this period. However the droplet center temperature is increased almost at a constant rate as nearly constant

amount of heat is being supplied to the liquid phase from the gas phase side. This period of burning can be defined as equilibrium burning period or d^2-law period. At the end of the burning, heat generated by the gas phase combustion may not be sufficient to meet the demand of heat losses for the self sustaining of the combustion wave, which leads to the extinction of the flame. This period is defined as flame extinction period. As a result the burning rate constant, K_b, is decreased drastically as shown in Fig. 5.1 (b). Based on the above discussion, the droplet burning regime can be divided into three major periods such as (I) Initial pre-heated period, (II) Stable d^2-law or equilibrium period and (III) Flame extinction period.

Flame Structure

Typical structure of flame at $(t/d_0{}^2)$ = 0.4 sec/mm^2 is shown in Fig. 5.3(a). It can be observed in this figure that the fuel and oxidizer species meet at the point where maximum temperature occurs at which flame is located. In this zone exothermic reactions take place as shown in Fig. 5.3 (b). As shown in the Fig. 5.3(a)-(b), very near to the droplet surface ($ln(r/r_d)$ towards zero), fuel concentration is higher and oxygen concentration is zero. In this zone fuel vaporizes from the droplet and subsequently diffuses to the gas phase. However, oxygen is also diffused to the gas phase from the ambient. At a certain distance from the droplet surface fuel and oxygen meet at their stoichiometric ratio. In this zone heat is being generated resulting high temperature. This high temperature zone, where fuel vapor and oxygen meet at their stoichiometric ratio, is defined as flame. The heat is being transferred to both the sides from the flame. Due to the reaction between fuel and oxidizer product species are generated at the flame zone. These product species are convected and diffuses to the ambient as well as towards the droplet surface. The typical variations of concentration of the product species are shown in Fig. 5.3(a).
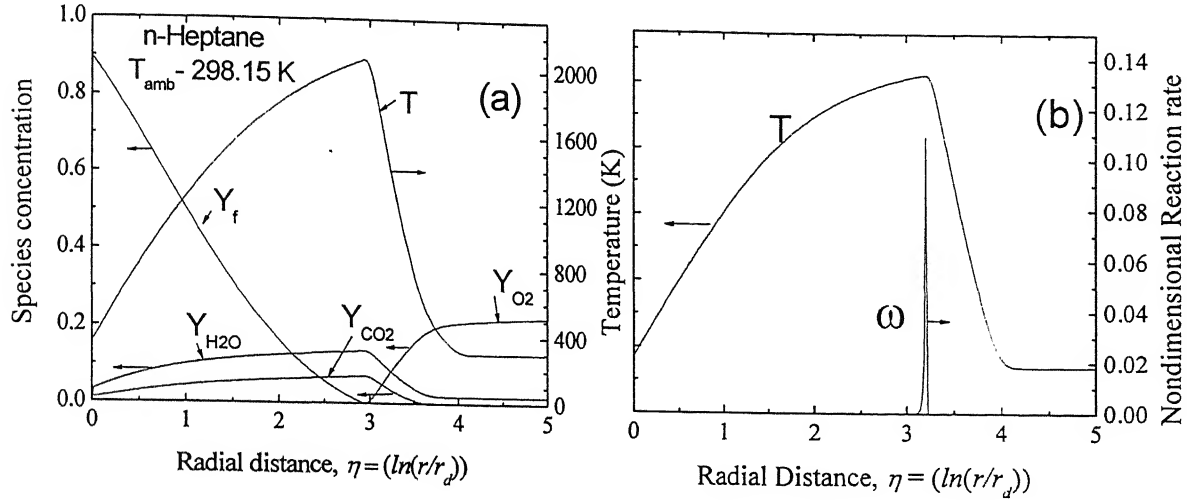
Fig. 5.3: (a) Structure of flame and **(b)** Radial distribution of reaction rate at the middle of droplet burning ($t/d_0^2 = 0.4$ sec/mm^2)

Flame Standoff Ratio and Flame Location

The variation of predicted flame stand off ratio during the droplet burning is plotted in Fig. 5.4(a). The flame standoff ratio increases monotonically with the time and then attains a maximum value in the stable d^2 law period as shown in Fig. 5.4(a). The present predicted flame stand-off ratio data are found to be in the range of 11 – 28. In contrast the numerical data predicted by Saito and Nagano [61] shows the flame stand off ratio increases from 4-35. It increases at a lower rate in the initial portion of burning but at a faster rate towards the end of the burning. These features may be due to the use of constant properties assumptions in their modeling.

The flame diameter first increases with time and after some time it decreases with the droplet diameter. The flame diameter observed from the present simulation matches qualitatively with the data presented by Okajima and Kumagai [52]. However, the present result fails to predict the experimental data of flame diameter quantitatively. This discrepancy might be caused due to the radiation heat loss. Although the flame diameter data predicted by Saito and Nagano [61] matches well in the initial phases with the experimental data but it departs drastically as can be seen in Fig. 5.4(b). It seems that the flame diameter prediction towards the ends of burning is quite unexpected as it is known that flame diameter drops down towards the end of the burning. This may be due to constant properties assumptions in their formulation.
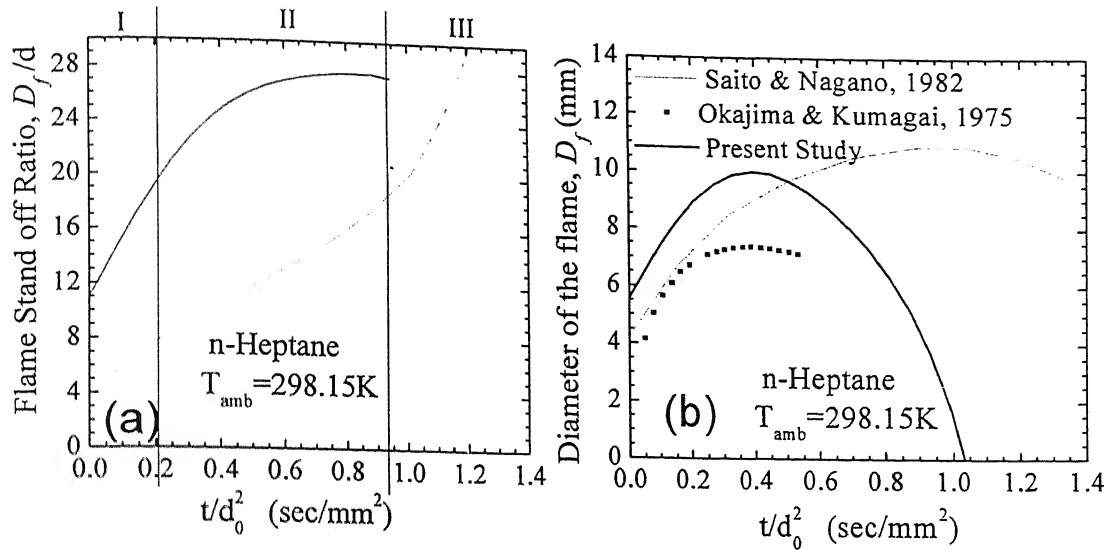
Fig. 5.4: Variation of (a) Flame Stand-off ratio and (b) Flame diameter during droplet burning.

Gas Phase and Liquid Phase Temperature Distribution

Transient variation of gas phase temperature distribution along the radial direction is plotted in Fig. 5.5 (a). It can be observed from Fig. 5.5(a) that the gas phase temperature increases from the surface temperature of the liquid droplet and attains a maximum value at the flame zone. Initially the gas phase temperature increases with time at a faster rate. After the initial pre-heated transient period it does not vary further with time. The reason may be attributed to the initial heat generation due to exothermic reactions, which is used to build up the temperature in the gas phase. After initial transient period it is expected that the heat generation due to chemical reactions is balanced by the heat loss to the droplet surface and ambient. In Fig. 5.5(b), the transient variation of liquid phase temperature is plotted along the radial direction. At the interface of liquid droplet and gas phase the surface temperature increases with time initially and attains a constant value. It can be observed from the Fig. 5.5(b) that the temperature gradient along the radial direction with time and attains almost uniform temperature profile across the liquid droplet towards the end of burning. This feature is well predicted as per the heat transfer due to conduction.
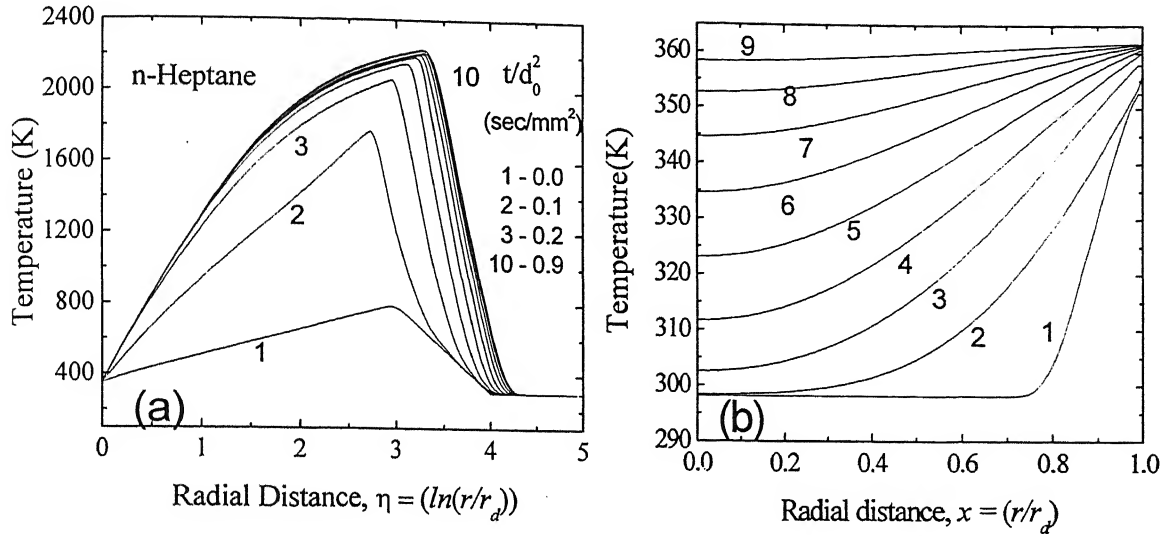
Fig. 5.5: (a) Gas phase and (b) Liquid Phase temperature distribution

5.1.2. Effect of Ambient Oxygen Concentration on Droplet Burning

The oxygen level in the actual combustion zone is likely to be changed with time. Hence it is very essential to study the effects of the ambient oxygen concentration on the droplet combustion. An attempt is made to investigate numerically the effect of ambient oxygen level on single isolated n-heptane fuel droplet burning.
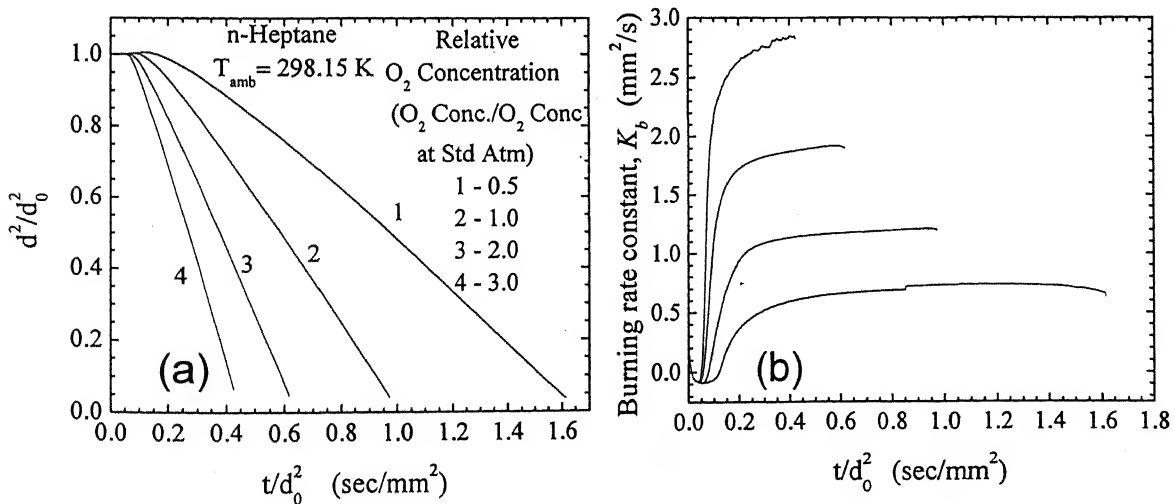
Fig: 5.6: Variation of (a) d^2 law and (b) burning rate constant, K_b with different O_2 concentration at ambient air.

The effect of ambient oxygen concentration level on the droplet burning history is plotted in Fig. 5.6(a). It can be observed from the Fig. 5.6 (a) that the burning rate increases with the ambient oxygen level. This might be attributed to increase in the heat generation rate, which is the function of $k(Y_{f_i})^m (Y_{O_2})^n$ in the single step chemistry model. Similar phenomenon can also be predicted by the classical quasi-steady theory.

It can be observed from the Fig. 5.6(a) that the initial preheat period is also affected due to the oxygen concentration level. In this regard, total burning time and initial preheat time are plotted in Fig. 5.7(a) and 5.7 (b) respectively with the relative oxygen concentration level, which is defined as the ratio of the oxygen concentration level at the atmosphere to the oxygen concentration level at standard condition. The burning time and preheat time decays exponentially with oxygen concentration level as shown Fig. 5.7(a) and (b). Besides this, the total burning time is more affected by the oxygen level than the initial preheat time.
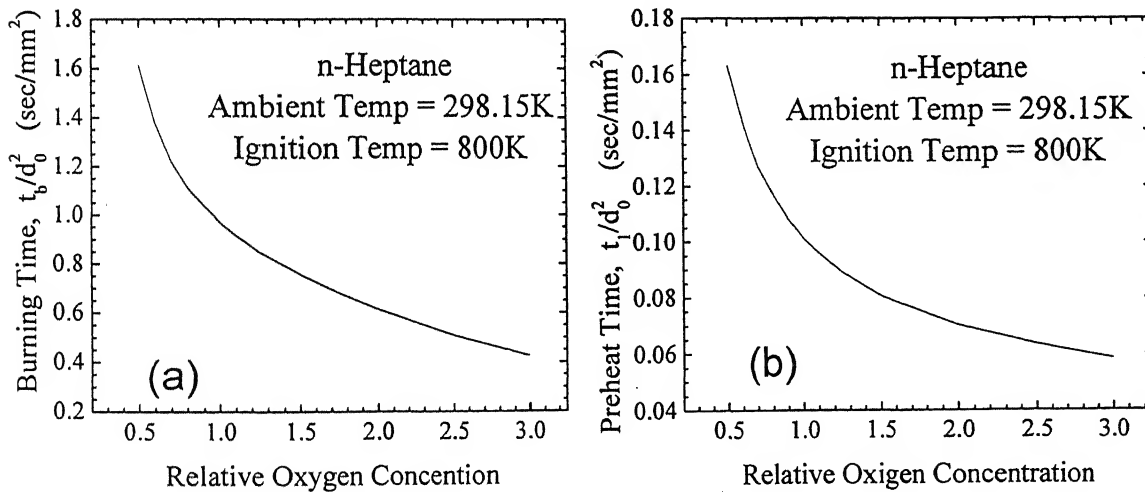
Fig: 5.7: Effect of relative oxygen concentration (O_2 Conc. / O_2 Conc. at standard atm) at the ambient on the (a) burning time (t_b) (b) Preheat time (t_i)

The transient variation of flame stand off ratio is plotted in Fig. 5.8(a). From Fig.5.8 (a) it can be observed that, the flame stand off ratio is increased with the ambient oxygen concentration level. It is known that the flame stand off ratio is controlled by balance between the gas phase radial velocity and the diffusional velocity of oxygen. In order to understand the increase of flame standoff ratio with oxygen level, the transient variation of the gas phase velocity, v_g, at the droplet

surface is plotted in Fig.5.9 (b) for different ambient oxygen concentration level. It can be observed that the flame temperature is increased with the ambient oxygen concentration level as shown in Fig. 5.9 (a) leading to the increase in the droplet regression rate as well as the gas phase radial velocity. Hence, flame is moved away further from the droplet surface with increase in gas phase velocity. In contrast, the diffusional velocity of oxygen, acting in inward radial direction is increased with the ambient oxygen concentration level. It attempts to push the flame front towards the droplet surface. However the magnitude of the diffusional velocity is less compared to the gas phase radial velocity at the flame surface. Hence, the flame stand off ratio increases with the ambient oxygen concentration level. Interesting to note that present prediction of flame standoff ratio is in contrast with the classical theory. These anomalies may be due to fact that the classical theory does not take account of the gas phase velocity, which is the determining factor in predicting the flame standoff ratio.
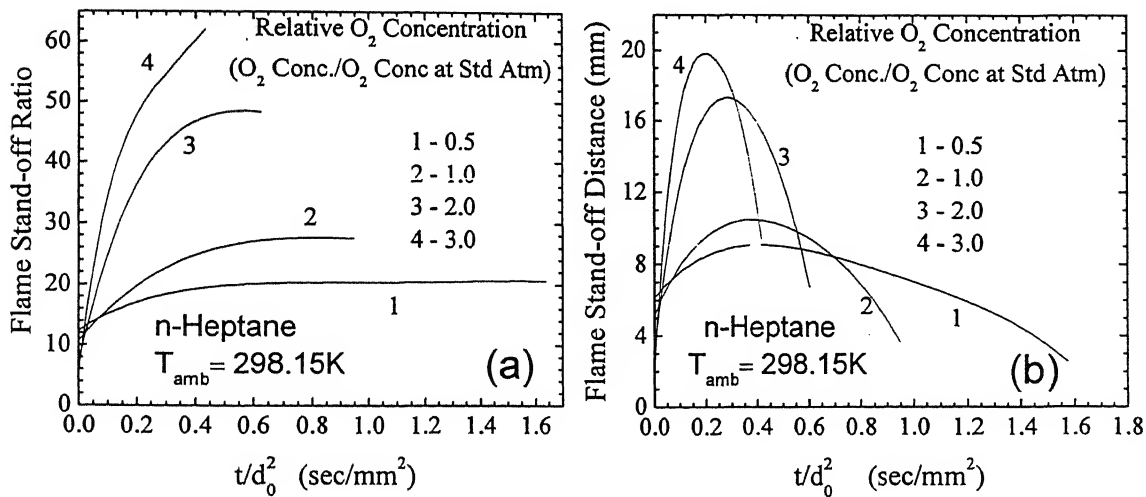
Fig: 5.8: Variation of (a) flame Stand-off ratio and (b) flame stand-off distance with different oxygen concentration of atmosphere.

Fig. 5.10. It can be observed that present numerical results matches well within the error band of experimental data of Mikami et al. [46].
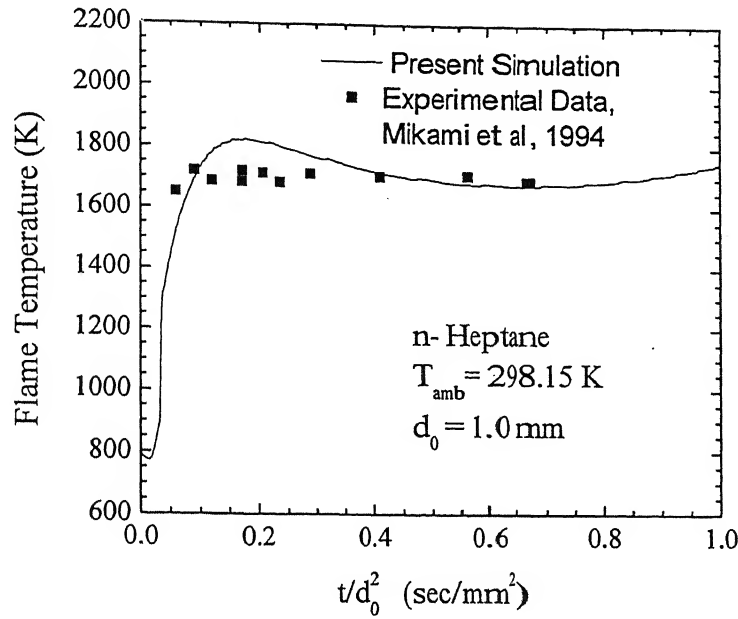
Fig.5.10: Variation of flame temperature as a function of time (t/d_0^2): predicting along with experimental values (Mikami et al., [46])

The normlalized droplet diameter square is plotted with normalized time (t/d_0^2) in Fig. 5.11(a). It is found from the Fig. 5.11(a) that the burning time is increased considerably due to the inclusion of radiation model. The data presented in the Fig. 5.11(a) are also compared with the compiled experimental data presented by Kumagai et al. [31] and the numerical prediction by Marchese et al. [46]. Only the stable d^2 law portions data are compared. Interesting to note that, by the inclusion of radiation model the present results of burning rate predicts well with the experimental data of Kumagai et al. [31] and numerical data of Marchese et al. [46] as shown in Fig. 5.11 (a).

The variation of burning rate constant, K_b at ambient temperature is plotted in Fig. 5.11(b). It can be observed that by inclusion of radiation model the burning rate constant, K_b decreases substantially as compared to results without radiation model. However when the ambient temperature is increased to 1093 K, the burning rate constant increases substantially as shown in Fig. 5.11 (b). Similar feature can also be observed in Fig. 5.11 (a) indicating that increase in ambient temperature reduces the burning time. This phenomenon can be attributed to the increase in

adiabatic flame temperature with increase in ambient temperature. Beside this the heat loss from the flame surface will be hindered due to the reduced temperature gradient between the flame surface and its surroundings.
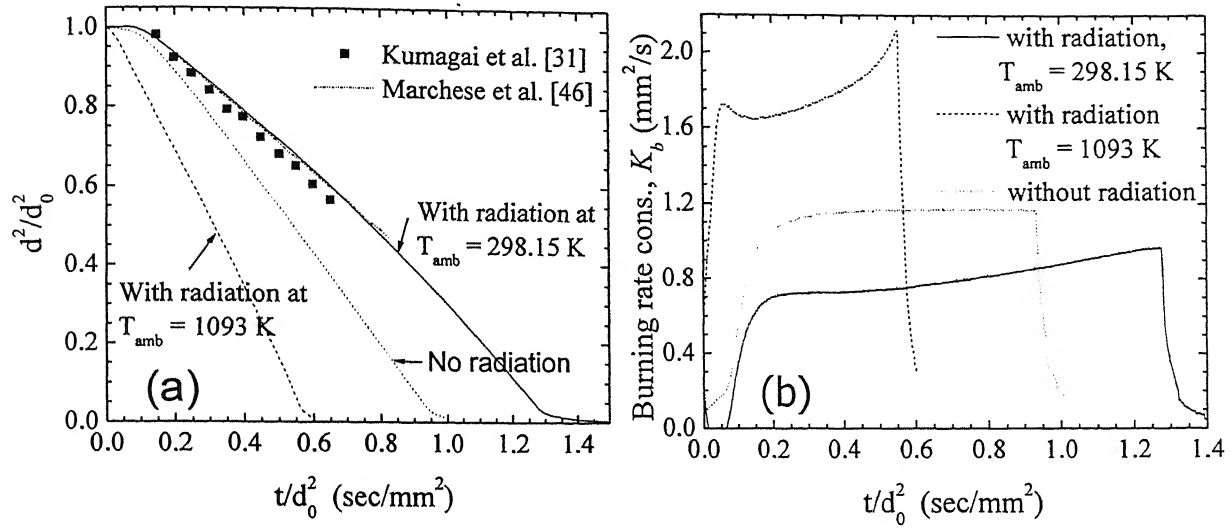
Fig. 5.11: Effect of radiation heat transfer on the **(a)** d^2-Law and **(b)** burning rate constant, K_b at different ambient temperatures for isolated droplet of initial Diameter 1.0 mm.
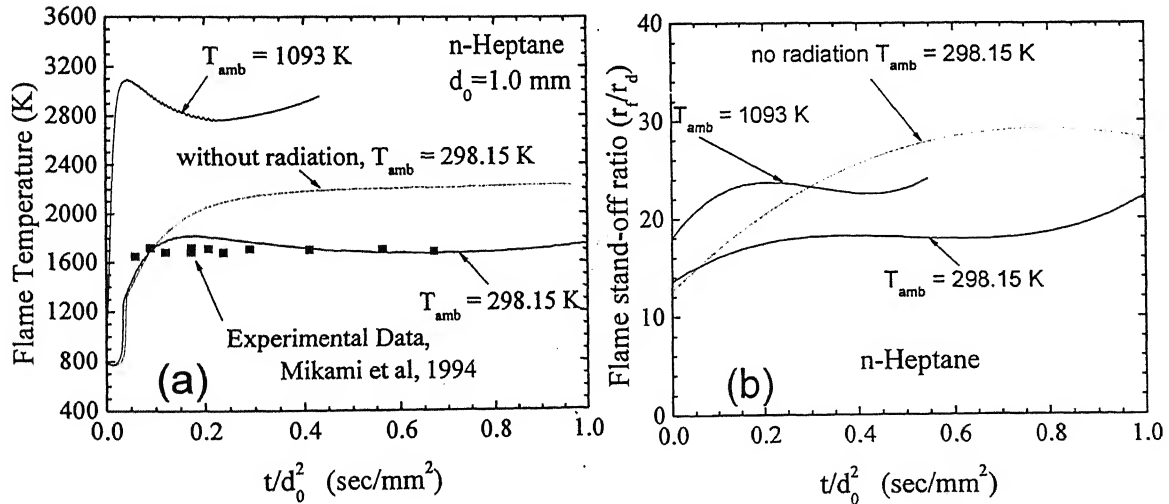
Fig. 5.12: Effect of radiation heat transfer on the **(a)** flame temperature and **(b)** flame stand off distances at different ambient temperatures for isolated droplet of initial diameter 1.0 mm.

An important feature can also be observed from the Fig. 5.11 (b) that the burning rate constant increases with time during stable portion of the droplet

combustion. However, it remains almost constant for no radiation model. This phenomenon can be explained in terms of the effects of geometry on droplet burning. The radiation heat loss from the flame front to its surrounding increases for larger size droplet due to increase in its surface area. In contrast radiation loss from the smaller droplet becomes less. Hence, the radiation heat loss from the flame surface is likely to be decreased with reduction in droplet diameter. As a result, more amount of heat can be transferred to the droplet surface leading to an increase in burning rate.

The flame temperature for n-Heptane fuel droplet combustion of initial diameter of 1 mm at two different ambient temperatures considering radiation heat transferred is compared in Fig.5.12 (a) with the predicted data of present numerical model without radiation. A considerable amount of flame temperature drop from 2200 K to 1700 K can be observed with the inclusion of the radiation model. By increasing the ambient temperature to 1093 K the present model predicts the flame temperature to be around 2800 K. But, this predicted flame temperature seems to be quite high for which gas phase dissociation reaction model may need to be considered.
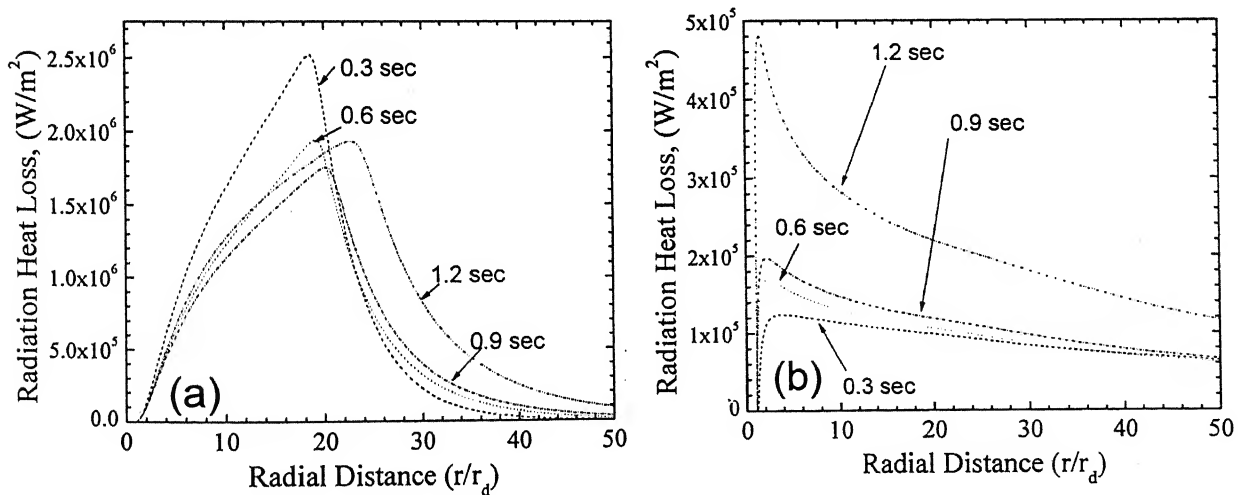
Fig. 5.13: Transient variation of radial distribution of (a) radiation heat loss and (b) heat gain in the gas phase.

In order to access the mechanism of radiation heat exchange during the droplet combustion, the variations of radiation heat loss and heat gain along the radial direction are plotted in the Fig. 5.13 (a) and 5.13 (b) respectively at different time intervals. It can be observed from the Fig. 5.13 (a)-(b) that, the maximum

radiation heat loss is occurred at the flame zone due to high temperature and it varies with the temperature. However the more radiation heat gain is likely to be occurring towards the droplet surface. Radiation heat gain is maximum at the droplet surface. It also increases with the time as the droplet diameter decreases.

Influence of Initial Droplet Diameter at Different Ambient Temperature

In order to study the influence of initial diameter on the n-Heptane fuel droplet combustion, three different representative initial droplet diameters such as 1.0 mm, 1.5 mm and 2.0 mm are considered at two different ambient temperatures. Figures 5.14 and 5.15 show the typical variation of normalized droplet diameter square and the burning rate constant, K_b, with time at two different ambient temperature of 298.15 and 1093 K respectively. The results are compared with the experimental data of Xu et al. [79].
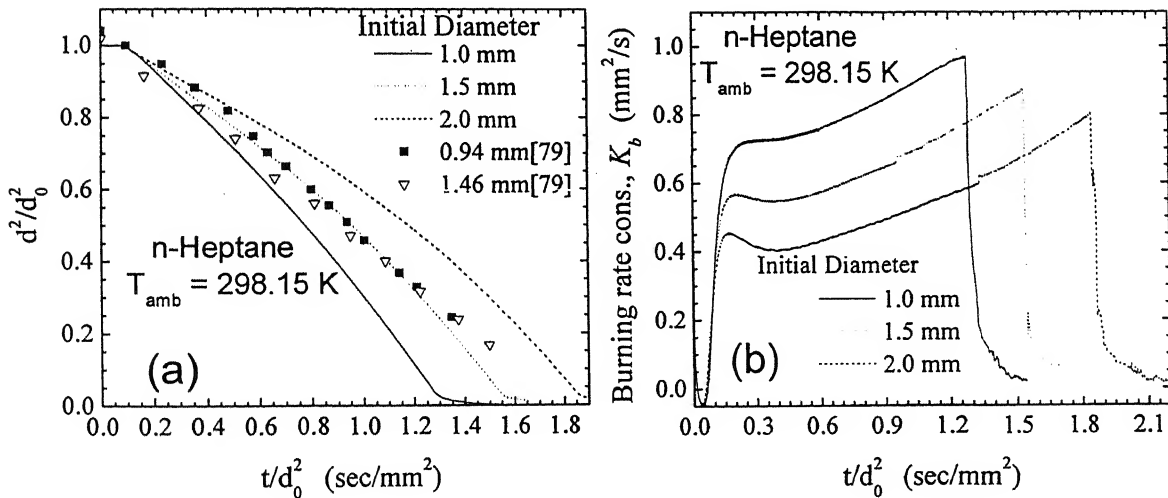
Fig.5.14: (a) d^2 law and (b) Burning rate constant for different droplet size (1.0 mm, 1.5 mm and 2.0 mm) at room temperature

It can be observed from the Fig. 5.14 that the burning rate decreases with the droplet diameter at low ambient temperature, 298.15 K. As a result the burning duration for complete combustion of droplet increases with the increase in droplet diameter. As the droplet diameter is increased the flame is located at a larger distance from the surface of the droplet. As a result, for a bigger droplet the heat loss from the flame surface to the ambient is likely to be more as compared to the smaller size droplet. Hence this is resulted in decrease in burning rate constant.
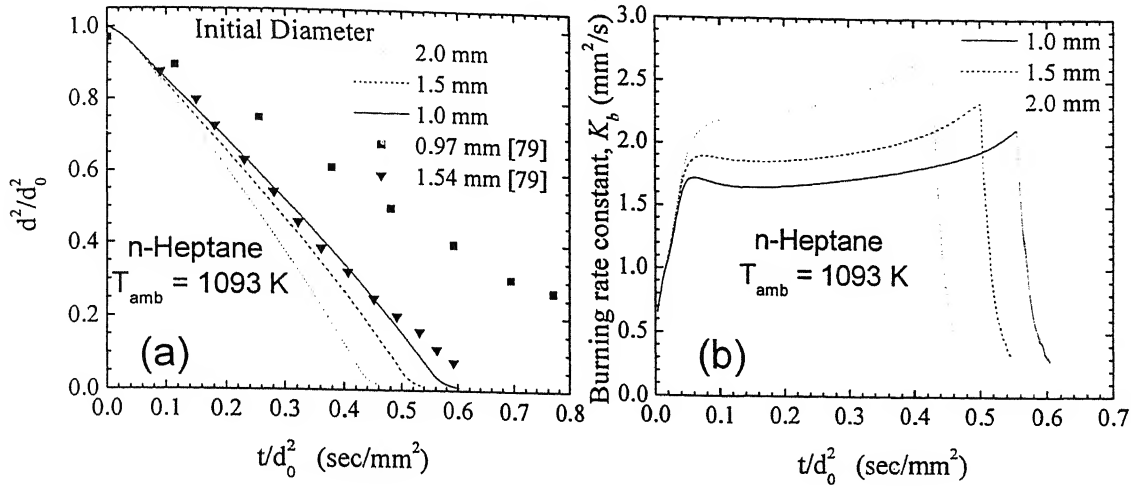
Fig.5.15: (a) d^2 law and (b) Burning rate constant for different droplet size (1.0 mm, 1.5 mm and 2.0 mm) at ambient temperature = 1093 K.

In contrast the predicted variation of burning rate at higher ambient temperature of 1093 K exhibits an opposite trend with increase in droplet diameter in comparison to the low ambient temperature case as shown in Fig. 5.15. Because at high temperature the heat gain from its surrounding is expected to be more as compared to the heat loss. This effect is more pronounced for bigger size droplet. Hence, the initial diameter effect has an opposite trend at high ambient temperature. Similar features can also be observed in the experimental data of Xu et al. [79].
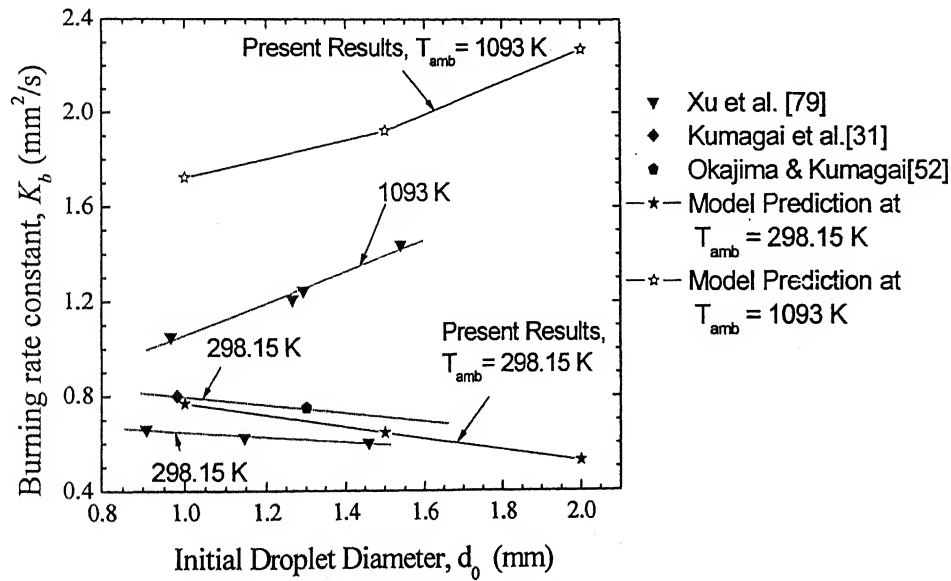
Fig. 5.16: Influences of initial droplet diameter on the average burning rate constant at different ambient temperature.

In order to compare the predicted burning rate constant with the experimental data available in the literature, the burning rate constant is averaged over the stable burning period and is plotted in Fig. 5.16 against the initial droplet diameter at two different ambient temperatures (298.15 K and 1093 K). The experimental data of Okajima & Kumagai [52], Kumagai et al. [31] and Xu et al. [79] are plotted in this figure. It can be observed that the present prediction matches well with the experimental data of Kumagai within the experimental error band. Although the experimental data of Xu et al. [79] exhibit the similar trend than that of the present numerical data and experimental data of Kumagai, but it is in the lower range. This difference may be caused by the heat loss to the support fiber of the fuel droplet. It can be noted that the Kumagai et al. conducted experiments using unsupported droplet and which may not have heat losses to the support fiber as compared to the data of Xu et al. [79]. Hence it is expected that the present prediction can match with the experimental data of Kumagai. This small difference may be due to consideration of gray gas radiation model and the finite rate chemistry. In contrast, the present predicted data at high temperature does not match well with the experimental data of Xu et al. [79]. However its trend is qualitatively similar to the experimental data.
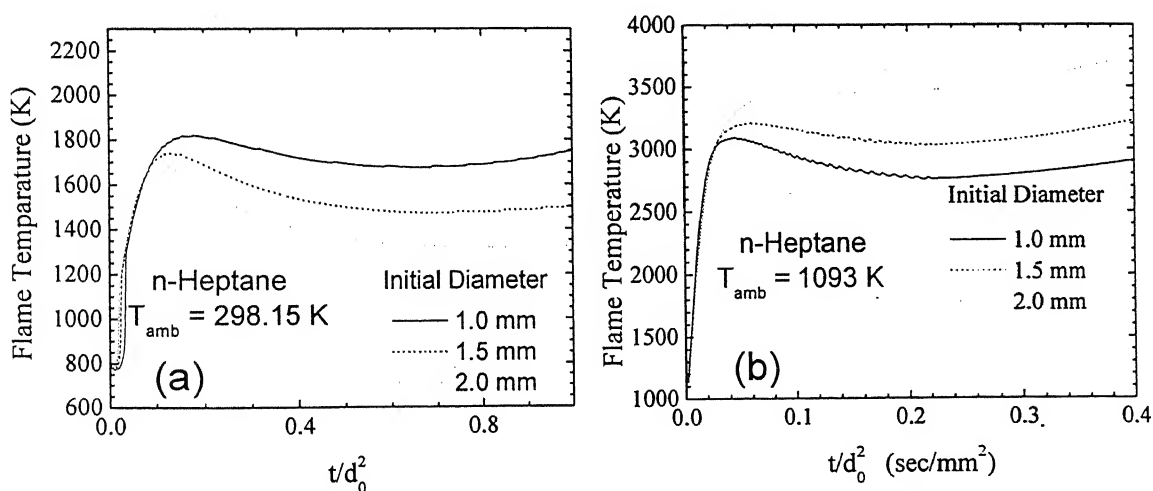
Fig.5.17: Transient variation of flame temperature for **(a)** ambient room temperature and **(b)** ambient temperature = 1093 K.

In order to investigate the present anomalies between the predicted data and the experimental data of Xu et al. [79] at the high temperature, the variation of the flame temperature during droplet burning is plotted in Fig. 5.17 (b) with different

initial droplet diameter. It can be observed from the Fig. 5.17(b) that at high ambient temperature the flame temperature become very high almost from 2800 K to 3600 K for droplet diameter of 1.0 to 2.0 mm. The predicted flame temperature seems to be quite high which may not be possible in the actual situation due to occurrence of endothermic dissociation reaction. However the present model does not contain the dissociation reactions which need to be included to predict this aspect.

The variations of flame temperature with time for three different initial droplet diameters are plotted in Fig 5.17 (a) at ambient temperature. It can be observed from Fig. 5.13 (a) that, the flame temperature is found to be decreased with the droplet diameter. In contrast the flame temperature increases with the diameter at high ambient temperature of 1093 K as shown in Fig. 5.17(b). This increase in flame temperature is expected to enhance the burning rate of the fuel droplet, which was discussed earlier at length.

5.2. Multicomponent Fuel Droplet Combustion

In modern days, practical fuels, used in combustion devices are blends of several hydrocarbons with different chemical and physical properties. The properties of such kind of fuels can be approximated with two hydrocarbons with different volatilities. Hence, the present study is carried out with a binary fuel consists of n-Heptane and n-Decane. Special efforts are made on the transient analysis of temperature, species mass fraction profile for both the gas phase and liquid phase by varying the initial fuel compositions. Transient variations of the surface parameters are very important to study in the case of multicomponent fuel droplet combustion. It has been considered in the literature that internal circulation takes place inside the droplet. Hence, the distillation curve model is being used in the present study by assuming the occurrence of proper mixing of fuels inside the droplet. The following subsections are devoted to discuss the results of multicomponent fuel droplet combustion.

5.2.1. Effect of Composition on Burning Parameters

In the present section the influences of the compositions of the binary fuel on the droplet burning are discussed. The droplet diameter square is plotted in Fig. 5.18 (a) with the time with variation in fuel compositions. It can be observed from this figure that burning rate and total time required for binary fuel droplet combustion vary as the composition of fuel components are changed. Average burning rate constant is found to be enhanced with the increase in high volatile fuel composition as per expectation. Although the pure fuel droplet combustion exhibit classical d^2 law behavior but results of binary fuel droplet with variation in compositions does not seem to follow the d^2 law behavior.
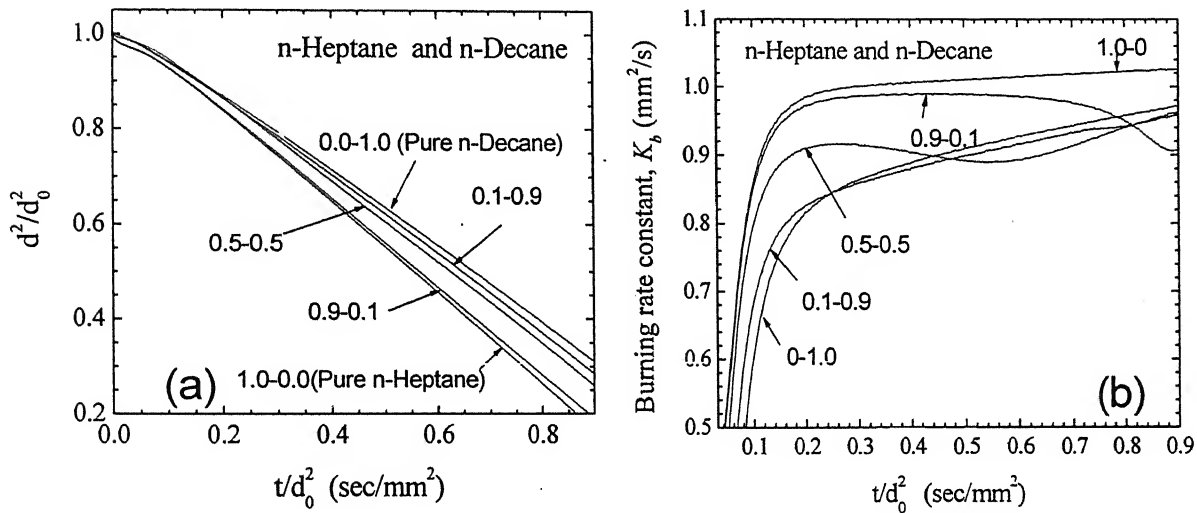
Fig.5.18: Effect of initial compositions of n-heptane and n-decane on **(a)** d^2 law and **(b)** Burning rate constant K_b.

To understand the burning rate behavior in details, the burning rate constant, K_b with the variation in fuel compositions is plotted with the time in Fig. 5.18 (b). A typical behavior corresponding to the binary fuel with compositions of 50% n-Heptane-50% n-Decane can be observed from this figure. Initially the burning rate constant, K_b increases very sharply in the initial preheat period. During this period droplet surface temperature also increases and attains a stable value. The vaporization of the high volatile substances is likely to be more than the less volatile fuel. It can be observed from the Fig. 5.18 (b) that the burning rate attains almost a peak value after the initial preheat period during which the vaporization of high volatile fuel is likely to occur at a faster rate. After certain time the high

volatile fuel will be depleted quickly. Then the burning rate constant starts decreasing and attains its minimum value. During this time both the components of the binary fuel droplet attains the same gasification rate as shown in Fig. 5.19. It can be noted that the surface temperature attains an inflection point at this time. Subsequently, the burning rate starts increasing due to the higher gasification rate of n-Decane fuel as shown in Fig. 5.19. It can also be observed in Fig. 5.19 that the surface temperature increases monotonically towards the boiling point temperature.

Fig.5.19: Transient variations of the Surface Parameters for n-Heptane and n-Decane fuel mixture of compositions ratio 50%-50%.

In case of briny fuel droplet with composition of 90% n-Heptane-10% n-Decane, the burning rate constant attains its minimum value towards the end of the burning as shown in Fig. 5.20 (a). As concentration of the high volatile n-Heptane fuel is higher than the low volatile n-Decane fuel, it is expected that the burning of n-Heptane fuel will dominant for longer period of time maintaining a lower temperature at its surface. As a result, n-Decane fuel can play an important role during the combustion of binary fuel after the complete consumption of n-Heptane fuel, which can be seen in Fig.5.20 (a). Thus the surface temperature increases at a faster rate towards the boiling point temperature of n-Decane fuel. As a result the burning rate drops down as shown in Fig. 5.20 (a).

However, in case of binary fuel, composed of 10% n-Heptane–90% decane n-Heptane gets vaporizes initially and gets depleted within short period of time. The

gasification rate of the heptane is found to be decreased with time as the percentage of n-Heptane is decreased in binary fuel. However the vaporization rate of n-Decane is predicted to be higher than the n-Heptane due to higher percentage of n-Decane in binary fuel. The temperature at droplet surface keeps increasing as shown in Fig. 5.20 (b) till n-Heptane fuel gets vaporized completely and then it maintains almost a constant value. As a result the burning rate increases with the time.

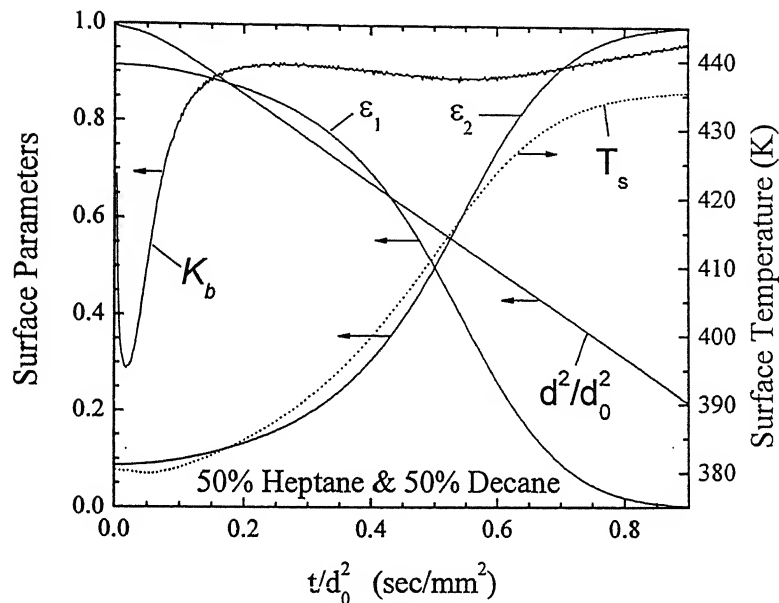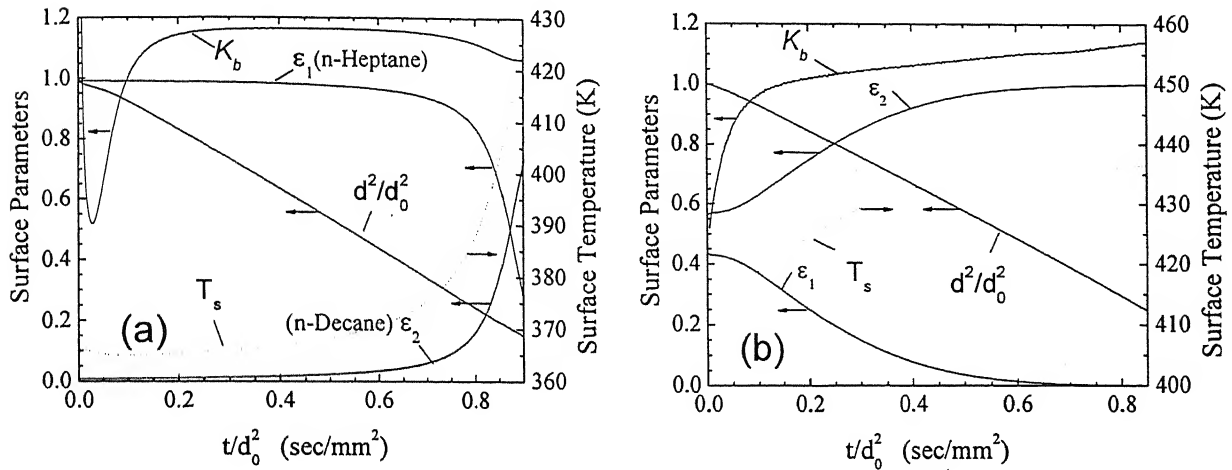**Fig.5.20:** Transient variations of the Surface Parameters for n-Heptane and n-Decane fuel mixture of compositions ratio of **(a)** 90%-10% and **(b)** 10%-90%.

Fig.5.21: Effect of initial compositions of n-heptane and n-decane on **(a)** droplet surface temperature and **(b)** variation in the droplet surface temperature with time.

The transient variations of droplet surface temperature are plotted in Fig. 5.21 (a). Depending on its compositions, the droplet surface temperature increases from a stable value towards the higher boiling point temperature (n-Decane). The temperature variation rate at the droplet surface is plotted in Fig. 5.21(b) with normalized time for binary fuel with representative composition. It can be observed that the temperature variation rate attains a maximum value after certain time from the initiation of droplet burning. Its peak moves forward and is increased in magnitude with the increase in the high volatility component in the binary fuel droplet. Interestingly, the temperature variation rate becomes steeper with increase in the high volatile component indicating that surface temperature increases at a faster rate towards the end of the burning.

The effects of the fuel compositions on the droplet center temperature are plotted in Fig.5.22 (a) with normalized time. For pure n-Heptane and n-Decane the droplet center temperature increases monotonically towards their respective boiling point temperature. The temperature variation rate at the center of droplet is plotted in Fig. 5.22 (b) for representative fuel compositions. It can be noted that the slope of temperature profile for the binary fuel droplet gets varied due to change in its surface temperature. A sharp change can be noticed towards end of burning for fuel composition of 90% n-Heptane-10% n-Decane. However for the fuel composition of 50% n-Heptane-50% n-Decane, the change in the slope is occurred almost in the middle of the droplet burning.
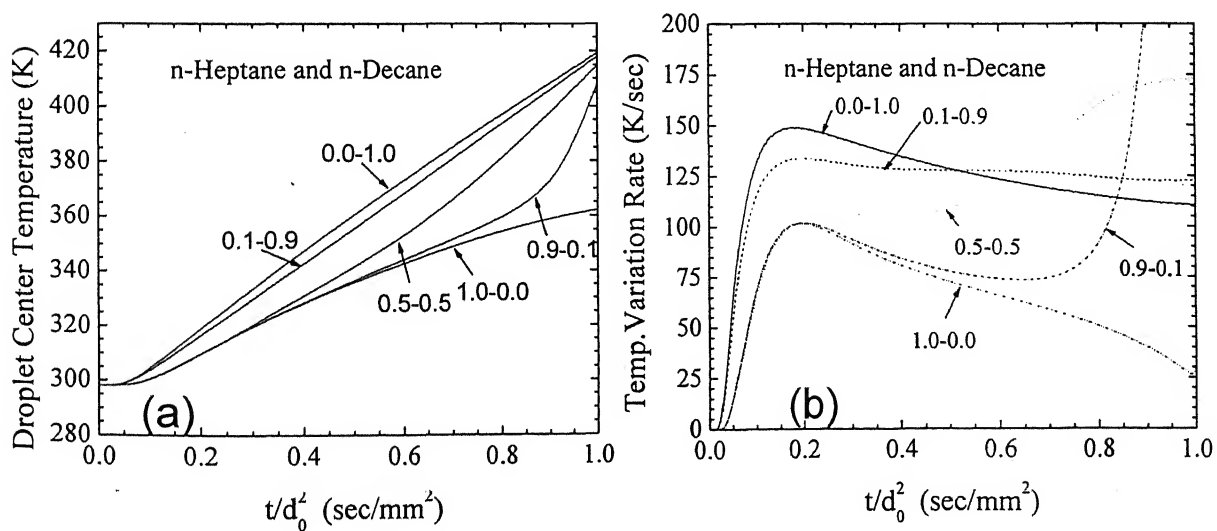
Fig.5.22: Effect of initial compositions of n-heptane and n-decane on **(a)** droplet center temperature and **(b)** variation in the droplet center temperature with time.

Furthermore, the fractional mass gasification rate for n-Heptane and n-Decane are plotted in Fig. 5.23 (a) and (b) respectively. The fractional mass gasification va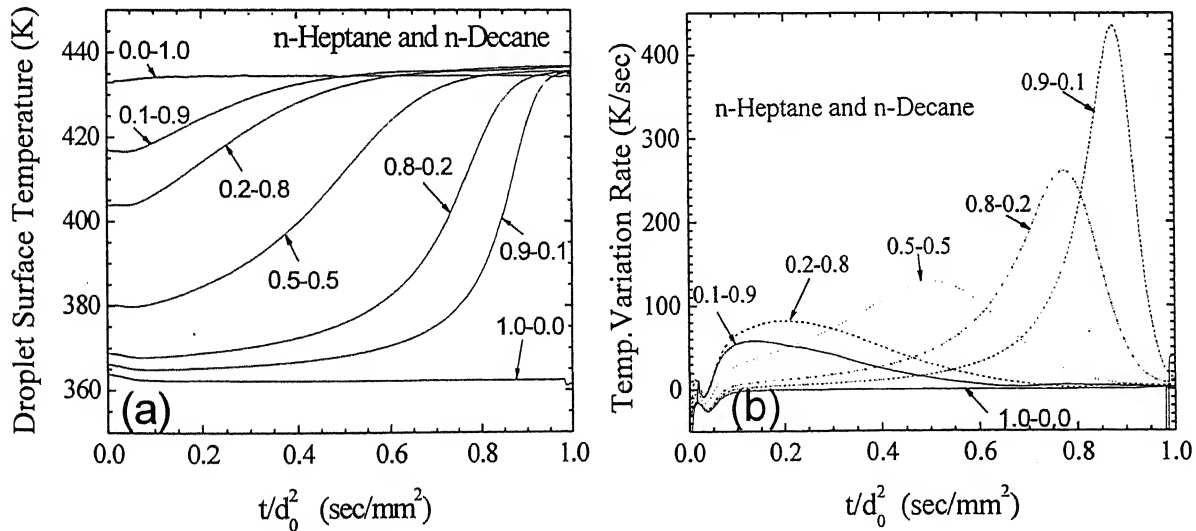riations rates for n-Heptane and n-Decane are plotted in Fig. 5.24 (a) and 5.24(b) respectively. It can be observed from the Fig. 5.23(a) that the fractional mass gasification rate for n-Heptane decreases with its concentration. In contrast, the fractional mass gasification rate for n-Decane increases with its concentration. Similar features can be also observed in the temporal variations of mass fractions as plotted in Fig. 5.25 (a) and (b).
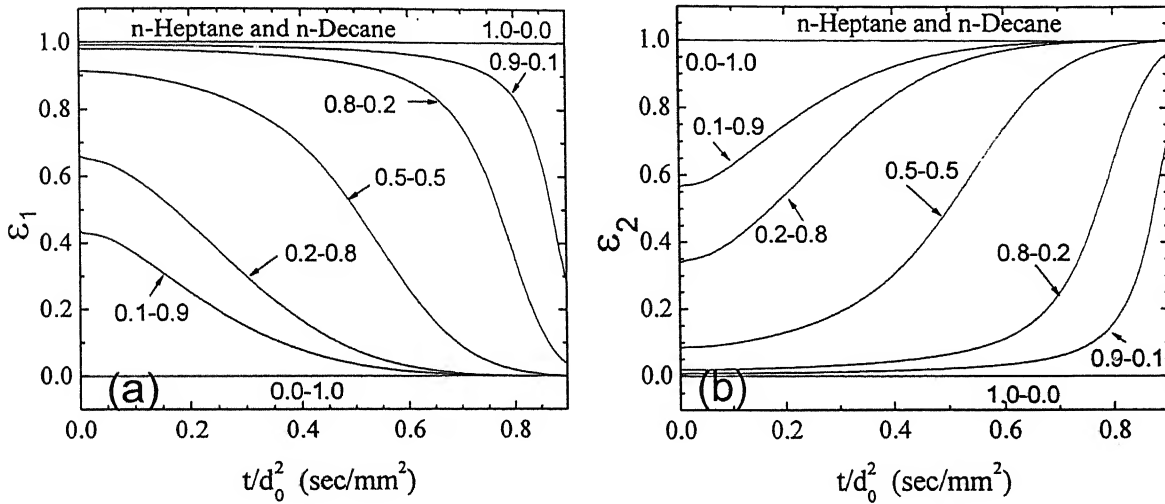
Fig.5.23: Effect of initial compositions of n-heptane and n-decane on fractional mass gasification rate for **(a)** n-Heptane and **(b)** n-Decane.
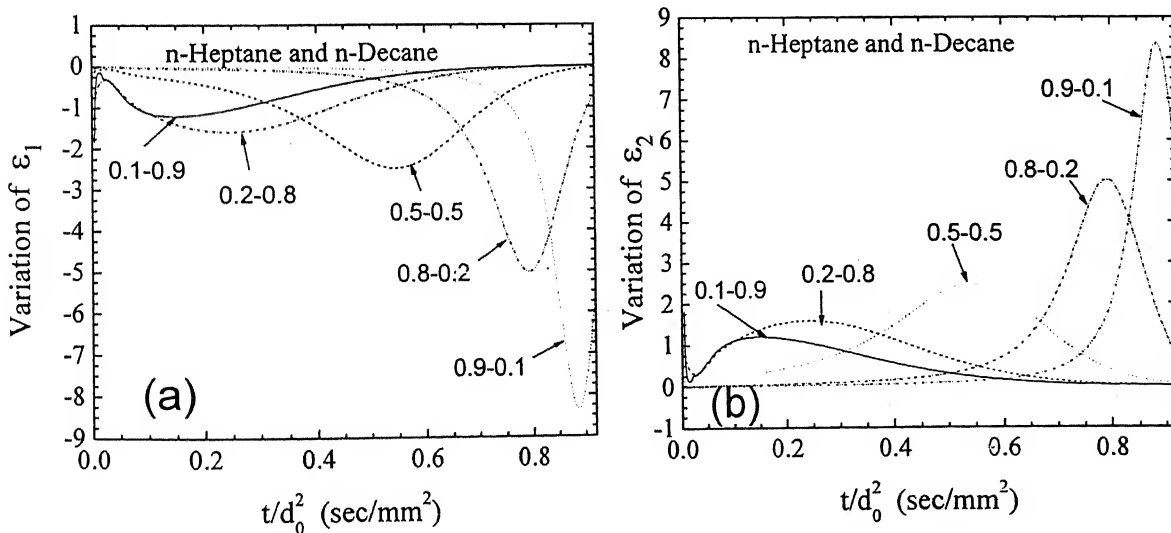
Fig.5.24: Effect of initial compositions of n-heptane and n-decane on rate of change of fractional mass gasification rate for **(a)** n-Heptane and **(b)** n-Decane.

Since the boiling point temperature of n-Heptane is less than n-Decane, the gasification of n-Heptane is expected to occur at higher temperature. Initially more amount of n-Heptane is likely to be gasified and its mass fraction inside the droplet gets decreased at faster rate. As a result, the gasification rate is decreased further leading to the complete depletion of n-Heptane fuel. Subsequently the n-Decane fuel gets gasified at higher surface temperature of the droplet.
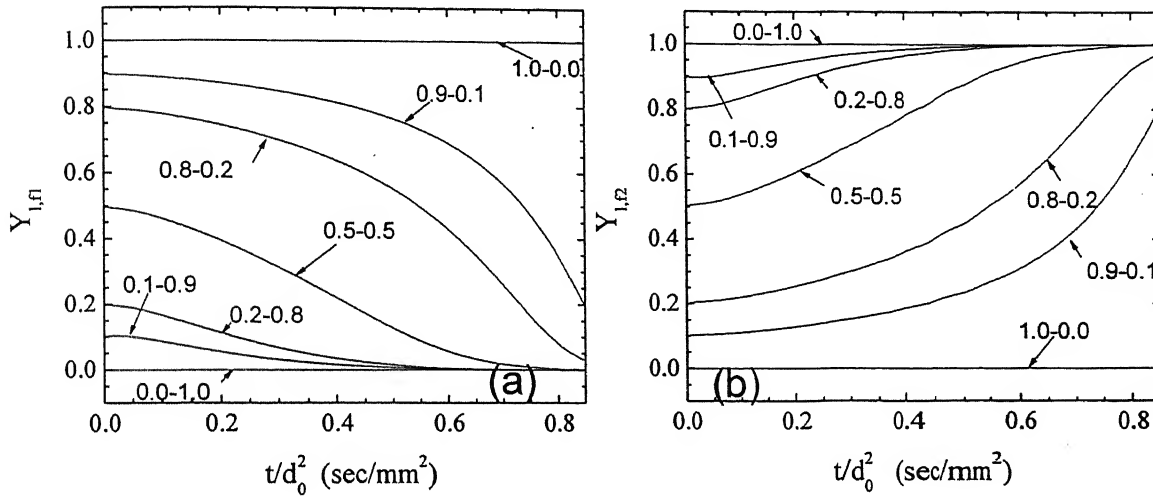
Fig.5.25: Effect of initial compositions of n-heptane and n-decane on liquid phase mass fractional profiles for (a) n-Heptane and (b) n-Decane.

Chapter 6

CONCLUSIONS

6.1. Conclusions

In this work the spherical symmetric combustion of single isolated fuel droplet has been investigated both experimentally and numerically. Experimental investigation of droplet combustion for both single and binary fuel has also been performed under normal gravity condition at ambient pressure and temperature. In order to simulate isolated droplet combustion, one dimensional, unsteady governing equations are solved numerically using Finite Difference Method. In present computation a single step chemistry model is employed. In this CFD code variable properties and gray gas model for radiation heat transfer have been considered. The effect of ambient oxygen level and effect of radiation heat transfer on the burning parameter at different temperatures have been studied extensively. The influence of initial droplet diameter on the droplet burning rate is also investigated. Besides this, the multicomponent fuel droplet combustion is simulated using Distillation Curve Model. The major conclusions of the present study are as follows;

Conclusions from the Experimental Data:

1.   Both the single and multicomponent fuel droplet combustion follow the classical d^2 law behavior under normal gravity at ambient pressure and temperature.

2.   Initially flame envelops increases and subsequently diminishes with time.

3.   The slope of the d^2 law curve known as the burning rate constant, K_b are found to be almost constant for both single and multicomponent fuel droplet combustion.

4.   The burning rate constant, K_b for both n-Heptane and n-Decane is found to be 1.12 and 1.03 respectively. For binary fuel droplet with composition of 50% n-Heptane and 50% n-Decane, the burning rate constant, K_b is found to be 1.1.

Conclusions from the Numerical Studies:

1. The burning rate of n-Heptane fuel droplet at normal ambient conditions is predicted to be higher than the existing experimental data. This discrepancies is attributed the considerable radiation heat transfer from the high temperature flame zone to its surrounding. Hence a suitable radiation model is thought to be included in the present code.

2. Initially, the flame standoff distance is found to be increased and subsequently diminishes with time. This phenomenon is commensurate to our experimental data. The flame stand-off ratio varies within 11-28. But in the literature the experimental flame standoff ratio is reported to be within 4-10. To predict the flame standoff ratio accurately radiation heat transfer model and multi step kinetics chemistry model may be required.

3. The present numerical prediction indicates that the burning rate gets enhanced with increase in ambient oxygen concentration level. The increase in the ambient oxygen concentration level is found to enhance the reaction rate, resulting in an increase in flame temperature. The heat transfer from the flame zone to the droplet surface causes the enhancement of gasification rate.

4. The flame stand-off ratio is found to be increased with the ambient oxygen level. This is in contradiction with the classical quasi-steady theory. These anomalies may be due to fact that the classical theory does not take account of the gas phase velocity, which is the determining factor in predicting the flame standoff ratio.

5. The gray gas model for radiation heat transfer is incorporated in the present code. As a result, the numerical prediction improves considerably in accordance with the experimental data. The predicted flame temperature is found to be closer to the experimental data with the inclusion of radiation heat transfer model. The burning rate data also matches well with the existing experimental data.

6. It is found out that the radiation heat transfer plays a predominant role in determining the burning rate particularly for bigger droplet. As the droplet diameter decreases the heat loss from the flame surface decreases leading to the rise in burning rate.

7. By varying the initial droplet diameter, it is found out that burning rate diminishes at ambient temperature. In contrast, an opposite trend in burning rate is observed at high ambient temperature. The present predicted data at low ambient temperature matches well with the experimental data of Xu et al [79]. However, at high ambient temperature the present prediction seems to match only qualitatively with the experimental data. The prediction may be improved by inclusion of dissociation reactions in the present model.

8. During the burning of multicomponent fuel droplet, a slight variation from the classical d^2 law is observed. The burning rate and total time for burning varies with the composition of the droplet.

9. Depending on the composition of fuel, the variation in the burning rate constant is observed. During the course of burning it has been observed that the droplet surface temperature is increased from a low value to a high value corresponding to the boiling point temperature of respective constituents in the binary fuel.

10. Initially the high volatile fuel is found to be getting consumed at a faster rate in comparison to low volatile fuel. It has been observed that the fractional mass gasification rate for n-Heptane decreases with its concentration. In contrast, the fractional mass gasification rate for n-Decane is found to be increased with its concentration.

6.2. Recommendations for Further Studies

During this work it has been observed that there are many issues that need further investigation. Some of them are listed below. ·

i) Multi-step chemistry model is to be incorporated in the computer code to improve its prediction.

ii) Droplet combustion at super critical pressure.

iii) The interaction between the droplets can be investigated.

iv) The model for multicomponent fuel droplet combustion can be improved further.

v) Soot production and soot radiation study may be carried out.

vi) High temperature dissociation effect can be considered.

Appendix A

Liquid and Gas Phase Thermal and Transport Properties Calculation

1. Gas Phase Properties

(a) Density:

The density of the gas mixture, ρ, has been obtained from the equation of state:

$$\rho = \frac{P \sum Y_{g,i} m_i}{R_u T} \qquad (A.1)$$

where, P is pressure; $Y_{g,i}$ is mass fraction of species i; m_i is molecular weight of species i, and R_u is universal gas constant.

(b) Specific Heat

The specific heat of the gas mixture has been estimated assuming it to be an ideal gas mixture of CO_2, H_2O, O_2, N_2 and fuel vapor. The specific heat, C_P, of mixture can be calculated by using the following relation.

$$C_P = \sum_{i=1}^{N} Y_i C_{P,i} \qquad (A.2)$$

The specific heat of component can be calculated from the curve-fit correlation. The data is taken from Sandia database and Toulokian et al. [72]. Then verify the data with Virgoftik [74].

$$\frac{C_{P,g}}{R_u} = \left(C_0 + C_1 T_g + C_2 T_g^{\,2} + C_3 T_g^{\,3} + C_4 T_g^{\,4} \right) \quad \text{for} \quad CO_2, H_2O, O_2, N_2 \quad (A.3)$$

$$C_{P,g}(J/kg\,K) = (C_0 + C_1 T_g + C_2 T_g^{\,2} + C_3 T_g^{\,3} + C_4 T_g^{\,4}) \times 4187 \quad \text{for fuel vapors} \quad (A.4)$$

The value of the coefficient C_0, C_1, C_2, C_3 and C_4 are listed in table A.1. The plot of the Specific Heat with time is shown in Fig. A.1.

Table A.1: Constants for the calculation of constant pressure specific heat.

Species	Temp. Range(K)	C_0	C_1	C_2	C_3	C_4
C_7H_{16}	300 - 800	0.0254671	1.37666e-3	-4.0004e-7	-1.1331e-10	0.0
C_7H_{16}	800 - 2000	0.0982018	1.30398e-3	-5.92804e-7	1.0105e-10	0.0
$C_{10}H_{22}$	300 - 780	0.1273	8.9679e-4	4.2932e-7	-5.1068e-10	0.0
$C_{10}H_{22}$	780 - 2000	0.0188191	1.5129e-3	-6.7117e-7	1.1236e-10	0.0
O_2	200 - 1000	3.2825	1.483e-3	-7.579e-7	2.0947e-10	-2.167e-14
O_2	1000 - 3500	3.7824	-2.9967e-3	9.847e-6	-9.6813e-9	3.2437e-12
CO_2	200 - 1000	3.8574	4.414e-3	-2.2148e-6	5.2349e-10	-4.7208e-14
CO_2	1000 - 3500	2.3567	8.9846e-3	-7.1235e-6	2.459e-9	-1.437e-13
H_2O	200 - 1000	3.03399	2.1769e-3	-1.640e-7	-9.704e-11	1.682e-14
H_2O	1000 - 3500	4.1986	-2.0364e-3	6.5204e-6	-5.4879e-9	1.772e-12
N_2	300 - 1000	2.9266	1.4879e-3	-5.684e-7	1.0097e-10	-6.7533e-15
N_2	1000 - 5000	3.2986	1.40824e-3	-3.9632e-6	5.6415e-9	-2.4448e-12
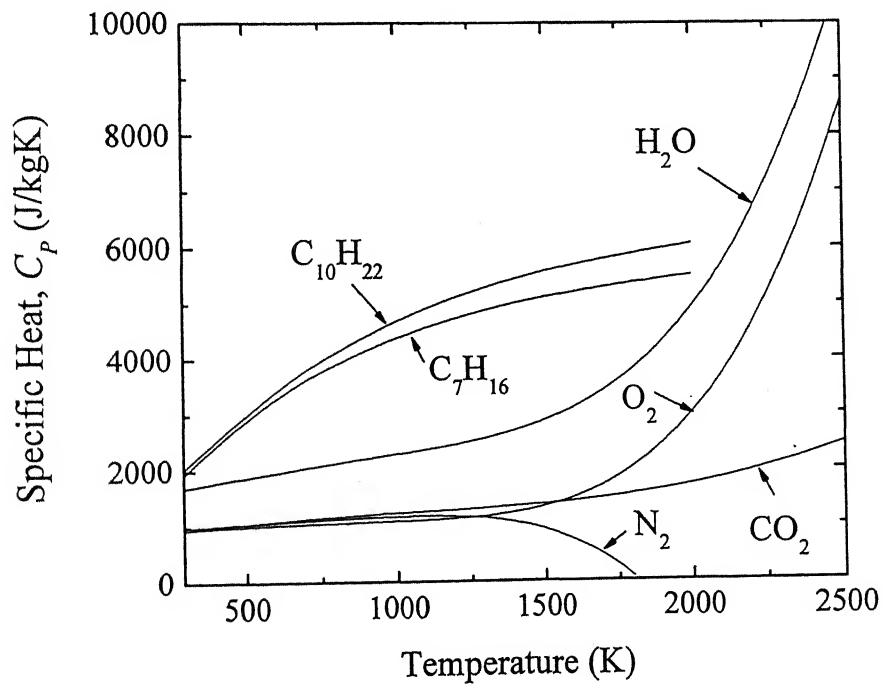
Fig.A.1: The variation of Specific Heat of Different Species with Gas Phase Temperature.

(c) Thermal Conductivity

Gas mixture thermal conductivity has been calculated by using Wassiljewa equation (1904) and Masomn and Sexana modification (1958), which has been recommended for both polar and non-polar gas mixtures (Reid et al. [59]).

$$\lambda_m = \sum_{i=1}^{N} \frac{X_i \lambda_i}{\sum_{j=1}^{N} X_j A_{ij}} \tag{A.5}$$

where, λ_m is the thermal conductivity of the gas mixture, λ_i thermal conductivity of pure componet i. X_i is the mole fraction of the component i. A_{ij} can be found out from the Mason and Saxena (1958) modification.

$$A_{ij} = \frac{\left[1 + \left(\frac{\lambda_i}{\lambda_j}\right)^{0.5} \left(\frac{m_i}{m_j}\right)^{0.25}\right]^2}{\left[8\left(1 + \frac{m_i}{m_j}\right)\right]^{0.5}} \tag{A.6}$$

where, m_i, m_j are the molecular weight of components i and j.

Table A.2: Constants for the calculation of Thermal conductivity (W/m s).

Species	C_0	C_1	C_2	C_3	C_4
C_7H_{16}	4.7317e-3	-4.3918e-8	2.8322e-7	-1.8841e-10	3.8818e-14
$C_{10}H_{22}$	3.9817e-3	-3.0918e-8	2.8352e-7	-1.8841e-10	3.882e-14
O_2	1.3708e-3	9.2262e-5	-2.8054e-8	6.3322e-12	-2.299e-16
CO_2	1.2528e-3	1.8145e-5	1.4728e-7	-1.3644e-10	3.7908e-14
H_2O	2.0878e-2	-9.4108e-5	3.6958e-7	-2.7724e-10	6.7850e-14
N_2	3.7894e-3	8.1514e-5	-2.339e-8	-3.2294e-12	4.3092e-15

The thermal conductivity of the pure component can be obtained by taking data from Toulokian et al. [72] and finding out curve-fit correlation.

$$\lambda_{g,i}(W/m\cdot s) = (C_0 + C_1 T_g + C_2 T_g^2 + C_3 T_g^3 + C_4 T_g^4) \tag{A.7}$$

The value of the coefficient C_0, C_1, C_2, C_3 and C_4 for thermal conductivity are listed in table A.2. The variations of thermal conductivity with the temperature

for different species have been plotted in Fig. A.2.
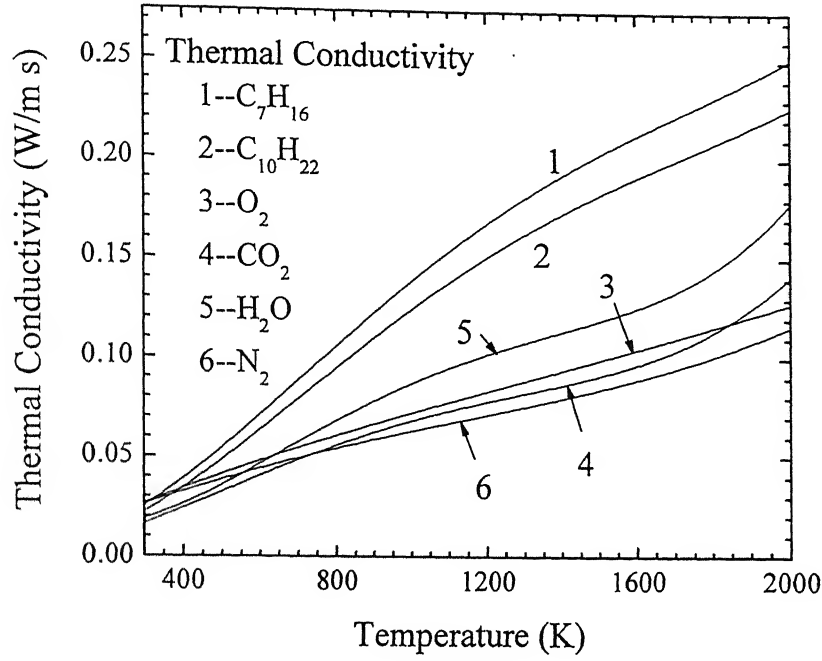
Fig. A. 2: The variation of Thermal Conductivity of Different Species with Gas Phase Temperature.

(d) Diffusion Coefficient

Diffusion coefficient of any component, D_i, in the mixture can be calculated as follows (Wilke, 1950)

$$D_i = \frac{1-X_i}{\sum_{j=1\neq i}^{N} \frac{X_j}{D_{ij}}} \tag{A.8}$$

The binary gas diffusion, D_{ij}, has been calculated from the following expression (Hirschfelder [22])

$$D_{ij} = 262.8 \times 10^{-9} \frac{\sqrt{T^3 \frac{(m_1 + m_2)}{2 m_1 m_2}}}{P \sigma_{ij}^2 \Omega_D} \tag{A.9}$$

where, P is the pressure in bar, m_1 and m_2 are the molecular weight of the components. σ_{ij} is the collision diameter in A, $\sigma_{ij} = 0.5(\sigma_i + \sigma_j)$. Ω_D is the collision integral, defined as Perry [56]

$$\Omega_D = \left(44.54 \times T_{ij}^{*-4.909} + 1.911 \times T_{ij}^{*-1.575}\right)^{0.1} \tag{A.10}$$

where, $T_{ij}^* = \sqrt{T_i^* T_j^*}$, and $T_i^* = \dfrac{T}{\in_0 / k}$. The value of σ_i and $\in_0 / k$ taken from Sandia

Database is tabulated in Table A.3.

Table A.3: Constants for the calculation of Transportation Data

Species	C_7H_{16}	$C_{10}H_{22}$	O_2	CO_2	H_2O	N_2
σ_i (A)	6.253	7.229	3.458	3.763	2.605	3.621
$\in_0 / k$ (K)	459.6	600.6	107.4	244	572.4	97.530

2. Liquid Phase Properties

The Liquid phase properties, density, specific heat and thermal conductivity have been calculated using curve-fit correlations given in Touloukian et al. [72] and checked from the experimental data given in Vargaftik, [74].

(a) Density

For calculating the density for n-Heptane and n-Decane following correlations are used respectively.

$$\rho_l (kg / m^3) = 720.0 - 0.892(T_l - 253.0) \qquad \text{for n-Heptane} \quad \text{(A.11)}$$

$$\rho_l (kg / m^3) = 923.4 - 0.5587 \times T - 0.0003 \times T^2 \qquad \text{for n-Decane} \quad \text{(A.12)}$$

(b) Specific Heat

Correlation used for specific heat of liquid is

$$C_{p,l}(J / kg\,K) = (C_0 + C_1 T_l + C_2 T_l^2 + C_3 T_l^3) \times 4187 \tag{A.13}$$

The values of the coefficients are as follows:

For n-Heptane this correlation is valid between 230K to 480K and

$$C_0 = 0.454958, \quad C_1 = -3.46073 \times 10^{-4}, \quad C_2 = 2.1482 \times 10^{-6}, \quad C_3 = -2.48653 \times 10^{-3}$$

For n-Decane this correlation is valid between 283 K to 493 K and

$$C_0 = 0.581718, \quad C_1 = -8.44526 \times 10^{-4}, \quad C_2 = 1.21946 \times 10^{-6}, \quad C_3 = 3.37247 \times 10^{-9}$$

(c) Thermal Conductivity

The following correlations are used to obtain the thermal conductivity for n-Heptane and n-Decane respectively

$$\lambda_l(J/mK) = (466.94 - 0.54892 \times T_l) \times 4.187 \times 10^{-4} \qquad \text{(A.14)}$$

$$\lambda_l(J/mK) = (564.599 - 0.781586 \times T_l) \times 4.187 \times 10^{-4} \qquad \text{(A.15)}$$

These correlations are gives substantially accurate values from 290 to 370 K and 230 K to 450 K respectively, and outside these range uncertainty increases. As our domain of interests is within these, these correlations are acceptable.

(d) Latent Heat of Vaporization

Latent heat of evaporation is a function of the surface temperature, T_d, at low pressure, is approximated by the following equation taken from Perry [55] and checked with Vargaftik [74].

$$L(J/kg) = C_0(T_C - T_d)^{C_1} \qquad \text{(A.16)}$$

where, T_C is the critical temperature, for n-Heptane and n-Decane 540.2K and 617.7K respectively. C_0 and C_1 are the two coefficients. For n-Heptane $C_0 = 55.53 \times 10^3$, $C_1 = 0.3436$ and for n-Decane $C_0 = 36.02 \times 10^3$, $C_1 = 0.39797$.

3. Radiative Properties (Planck Mean Absorption Coefficient)

The Planck Mean Absorption Coefficient of CO_2 and H_2O, k_{CO_2} and k_{H_2O}, have been determined by the curve-fit data taken from RADCAL program 1993 [19] as sited in http://www.ca.sandia.gov/TNF/radiation.html. These curve fits were generated for temperatures between 300K and 2500K and may be very inaccurate outside this range.

$$k_{P,g} = C_0 + C_1 \times (1000/T_g) + C_2 \times (1000/T_g)^2 + C_3 \times (1000/T_g)^3$$
$$+ C_4 \times (1000/T_g)^4 + C_5 \times (1000/T_g)^5 \qquad \text{(A.17)}$$

The values of the Coefficients are given in Table A.4. The Planck Mean Absorption Coefficients for CO_2 and H_2O are plotted in Fig. A.4.

`Table A.4: Constants for the Calculation of Planck Mean Absorption Coefficient

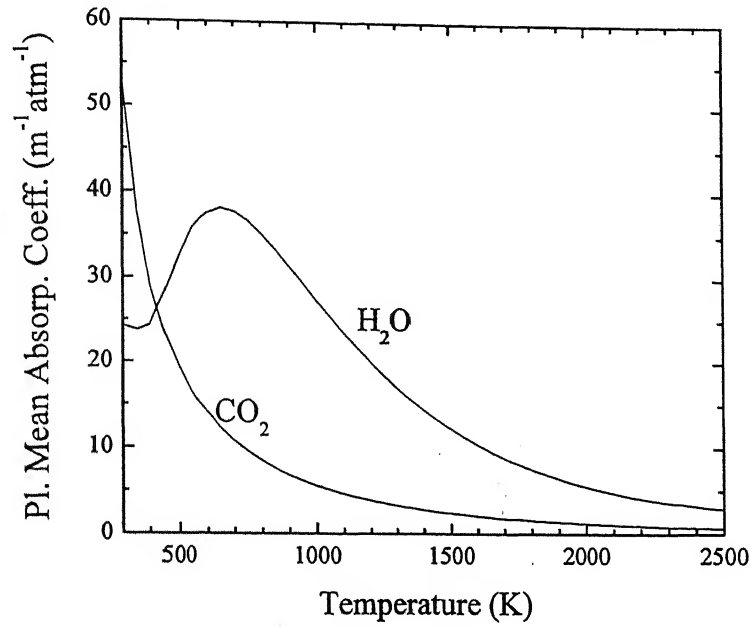| Coefficients	C_0	C_1	C_2	C_3	C_4	C_5
CO_2	18.741	-121.310	273.5	-194.05	56.310	-5.8169
H_2O	-0.23093	-1.12390	9.41530	-2.99880	0.51382	-1.8684e-5

Fig.A.3: Planck Mean Absorption Coefficients for H_2O and CO_2.

BIBLIOGRAPHY

[1] Abdel-Khalik, S.I., Tamaru, T., and El-Wakli, M., "A chromatographic and interferometer study of the diffusion flame around a simulated fuel drop", *Fifteenth Symposium (International) on Combustion,* 1975, pp. 389-399.

[2] Anderson, J.D.(Jr.), "Computational Fluid Dynamics", *Mcgraw-Hill International editions,* 1995.

[3] ASME Boiler and Pressure Vessel Design Handbook, American National Standard, 1975.

[4] Baek, S.W., Park, J.H., and Choi, C.E.,"Investigation of droplet combustion with nongray gas radiation effects", *Combustion Science and Technology,* Vol.142, 1999, pp.55-79.

[5] Beer, J.M., and Howarth, C.R., "Radiation from flames and furnaces", *Twelfth Symposium (International) on Combustion,* 1969, pp.1205-1217.

[6] Burger, M., Schmehl, R., Prommersberger, K., Schafer, O., Koch, R., and Wittig, S., "Droplet evaporation modeling by the distillation curve model: accounting for kerosene fuel and elevated pressures", *Int. J. of Heat and Mass Transfer,* 46, 2003, pp- 4403-4412.

[7] Chervinsky, A.,"Supercritical burning of liquid droplet in stagnant environment", *AIAA J.,* Vol. 7, 1968, pp. 1815-1817.

[8] Chio, M. Y., and Dryer, F. L., "Microgravity Droplet Combustion", *Microgravity Combustion: Fire in free fall,* Academic Press, 2001, pp. 183-297.

[9] Chiu, H.H., "Advances and challenges in droplet and spray combustion. I. Toward a unified theory of droplet aero-thermo-chemistry", *Progress in Energy and Combustion Science,* Vol. 26, 2000, pp. 381-416.

[10] Cho, S.Y., Yetter, R.A., and Dryer, F.L., "A computer model for one-dimensional mass and energy transport in and around chemically reacting particles, including complex gas-phase chemistry, multicomponent molecular diffusion, surface evaporation, and heterogeneous reaction", *Journal of Computational Physics,* 102, 1992, pp. 160-179.

[11] Delplanque, J.P., and Sirignano, W.A., "Numerical study of the transient vaporization of an oxygen droplet at sub and supercritical conditions", *Int. J. of Heat and Mass Transfer,* Vol. 36, No. 2, 1993, pp.303-314.

[12] Egawa, T., Kawakami, S., Okajima, S., "Pressure effects om combustion of fuel droplets under zero gravity", *Archivum Combustionis,* Vol.6.No.1, 1986, pp.51-59.

[13]   Faeth, G.M., Dominicis, D.P., Tulpinsky, J.F., and Olson, D.R., "Supercritical bipropellant droplet combustion", *Twelfth Symposium (International) on Combustion*, 1969, pp.18.

[14]   Faeth, G. M., *AIAA Paper* A70-18141, 1970.

[15]   Ghenai, C., Smith, O.I., and Karagozian, A.R., "Acoustical excitation of burning fuel droplets", *39th AIAA Aerospace Sciences Meeting and Exhibit, January 2001, Reno, Nevada*, 2001.

[16]   Givler, S.D., and Abraham, J., "Supercritical droplet vaporization and combustion studies", *Progress in Energy and Combustion Science*, Vol. 22, 1996, pp. 1-28.

[17]   Glassman, I., "Combustion" 3rd edition, *Academic Press*, Orlando, 1995.

[18]   Godsave, G. A. E., "Studies of the combustion of drops in the fuel spray - The burning of single drop of fuel", *Fourth Symposium (International) on Combustion*, 1953, pp. 818-830.

[19]   Grosshandler, W. L., "A Narrow-Band Model for Radiation Calculations in a Combustion Environment", *RADCAL, NIST technical note 1402*, 1993. (http://www.ca.sandia.gov/TNF/radiation.html.)

[20]   Hara, H. and Kumagai, S., *12th International Colloquium on Dynamics of Explosion and Reactive Systems*, 1989.

[21]   Heidemann, Robert A., and Khalil, Ahmed M., "The calculation of critical points", *AIChE Journal*, Vol. 26, No. 5, 1980, pp.769-779.

[22]   Hirschfelder, J.O., Curtiss, C.F., and Bird, R. B, *Molecular theory of Gases and liquids*, John Wiley and Sons, Inc, New York, 1954.

[23]   Hottel, H.C., Williams, G.C., and Simpson, H.C., "Combustion of heavy liquid fuels", *Fifth Symposium (International) on Combustion*, 1995, pp. 101-129.

[24]   Hubbard, G.L., Denny, V.E., and Mills, A.F., "Droplet evaporation: Effects of transient and variable properties", *Int. J. of Heat and Mass Transfer*, Vol.18, 1975, pp- 1003-1008.

[25]   Jackson, G.S., and Avedisian, C.T., "Combustion of unsupported water in n-heptane emulsion droplets in a convection free environment", *Int.J. of Heat and Mass Transfer*, 41:16, 1998, pp- 2503-2515.

[26]   Jia, H., and Gogos, G., "High pressure droplet vaporization; effects of liquid-phase gas solubility", *Int. J. of Heat and Mass Transfer*, Vol. 36, No. 18, 1993, pp. 4419-4431.

[27] Kazakov, A., Conley, J., and Dryer, F.L., "Detailed modeling of an isolated, ethanol droplet combustion under microgravity conditions", *Combustion and Flame*, 134, 2003, pp-301-314.

[28] Kumagai, S., and Isoda, H., "Combustion of fuel droplets in a vibrating air field", *Fifth Symposium (International) on Combustion*, 1955, pp. 129-141.

[29] Kumagai, S., "Combustion of Fuel sprays", *Sixth Symposium (International) on Combustion*, 1957, pp. 668-674.

[30] Kumagai, S., and Isoda, H., "Combustion of fuel droplets in a falling chamber", *Sixth Symposium (Inter-national) on Combustion*, 1957, pp. 726-731.

[31] Kumagai, S., Sakai, T., and Okajima, S., "Combustion of free fuel droplets in a freely falling chamber", *Thirteenth Symposium (Inter-national) on Combustion*, 1971, pp. 779-785.

[32] Kumar, S., "Influences of soot formation and radiation on spherically symmetric droplet combustion", *Ph. D. Thesis*, submitted to Dept of Mech. Engg. IIT Delhi, India, 2000.

[33] Kumar, S., Ray, A., and Kale, S., "A soot model for transient, spherically symmetric n-heptane droplet combustion", *Combustion Science and Technology*, 174, 2002, pp-67-102.

[34] Kuo, K.K., *Principles of Combustion*, John Wiley, Singapore, 1986.

[35] Law, C.K., "Multicomponent droplet combustion with rapid internal mixing", *Combustion and Flame*, 26, 1976a, pp-219-233.

[36] Law, C.K., "Unsteady droplet combustion with droplet heating", *Combustion and Flame*, 26, 1976, pp. 17-22.

[37] Law, C.K., and Sirignano, W.A., "Unsteady droplet combustion with droplet heating-II: Conduction limit", *Combustion and Flame*, 28, 1977, pp. 175-186.

[38] Law, C.K., "Internal boiling and superheating in vaporizing multi-component droplets" *AIChE Journal*, 24, 1978, pp. 626-632.

[39] Law, C.K., "On the fire resistant nature of oil-water emulsion", *Fuel*, 60, 1981, pp. 998-999.

[40] Law, C.K., and Law, H.K., "D^2-Law for multicomponent droplet vaporization and combustion", *AIAA Journal*, Vol.20, No.4, 1982, pp.522-527.

[41] Makino, A., and Law, C.K., "On the controlling parameter in the gasification behavior of multicomponent droplets", *Combustion and Flame*, 73, 1988, pp- 331-336.

[42] Mandal, S., "Modeling of Multicomponent Fuel Droplet Combustion", *Ph. D. Thesis,* submitted to Dept of Mech. Engg. IIT Kanpur, India, 1995.

[43] Marchese, A.J., and Dryer, F.L., "The effect of non luminous thermal radiation in micro-gravity droplet combustion", *Combustion Science and Technology,* Vol.124, 1997, pp. 371-402.

[44] Marchese A.J., Dryer F.L., and Naygam, V., "Numerical modeling of isolated n-alkane droplet flames: initial comparisons with ground and space-based microgravity experiments", *Combustion and Flame,* Vol.116, 1999, pp.432-459.

[45] Mawid, M., and Agarwal, S.K., "Analysis of transient Combustion of a Multicomponent Liquid Fuel Droplet", *Combustion and Flame,* 84, 1991, pp. 197-209.

[46] Mikami, M., Kato, M., Sato, M., Kono, M., "Clarification of the structure of droplet burning based on temperature measurement in microgravity", *Twenty Fifth Symposium (International) on Combustion,* 1994, pp.431-438.

[47] Mishra, D.P., "Fundamentals of Combustion", 2005 (Under preparation).

[48] Miyasaka, K., and Law, C.K., "Combustion of strongly interacting linear droplet arrays", *Eighteenth Symposium (International) on Combustion,* 1981, pp. 283-292.

[49] Nagreli, D.E., Lloyd, J.R., and Novonty, J.L., "A theoretical and experimental study of radiation-convection interaction in a diffusion flame", *Journal of Heat Transfer,* Vol. 99, 1977, pp. 212-220.

[50] Okai, K., Moriue, O., Tsue, M., Kono, M., Sato, J., Dietrich, D., L., and Williams, F., A., "Pressure effects on combustion of methanol and methanol / dodecanol single droplet and droplet pairs in microgravity", *Combustion and Flame,* 121, 2000, pp-501-512.

[51] Okai, K., Tsue, M., Kono, M., Sato, J., Dietrich, D., L., and Williams, F., A., "An experimental study of microgravity combustion of a droplet near a wall", *Combustion and Flame,* 133, 2003, pp.169-172.

[52] Okajima, S., and Kumagai, S., "Further investigations of combustion of free droplets in a freely falling chamber including moving droplets", *Fifteenth Symposium (Inter-national) on Combustion,* 1975, pp. 401-407.

[53] Okajima, S., and Kumagai, S., "Experimental studies on combustion of fuel droplets in flowing air under zero- and high gravity conditions", *Nineteenth Symposium (International) on Combustion,* 1982, pp-1021-1027.

[54] Orbey, Hasan, and Sandler, Stanley I., "Modeling Vapor-Liquid Equilibria", *Cambridge Series in Chemical Engineering,* 1998.

[55] Peng, D.Y., and Robinson, D.B., "A rigorous method for predicting the critical properties of multicomponent systems from an equation of state", *AIChE Journal*, Vol. 23, No. 2, 1977, pp.137-143.

[56] Perry, R.H. and Green, D.W., *Perry's Chemical Engineering Handbook*, Seventh Edition, McGraw-Hill International Publication, 1997.

[57] Prakash, S., and Sirignano, W.A., "Liquid fuel droplet heating with internal circulation", *Int. J. of Heat and Mass Transfer*, Vol.21, 1978, pp.885-895.

[58] Prakash, S., and Sirignano, W.A., "Theory of convective droplet vaporization with unsteady heat transfer in the circulating liquid phase", *Int. J. of Heat and Mass Transfer*, Vol.23, 1980, pp.253-268.

[59] Reid, R.C., Prausnitz, J.M., and Sherwood, T.K., *The Properties of Gases and Liquids*, 4th Ed., McGraw-Hill, New York, 1988.

[60] Rosner, D.B., "On liquid droplet combustion at high pressures", *AIAA J.*, Vol.5, No.1, 1967, pp-163-166.

[61] Saitoh, T., and Nagano,O., "Transient combustion of a fuel droplet with finite rate of chemical reaction", Combustion and Flame, Vol. 108, 1980, pp. 71-86.

[62] Saitoh, T., Yamazaki, K., and Viskanta, R., "Effect of thermal radiation on transient combustion of fuel droplet", *Journal of Thermophysics and Heat Transfer*, Vol. 22, 1993, pp. 227-234.

[63] Saito, M., Hoshikawa, M., and Sato, M., "Enhancement of evaporation / combustion rate coefficient of a single fuel droplet by acoustic oscillation", *Fuel*, Vol. 75, No. 6, 1995, pp. 669-674.

[64] Sato, J., Tsue, M., Niwa, M., and Kono, M., "Effcts of natural convection on high pressure droplet combustion", *Combustion and Flame*, Vol. 82, 1990, pp. 142-150.

[65] Shaw, B. D., Dryer, F. L., Williams, F. A., and Haggard Jr, J.B., *Acta Astronaut.* 17, 1988, 1195-1202.

[66] Shaw, B.D., "Studies of influence of liquid-phase species diffusion on spherically symmetric combustion of miscible binary droplets", *Combustion and Flame*, Vol. 81, 1990, pp. 277-288.

[67] Shaw, D.B., and Williams, F.A., "Theory of influences of a low-volatility, soluble impurity on spherically-symmetric combustion of fuel droplets", *Int. J. of Heat and Mass Transfer*, Vol. 33 No. 2, 1990, pp. 301-317.

[68] Spalding, D. B., "The combustion of liquid fuels", *Fourth Symposium (International) on Combustion*, 1953, pp. 847-864.

[69] Stengele, J., Prommersberger, K., Willmann, M., and Wittig, S., "Experimental and theoretical study of one and two component droplet vaporization in a high pressure environment", *Int. J. of Heat and Mass Transfer*, Vol. 42, 1999, pp. 2683-2694.

[70] Tien, C.L., and Lee, S.C., "Flame radiation", *Progress in Energy and Combustion Science*, Vol. 8, 1982, pp. 41-59.

[71] Tong, A.Y., and Sirignano, W.A., "Multicomponent transient droplet vaporization with internal circulation: Integral equation formulation and approximate solution", *Numerical Heat Transfer*, 10, 1986, pp- 253-278.

[72] Toulokian Y. S., and Makita Tadashi, *Thermophysical Properties of Matter*, TPRC data series, IFI/PLENUM, New York, 1970.

[73] Turns, S. R., *An Introduction to Combustion*, McGraw-Hill, New York, 1996.

[74] Vargaftik, N. B., *Tables on the Thermophysical Properties of Liquid and gases*, 2nd Ed., Hemisphere, Washington, 1975.

[75] Viskanta, R., and Merriam, R.L., "Heat transfer by combined conduction and radiation between concentric spheres separated by radiating medium", *Journal of Heat Transfer*, Vol. 90, 1968, pp.248-256.

[76] Wang, C. H., Liu, X. Q., and Law, C. K., "Combustion and micro-explosion of Freely Falling Multi-component Droplets", *Combustion and Flame*, Vol. 56, 1984, pp. 175-197.

[77] Williams, F.A., *Combustion Theory*, Addision-Wiley, New York, 1985.

[78] Xiong, T.Y., Law C.K., and Miyasaka, K., *Twentieth Symposium (Internatioal) on Combustion*, 1984, pp. 1781.

[79] Xu, G., Ikegami, M., Honma, S., Ikeda, K., Ma, X., Nagaishi, H., Dietrich, D.L., and Struk, P.M., "Inverse influence of initial diameter on droplet burning rate in cold and hot ambiences: a thermal action of flame in balance with heat loss", *Int. J. of Heat and Mass Transfer*, 46, 2003, pp. 1155-1169.

[80] Yang, J.C., and Avedisian, C.T., "The combustion of unsuspended heptane/hexadecane mixture droplet at low gravity", *Twenty Second Symposium (Inter-national) on Combustion*, 1988, pp-2037-2044.

[81] Yang, Jeng-Renn, Wong, Shwin-Chung, "On the discrepancies between theoretical and experimental results for microgravity droplet evaporation", *Int. Journal of Heat and Mass Transfer*, Vol. 44, 2001, pp.4433-4443.

[82] Yang, Jeng-Renn, Wong, Shwin-Chung, "An experimental and theoretical study of the effects of heat conduction through the support fiber on the evaporation of a droplet in a weakly convective flow", *Int. Journal of Heat and Mass Transfer*, Vol. 45, 2002, pp.4589-4598.

[83] Zhu, G.S., and Aggarwal, S.K., "Transient supercritical droplet evaporation with emphasis on the effects of equation of state", *Int. J. of Heat and Mass Transfer,* Vol.43, 2000, pp.1157-1171.

[84] Zhu, G.S., Reitz, R.D., and Aggarwal, S.K., "Gas phase unsteadiness and its influence on droplet vaporization in sub and super critical environments", *Int. J. of Heat and Mass Transfer,* Vol.44, 2001, pp.3081-3093.

[85] http://mathworld.wolfram.com/En-Function.html